JRC TECHNICAL REPORTS

Determination of high temperature material properties of 15-15Ti steel by small specimen techniques

EERA JPNM Pilot project TASTE

S. Holmström	JRC
I. Simonovski	JRC
F. de Haan	JRC
J-M. Lapetite	JRC
D. Baraldi	JRC
M. Serrano	CIEMAT
E. Altstadt	HZDR
J. Aktaa	KIT
V. Radu	INR
H. Namburi	CV-REZ
C. Cristalli	ENEA
R. Pohja	VTT
R. Delville	SCK·CEN
A. Courcelle	CEA

2017

Joint Research Centre

EUR 28746 EN

JRC Science Hub
https://ec.europa.eu/jrc

JRC105589

EUR 28746 EN

PDF ISBN 978-92-79-75429-6 ISSN 1831-9424 doi:10.2760/49859

Luxembourg: Publications Office of the European Union, 2017

How to cite this report: Holmström, S. et al, Determination of high temperature material properties of 15-15Ti steel by small specimen techniques, EUR 28746 EN, Publications Office of the European Union, Luxembourg, 2017, ISBN 978-92-79-75429-6, doi:10.2760/49859, JRC105589.

The following is a re-edition of Holmström, S. et al, *Determination of high temperature material properties of 15-15Ti steel by small specimen techniques,* EUR 28746 EN, Publications Office of the European Union, Luxembourg, 2017, ISBN 978-92-79-72278-3, doi:10.2760/259065, JRC105589.

Contents

Foreword 2
Acknowledgements 3
Abstract 4
1 Introduction 5
2 Materials and Methods 6
2.1 Test programs 7
2.1.1 Tensile properties 8
2.1.2 Creep properties 8
3 Results on 24%CW and 46%CW tube material 9
3.1 Tensile test results on 24%CW and 46%CW sub-sized uniaxial specimen 9
3.2 MT test results on 24%CW and 46%CW uniaxial specimen 11
3.3 Ring tension tests on 24%CW and 46%CW material (INR) 14
3.4 Ring compression tests on 24%CW and 46%CW material (ENEA, CVCREZ, JRC) 16
3.5 SP tests on 24%CW, 46%CW and 22%CW (CEA) material (JRC, HZDR, CIEMAT) 19
4 Results on annealed and 20%CW bar material 28
4.1 Tensile test results on annealed and 20%CW bar material 28
4.2 SP test results on annealed and 20%CW bar material 30
5 SPC (creep) testing on cold worked 1515Ti tubes and bars 33
6 Discussion 36
7 Conclusions and recommendations 38

Foreword

This report presents the final results from the round robin test program on thin-walled cladding tubes in the EERA-JPNM pilot project TASTE. The test methods and assessment procedures used for the assessment of 15-15Ti steel have been presented in an earlier TASTE report. In this report the test results from different test types are assessed, compared and evaluated. The collation of tests, mainly on tensile properties show good agreement between tests, and it can be seen that there is an indication of anisotropy between the axial and the hoop direction. The most applied test technique, i.e. the small punch tests has been used in a large temperature range from cryogenic to 800°C. A range of finite element simulations (FEA) have been performed for the SP test confirming that tests conducted on curved specimens (tube sections) can give a good estimate on the tensile strength within about 4% in comparison to using smaller standard type (flat specimen).

The small punch tests, the ring compression and ring tension test seem to complement each other well to give an overall estimation of the tube properties in comparison with miniature axial tensile test results. The ring compression tests gave a good correlation between collapse load and tensile strength despite of the complex stress − strain evolution during a test.

The small punch creep (SPC) tests performed on curved samples were not successful in determining the creep properties of the tubes due to cracking at an early stage (small deflection) of the test.

Acknowledgements

The authors wish to acknowledge the Joint Programme on Nuclear Materials (JPNM) of the European Energy Research Alliance (EERA).

Authors

S. Holmström JRC

I. Simonovski JRC

F. de Haan JRC

J-M. Lapetite JRC

D. Baraldi JRC

M. Serrano CIEMAT

E. Altstadt HZDR

J. Aktaa KIT

V. Radu INR

H. Namburi CV-REZ

C. Cristalli ENEA

R. Pohja VTT

R. Delville SCK·CEN

A. Courcelle CEA

Abstract

This report presents the final results from the round robin test program on thin-walled cladding tubes in the EERA-JPNM pilot project TASTE. The test methods and assessment procedures used for the assessment of 15-15Ti steel are presented in a previous TASTE report 1. In this report the test results from different test types are assessed, compared and evaluated. The collation of results, mainly on tensile properties shows good agreement between tests methods. An open question remains if there is some anisotropy between the axial and the hoop direction of the tubes. Results from ring tension indicate lower strength values than the test performed in the axial direction. However, the ring tension calculated estimates do not take bending and friction into account. Tensile strength estimates from miniature Small punch tests samples (3 mm in diameter and 0.25 mm thick) indicate no anisotropy whereas tests on the full wall thickness (0.45 mm) with larger puncher balls indicate a reduction towards the INR measured tensile strength (Ring Tension) in the hoop direction. The ring compression test estimates based on calibration at room temperature by ENEA showed surprisingly good performance in estimating the tensile strength at higher temperatures despite the complex stress distribution for this type of test.

The few tests performed for determining creep properties, i.e. small punch creep tests, were not successful in describing the expected creep properties. The SPC specimen (as was the case for some SP "tensile test") showed premature cracking at a very early stage of the test for the cold worked material.

As a whole it seems that the different types of tests complement each other and together gives an overall picture of the strength and ductility of the tube material. The classical tests such as the ring compression test and the ring tension test gave good estimates on the hoop strength whereas the small punch tests seemingly give an estimate for the weaker direction.

1 Introduction

The integrity of the fuel cladding in present and future nuclear fuel concepts is critical for the safe performance of the power plants. Presently the material performance and mechanical properties of thin walled fuel cladding tubes are evaluated through a number of testing techniques and evaluation methodologies. Within the pilot project TASTE under the umbrella of EERA-JPNM an inter-laboratory test programme of selected methods incorporating both currently used and new promising methods as well as miniature techniques has been performed. The main test materials were 24% and 46% cold worked fuel cladding tubes with an outer diameter of 6.55 and an inner diameter of 5.65 (nominal wall thickness 0.45 mm). The material was made available by SCK·CEN. Secondary test materials were annealed and a cold worked 15-15Ti bars (by SCK·CEN) and a 22% CW 15-15Ti tube from CEA.

The main objective of this report is to determine the material properties of the test tubes and compare results between different test types.

This report consists of the presentation of the TASTE data acquired within the round-robin and the comparison of material property estimates. The reports written by the different participating organisations are included in separate appendixes.

2 Materials and Methods

The primary project steel 15-15Ti (X10CrNiMoTiB15-15 or 1.4970) is a stabilized heat resistant stainless steel designed for fuel element claddings. The main test material heats were made available by SCK·CEN. The secondary 1515Ti test material provided by CEA was also tested by JRC.

The material chemical composition specifications for 15-15Ti material from the 1970s 2 is presented in Table 1 together with the main TASTE project material compositions (SCK·CEN tube and bar) 34. The TASTE 1515Ti materials include tubes with 22%, 24% and 46% cold work as well an annealed and a 19.6% cold worked bar (designation CW20%). The CEA material specific chemical composition and the material meta-data is confidential and have not been made available for this report. Microstructural investigation was conducted by CV-REZ for the 24%CW and 46%CW tubes. The micrographs are presented in Appendix A.

Table 1. Chemical composition of 15-15Ti, classical specification (1.4970), the SCK·CEN requirements and the measured values of the TASTE materials.

1.497 (FZKA6864)								
C, %	**Si, %**	**Mn, %**	**Cr, %**	**Mo, %**	**Ni, %**	**Ti, %**	**B, %**	
0.08-0.12	0.3-0.5	1.6-2.0	15.0-16.0	1.05-1.25	14.5-15.5	0.35-0.55	0.003-0.006	
P, %	**S, %**	**Fe, %**						
≤0.03	≤0.015	bal						
SCK·CEN requirements								
C, %	**Si, %**	**Mn, %**	**Cr, %**	**Mo, %**	**Ni, %**	**Ti, %**	**B, %**	
0.08-0.12	0.5-0.7	1.0-2.0	14.5-15.5	1.0-1.4	14.5-15.5	0.33-0.55	0.003-0.007	
P, %	**S, %**	**Co, %**	**N, %**	**V, %**	**Ta, %**	**Cu, %**	**Ca, %**	**Fe, %**
≤0.015	≤0.015	≤0.03	≤0.015	≤0.05	≤0.02	≤0.05	≤0.03	bal
TASTE (SCK·CEN tube)								
C, %	**Si, %**	**Mn, %**	**Cr, %**	**Mo, %**	**Ni, %**	**Ti, %**	**B, %**	
0.096	0.57	1.86	15.06	1.21	15.05	0.44	0.0031	
P, %	**S, %**	**Co, %**	**N, %**	**V, %**	**Ta, %**	**Cu, %**	**Ca, %**	**Fe, %**
0.013	<0.001	0.02	0.011	0.034	<0.02	<0.05	<0.03	bal
TASTE (SCK·CEN bar)								
C, %	**Si, %**	**Mn, %**	**Cr, %**	**Mo, %**	**Ni, %**	**Ti, %**	**B, %**	
0.1	0.58	1.92	15.09	1.21	15.08	0.34	0.004	
P, %	**S, %**	**Co, %**	**N, %**	**V, %**	**Ta, %**	**Cu, %**	**Ca, %**	**Fe, %**
0.013	<0.001	0.019	0.007	0.033	0.005	0.026	0.0005	bal

The SCK·CEN bar material is used as reference to evaluate the potential material property differences caused by product form, i.e. tube vs. bar. The bar material (∅13 mm) was delivered in two material states, as annealed bar and cold drawn to 19.6% cold work. The grain size of the cold drawn bar is in transversal direction G=6 (~500 grains/mm^2) and the annealed transversal grain size is G=8 (~2000 grains/mm^2). This

means that in a SP specimen with a wall thickness of 0.5 mm there are about 11 grains over the specimen thickness for the cold worked case and 22 in the annealed case.

The SCK·CEN tube material dimensions are $\varnothing_o = 6.55^{+0.03-0.05}$ and $\varnothing_i = 5.65^{\pm 0.03}$ mm with a wall thickness $h \geq 0.45$ mm. The ovality criterion is <0.04mm. As mentioned before there is two levels of cold work, namely 24%CW and 46%CW. The grain size of the 24%CW tube is G=9-9.5 transversal and G=9 longitudinal, corresponding to about 28-34 grains over the wall thickness of 0.45 mm. The average tensile strength and yield stress at RT in the axial direction for the 24%CW tube are R_m=809 and R_{p02}=691 MPa (3 tests). The average tensile fracture elongation (A%) is 25.4%. Note that for these tests were performed by loading a full tube (non-machined). The non-machined test will generally show lower tensile strength values and lower uniform elongations in comparison to the test conducted on tube sections with narrowed gauge length 5.

For the 46%CW tube the given grain size is G=10 transversal and G=9.5 longitudinal or 34-40 grains over the wall thickness of 0.45 mm. The tensile strength and yield stress at room temperature are R_m=950 and R_{p02}=926 MPa. The tensile fracture elongation A=10.3%.

The CEA tube material dimensions are $\varnothing_o$=8.5 mm and $\varnothing_i$=7.37 mm with a wall thickness h=0.565 mm. No axial material strength values have been disseminated.

Post-test evaluation was performed for some of the small punch test samples using a nano-CT X-ray tomography system for full 3D imaging (XCT). the from General Electric). The Phoenix Nanotom S 180 XCT is equipped with an ultra-high performance nanofocus X-ray tube with a Hamamatsu 2304 x 2304 pixel flat panel sensor. The software packet (Phoenix datos/x software) offers detectability up to 200 nm and a minimum voxel ("volume pixel") size of 500 nm. The sample is scanned at an angle of approximately 45° to avoid artefacts. The scans in the present study were carried out with a voltage of 130 kV and a current of 110 mA. A 0.5 mm Sn filter was used to cut-off the low-energetic radiation. For the data visualization the VGStudio Max 2.2 (Volume Graphics) software was used.

2.1 Test programs

The wide spread of test methods and the amount of test materials has restricted the coverage of tests for all materials. The structure of this report will be material based and have subsections for all tests types performed on them. Thus the main material for comparison of test types is the 1515Ti 24%CW steel. For creep only a few tests were performed in TASTE, mainly small punch creep tests (SPC) but a few internal pressure creep tests were performed by VTT on Zircaloy 4 (Zr4). The tests performed are given in Table 2 together with the performing testing labs.

Table 2. test types and materials tested in the TASTE round robin.

Test method and designation	Laboratories	Materials
Sub-size tensile tests on tube segments (**ST**)	CIEMAT, HZDR, SCK-CEN	24%CW, 46%CW
Micro tensile and creep test (**MT**, MC)	KIT	24%CW, 46%CW
Ring Tension testing (**RT**)	INR	24%CW, 46%CW

Segmented expanding cone mandrel test (SCM)	JRC	Zr4[1)]
Small Punch test − tensile (**SP**)	HZDR, CIEMAT, ENEA, JRC	24%CW, 46%CW, annealed bar, CW20% bar
Small Punch test − creep (SPC)	JRC	24%CW, 46%CW
Ring Compression testing (RC)	ENEA, JRC, CVR	24%CW, 46%CW
Internal Pressure testing (IP)	VTT	Zr4[1)]

1) Not assessed in this report

The main comparison activity was made on the tensile properties of the 24% cold worked 1515Ti steel for ST, MT, RT, SP and RC test. The properties of the 46% cold worked steel was performed using the same test specifications and correlation coefficients as for the 24%CW steel.

2.1.1 Tensile properties

The targeted properties are; the ultimate tensile strength R_m, the yield stress R_{p02} and the fracture elongation ε_f (%). The test specifics and the extraction of the target properties are describe in the test procedure TASTE report.

2.1.2 Creep properties

The targeted properties are; time to rupture as a function of stress and temperature and the creep fracture elongation ε_{cf} (%).

The only test methods used in TASTE were the internal pressure tests by VTT and the JRC spall punch creep tests. Since the internal pressure tests were performed on Zircaloy-4 only, the SPC tests are the only tests that can be compared against the SCK·CEN estimates for time to rupture on 1515Ti. These estimated rupture times are based on internal pressure burst tests.

3 Results on 24%CW and 46%CW tube material

3.1 Tensile test results on 24%CW and 46%CW sub-sized uniaxial specimen

The tensile estimates from the non-uniaxial test methods are mainly compared to the sub-sized uniaxial test results by HZDR [8] for 24%CW and 46%CW (see Figure 1) as given in Table 3-4. Uniaxial tests were also conducted by CIEMAT with a slightly longer specimen (see Figure 2): The CIEMAT results are given in Table 5. These results can be compared against the SCK·CEN tests with a full tube section at room temperature, i.e. R_m=809 and R_{p02}=691 MPa for the 24%CW and R_m=950 and R_{p02}=926 MPa for the 46%CW material. The tensile fracture elongations (A_t) were in this case 25.4% and 10.3% correspondingly.

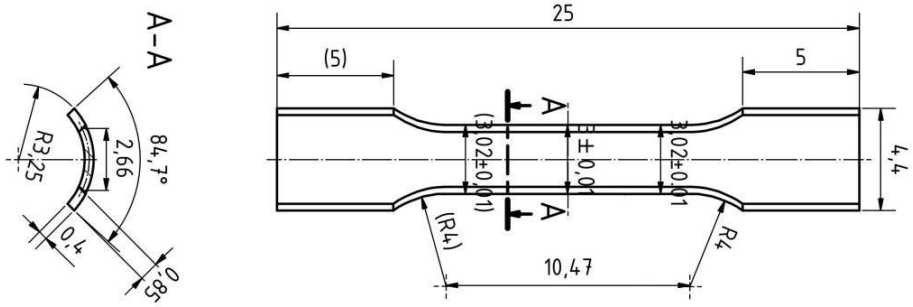

Figure 1. HZDR specimen machined from the tube.

Table 3. sub-sized uniaxial test matrix on 24%CWCW and 46%CW 1515Ti steel conducted by HZDR.

Temperature	Number of valid tests 24%CW	Number of valid tests 46%CW
RT	3	3
300 °C	4	3
500 °C	3	4
800 °C	2	2

Table 4. Sub-sized uniaxial test results on 24%CWCW and 46%CW 1515Ti steel conducted by HZDR.

	24%CW				46%CW			
(°C)	$R_{p0.2}$ (MPa)	R_m (MPa)	A_g (%)	A_t (%)	$R_{p0.2}$ (MPa)	R_m (MPa)	A_g (%)	A_t (%)
RT	740	857	5.4	13.1	918	929	1.6	9.0
300 °C	646	758	2.0	5.1	754	820	1.2	3.9
500 °C	613	716	3.1	6.4	689	756	1.7	3.9
800 °C	278	300	0.9	20.7	311	325	0.8	25.9

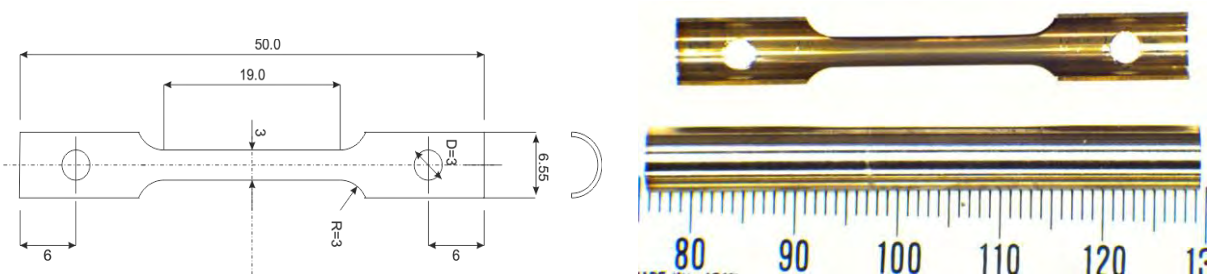

Figure 2. CIEMAT specimen machined from the tube.

Table 5. Sub-sized uniaxial test results on 24%CWCW and 46%CW 1515Ti steel conducted by CIEMAT.

	24%CW				46%CW			
(°C)	$R_{p0.2}$ (MPa)	R_m (MPa)	A_g (%)	A_t (%)	$R_{p0.2}$ (MPa)	R_m (MPa)	A_g (%)	A_t (%)
RT	723	813	11.0	18.0	884	909	4.0	7.0
300 °C	677	793	3.5	4.9	731	819	2.5	3.6
500 °C	729	806	6.0	7.4	752	816	4.3	5.3

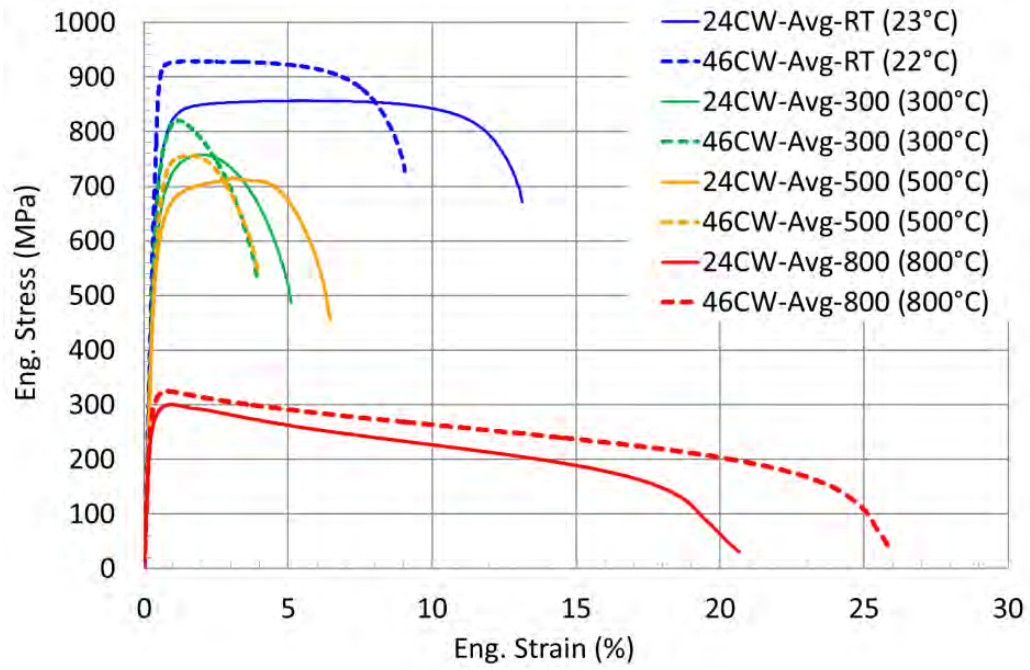

Figure 3. Comparison of HZDR averaged stress-strain curves at different temperatures; solid lines: 24%CW, dashed lines: 46%CW (see Appendix B).

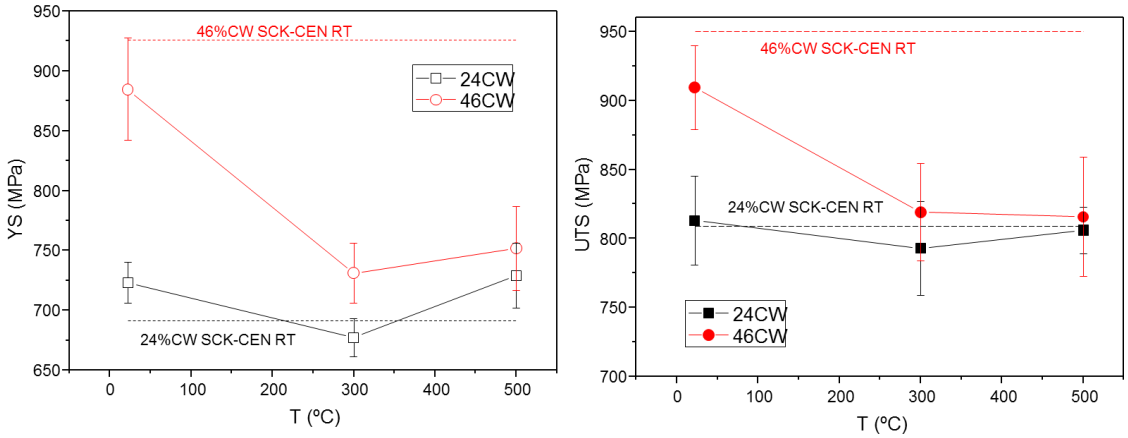

Figure 4. Comparison of yield strength (YS=R_{p02}) and tensile strength (UTS=R_m) for the CIEMAT tests on tube sections (see Appendix C)

3.2 MT test results on 24%CW and 46%CW uniaxial specimen

3.2.1 General Test setup details

Micro-tensile testing is performed as for larger standard samples but with much smaller samples. The main difference in test setup is that conventional strain (elongation) measurement is not possible and a camera system measures strain by means of digital image correlation (DIC). The small loads are measured with sensitive load cells. For high temperature tests, this is done by monitoring the specimen through the optical window of the furnace (see schematic view below, Figure **5**a). The specimens are micro "dog bone" specimen extracted from the material of interest (Figure **5**b). For claddings with sufficient large diameter the small sample size allows for both testing in radial and axial direction, hence possible anisotropy in the behavior of thin cladding tubes can be characterized. The samples are extracted by wire erosion (electrical discharge machining (EDM)) or laser cutting techniques and if necessary thinned to the desired thickness.

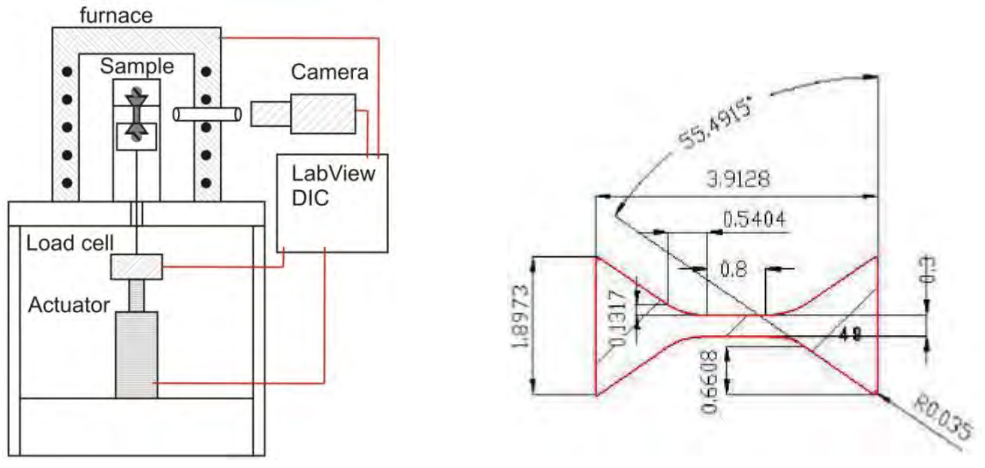

(a) (b)

Figure 5: Schematic view of the micro-tensile testing setup at KIT (a) and dimensions of a the micro specimen (b)

3.2.2 Tested materials and experimental procedure

Two distinct 15-15Ti austenitic cladding tubes with different cold-working (CW) levels were provided by partners for testing. While tube194 was 24% CW, another tube27 was 46% CW. Nevertheless, both tubes have similar outer- and inner-diameters of 6.5 mm and 5.6 mm, respectively.

For fabricating specimens, firstly, thin strips were longitudinally cut out from the as-received cladding tubes using EDM. To eliminate tubes curvatures from these thin strips, they were subsequently grinded carefully which brought their thickness down to ~ 0.1 mm. Thereafter, using EDM, final dog bone shaped specimens, with gauge length of 1 mm and cross-section of 0.3 x 0.1 mm^2 at an overall length of 4 mm, were precisely cut from these grinded strips (Figure 6). The obtained micro-specimens were then directly used for micro-tensile testing.

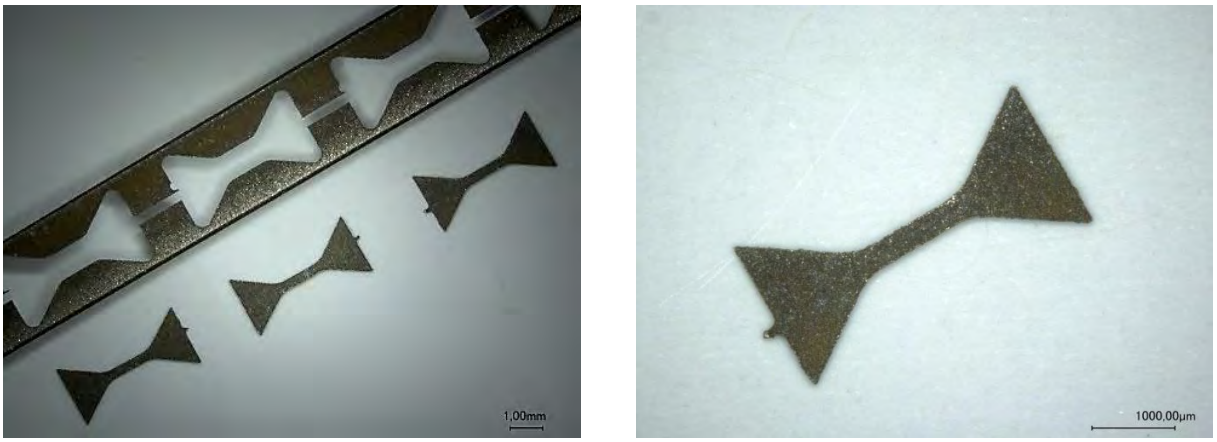

(a) (b)

Figure 6. Dog bone shaped micro-specimens taken out via EDM from the grinded thin strip (a) and an enlarged view of the dog bone shaped micro-specimen (b).

The tensile tests were carried out in air at four different temperatures (i.e. room temperature (RT), 300°C, 500°C and 600°C) with a nominal strain rate of $10^{-3}s^{-1}$. At elevated temperatures, the dwell time prior to the test start was at least 20 min. The images taken during the test were then carefully analyzed to estimate the strain using DIC by employing a Matlab script. The obtained stress-strain curves (see for example Figure 3) were then used to obtain various tensile properties namely yield strength ($R_{p0.2}$) and ultimate tensile strength (R_m), uniform elongation (A_g) and total elongation (A).

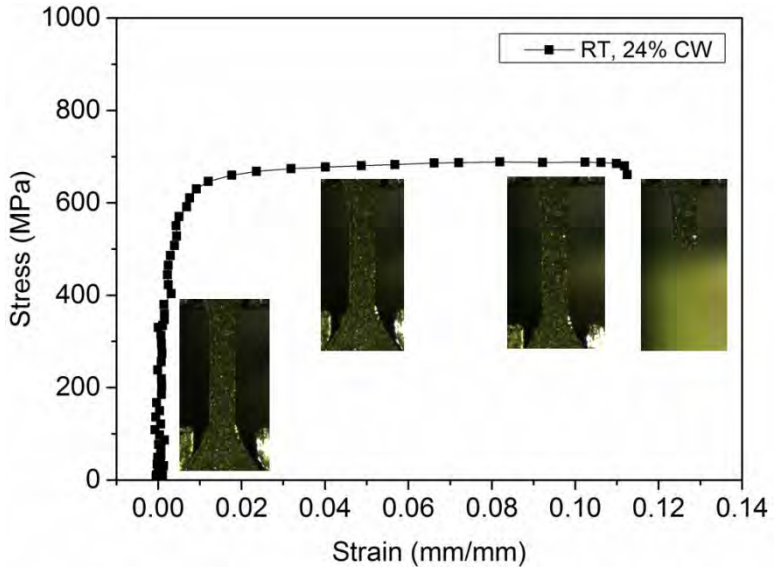

Figure 3: A typical stress-strain curve obtained at room temperature (RT) for 24% CW tube material.

3.2.3 Results

Figure 7 presents the stress-strain curves for both materials at all test temperatures. The comparison of strength and elongation are shown in Figure 8. Clearly, 46% CW tube material exhibit higher strength and obviously lower elongation than the 24% CW tube material at all tested temperatures. Although strength decreases for both materials with increase in temperature, the 46% CW tube material manifest weaker temperature dependence than 24% CW tube material. The main averaged tensile properties for both materials are also summarized in Table 6.

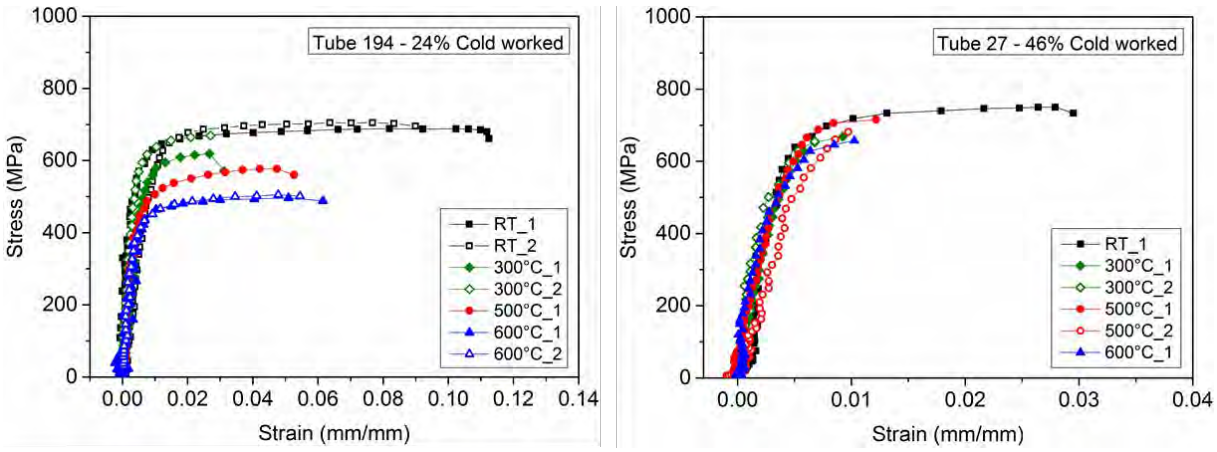

(a) (b)

Figure 7. Stress-strain curves for 24% CW tube (a) and 46% CW tube (b).

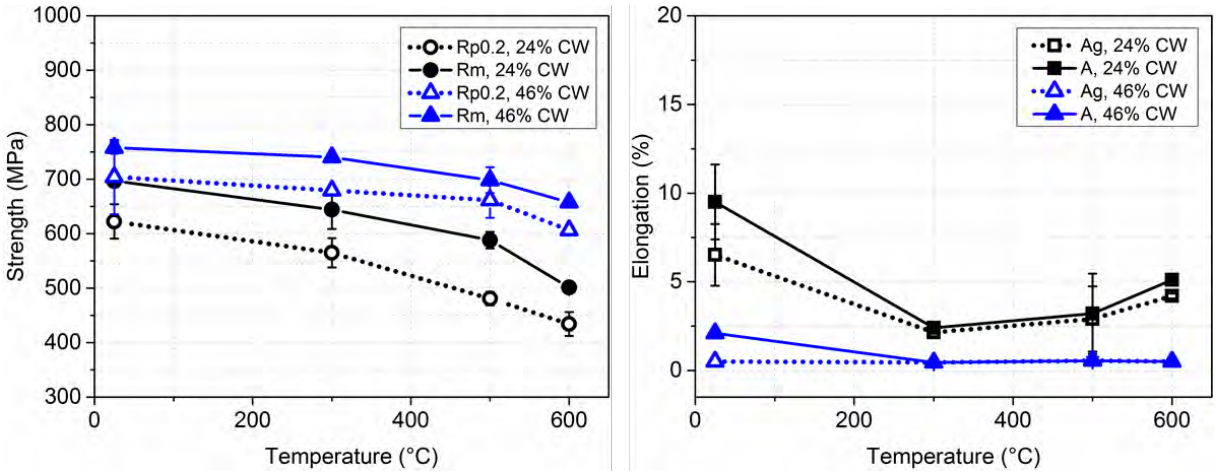

:

Figure 8. Yield ($R_{p0.2}$) and ultimate tensile (R_m) strength and (a) uniform (A_g) and total elongation (A) variation with temperature (b).

Table 6: Micro uniaxial test results on 24%CW and 46%CW 15-15Ti steel conducted by KIT.

	24%CW				46%CW			
(°C)	$R_{p0.2}$ (MPa)	R_m (MPa)	A_g (%)	A_t (%)	$R_{p0.2}$ (MPa)	R_m (MPa)	A_g (%)	A_t (%)
RT	622.5	696.8	6.5	9.5	704	757.7	0.5	2.1
300 °C	564.8	644.2	2.2	2.4	680.5	740.7	0.45	0.45
500 °C	472.0	577.4	4.2	4.8	660.7	698.4	0.6	0.6
600 °C	434.2	500.9	4.2	5.2	606.5	657.6	0.5	0.5

3.3 Ring tension tests on 24%CW and 46%CW material (INR)

The ring tension test results (R_m) are given in Table 7 and plotted against the HZDR uniaxial test results in Figure 9 and Figure 10. Note that the R_m estimates do not take bending and friction into account (see Appendix D).

Table 7. Ring tension test results on 24%CW and 46%CW 1515Ti steel conducted by INR.

	24%CW				46%CW			
(°C)	$R_{p0.2}$ (MPa)	R_m (MPa)	A_g (%)	A_t (%)	$R_{p0.2}$ (MPa)	R_m (MPa)	A_g (%)	A_t (%)
RT	-	746; 745	-	-	-	844; 864	-	-
500 °C	-	595; 610	-	-	-	688; 694	-	-
600 °C	-	590	-	-	-	670	-	-

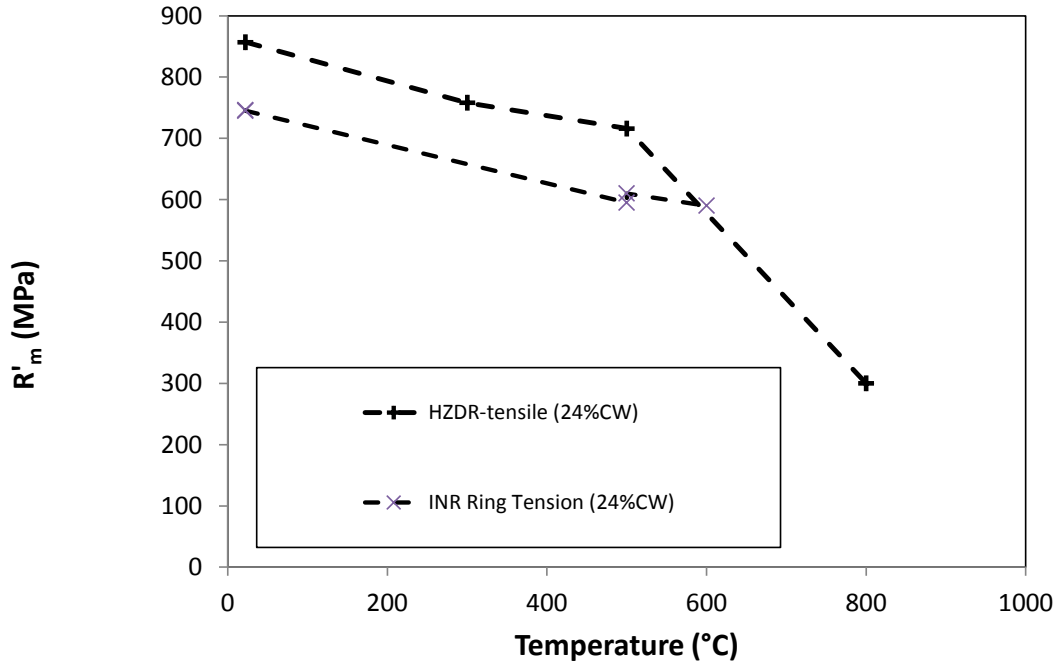

Figure 9. Comparison of tensile strength (R_m) estimates for the INR ring tension (RT) tests on 24%CW material in comparison to the HZDR uniaxial test.

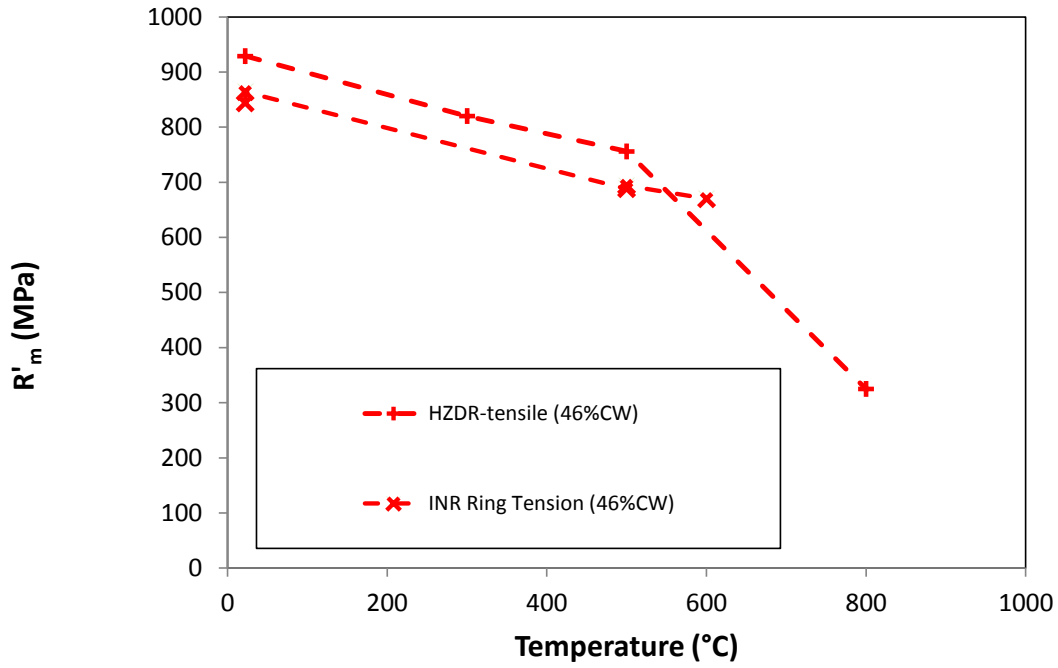

Figure 10. Comparison of tensile strength (R_m) estimates for the INR ring tension (RT) tests on 46%CW material in comparison to the HZDR uniaxial test.

3.4 Ring compression tests on 24%CW and 46%CW material (ENEA, CVCREZ, JRC)

Ring compression tests at room temperature were conducted by ENEA with a range of ring lengths as described in Appendix E (ENEA report). The correlation between the collapse load and the tensile strength was calibrated by ENEA at room temperature for the 24%CW case and used for assessing the data from CV-REZ and JRC.

The collapse stress (σ_0) and the tensile strength are correlated by;

$R_m = \sigma_0 / K_{UTS}$

Where σ_0 is calculated from the collapse force (P_0). P_0 is extracted from the force-deflection curve by the two-secants method (intersection of linear fits to before and after collapse). The $\sigma_0 = \alpha \cdot P_0 \cdot R_0 / (h^2 \cdot L)$ where R_0 is the outer radius of the tube, h is the wall thickness and L is the length of the tube. Note that $\alpha = 1$ for thin rings (not longer than a few wall thicknesses) and $\alpha = 0.866$ for longer tubes with L>one tube diameter. Note that in this work $\alpha = 0.866$ is also used for the rings that are marginally shorter than one tube diameter.

The correlation between collapse load and tensile strength was done by ENEA for 3 different tube lengths (L=6, 20 and 65mm) as given in Table 8. However the 3 test results from the 20 mm long tubes for 24%CW material was chosen as calibration point for comparing test results from the different labs. At the calibration point the σ_0 was optimized to give a R_m= 818 MPa. Two out of the 3 test gave a K_{UTS} =1.18. This value is used for estimating the R_m for all the other RC test results. Note that the choice of method for extracting the collapse load will have a direct impact on the estimated tensile properties.

The CV-REZ results are given in Table 9 and the JRC results from the wider temperature range RT-800°C are given in Table 10. The JRC estimates at room temperature to 800°C are shown in comparison to the HZDR tensile tests in Figure 13 and Figure 14. The ring tensile test results seem to estimate the axial R_m very well.

Table 8. Ring compression test results on 24%CW and 46%CW 1515Ti steel conducted by ENEA at room temperature.

	24%CW				46%CW			
Ring length	P_0 (N)	R'_m (MPa)	A_g (%)	A_t (%)	P_0 (N)	R'_m (MPa)	A_g (%)	A_t (%)
6 mm		882	-	-	-	965	-	-
20 mm		**818**[1)]	-	-	-	902	-	-
65 mm		782	-	-	-	897	-	-

([1]) Calibration point.

Table 9. Ring compression test results on 24%CW and 46%CW 1515Ti steel conducted by CV-REZ at room temperature. The ring length L ranges from 6.06 mm to 7.6 mm in length

	24%CW				46%CW			
Ring length	P_0 (N)	R_m (MPa)	A_g (%)	A_t (%)	P_0 (N)	R_m (MPa)	A_g (%)	A_t (%)
6.1-7.6		775	-	-		875	-	-

Table 10. Ring compression test results on 24%CW and 46%CW 1515Ti steel conducted by JRC with a ring length L=6.8 mm. The reported collapse stress P_0 is an average.

	24%CW				46%CW			
(°C)	P_0 (N)	R_m (MPa)	A_g (%)	A_t (%)	P_0 (N)	R_m (MPa)	A_g (%)	A_t (%)
RT	-	881	-	-	-	969	-	-
300°C	-	804	-	-	-	882	-	-
500°C	-	725	-	-	-	892	-	-
600°C	-	672	-	-	-	859	-	-
700°C	-	628	-	-	-	836	-	-
750°C	-	435	-	-	-	843	-	-
800 °C	-	384	-	-	-	725	-	-

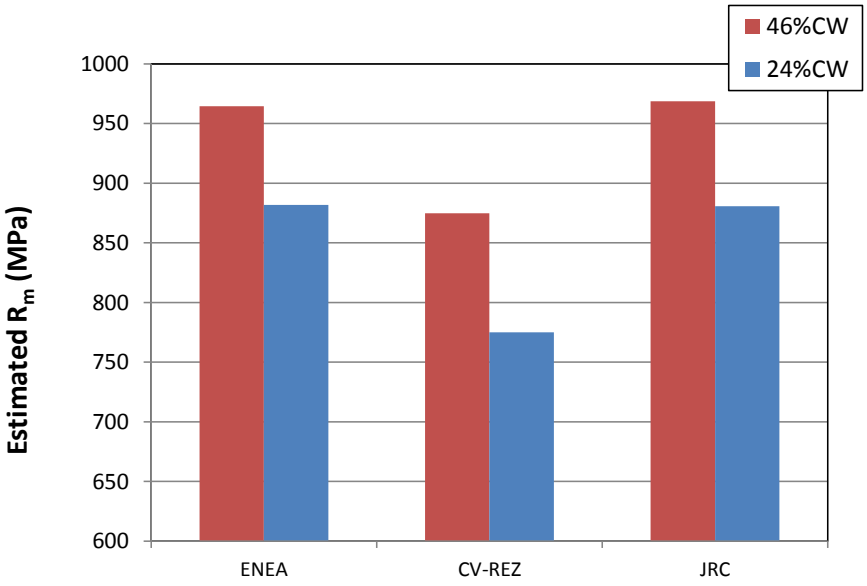

Figure 11. Comparison of estimated tensile strength R_m at room temperature for RC tests with ring lengths L of around 6 mm.

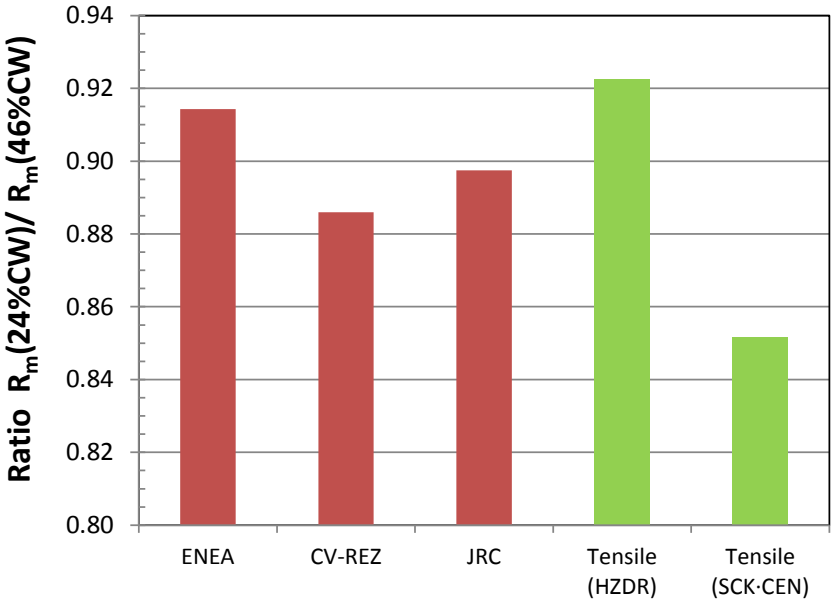

Figure 12. Comparison of the tensile strength ratios $R_{m\text{-}24\%CW}/R_{m\text{-}46\%CW}$ at room temperature for RC tests (red) with a length L~ 6 mm. The corresponding ratios for uniaxial tensile test are shown as reference (green).

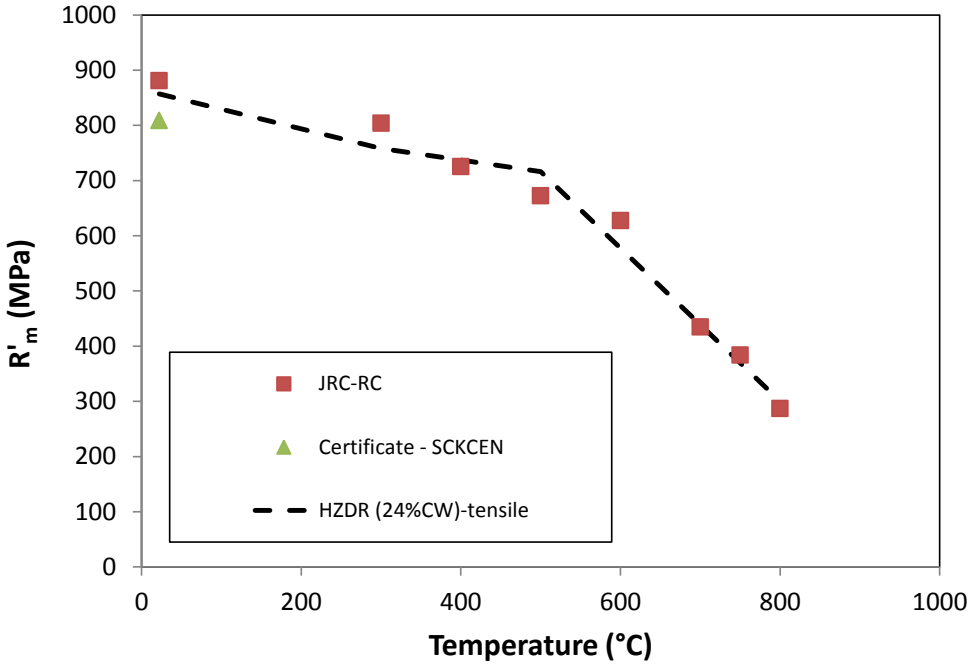

Figure 13. Comparison of the 24%CW tensile strength estimates from the JRC ring compression tests and the uniaxial tensile test results from HZDR.

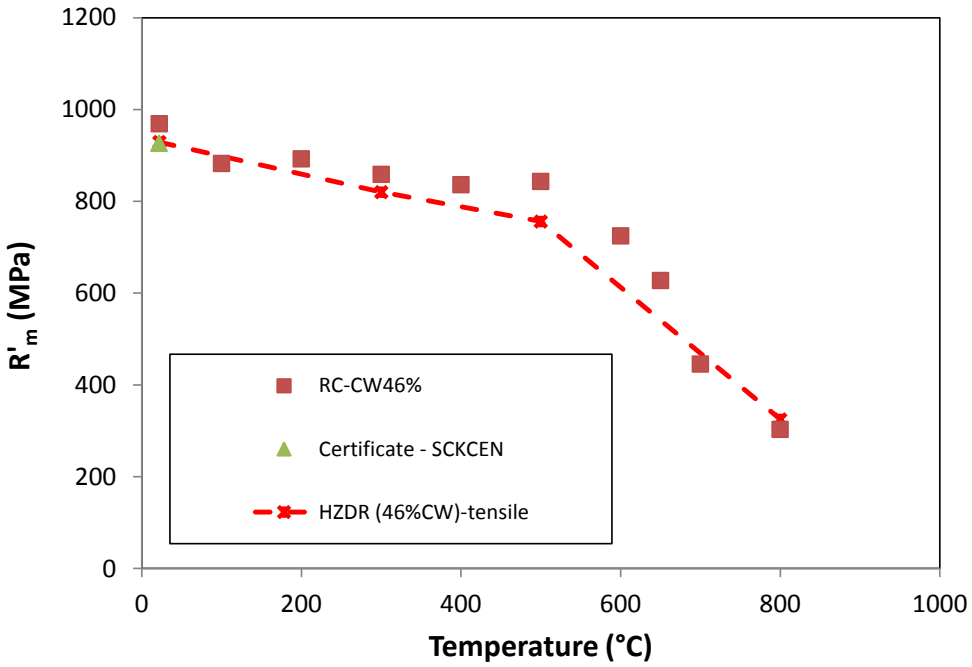

Figure 14. Comparison of the 46%CW tensile strength estimates from the JRC ring compression tests and the uniaxial tensile test results from HZDR.

3.5 SP tests on 24%CW, 46%CW and 22%CW (CEA) material (JRC, HZDR, CIEMAT)

The small punch test programme on the 24%CW and 46%CW claddings comprises of test performed by 3 laboratories. All 3 laboratories have a different test set-up and target test temperatures. HZDR is targeting the cryogenic temperatures for estimating the ductile to brittle transition temperature (Appendix A) while CIEMAT and JRC are targeting the high temperature properties as given in Table 11.

Note that JRC is testing two different sizes of punching ball. The differences in the specimen and test-setup dimensions are naturally causing difficulties in comparing results. The overlap condition of all laboratories is at room temperature. These tests are used for studying the effect of the test set-up differences.

Table 11. Test-setup specifics for testing 24%CW, 46%CW and 22%CW claddings with SP. The radial clearance is a measure that gives describes the available space for "deep drawing" deformation. The recommended radial clearance for cup drawing to avoid "wrinkling" and "tearing" is between 7-14%.

Testing lab set-up	Spec. thickness h_0 (mm)	Ball diameter d (mm)	Receiving hole diameter D (mm)	Radial clearance ((D-(d+2*h_0))/D)	Test temperatures
CIEMAT	0.25	1	1.5	0%	22, 300, 500 °C
HZDR	0.45	1	2	5%	-196 to 22 °C
JRC-A	0.45	2	4	27.5%	22-800 °C

JRC-B	0.45	2.5	4	15%	22-800 °C
JRC-C	0.565	2	4	21.8%	22
JRC-D	0.565	2.5	4	9.3%	22-800 °C

Both JRC and HZDR tested on curved samples with the original tube wall thickness (nominal 0.45 mm) whereas CIEMAT prepared miniature samples from the tube and grounded/polished them to a thickness of 0.25 mm. In this case the material under the punch is close to the inner surface of the cladding tube.

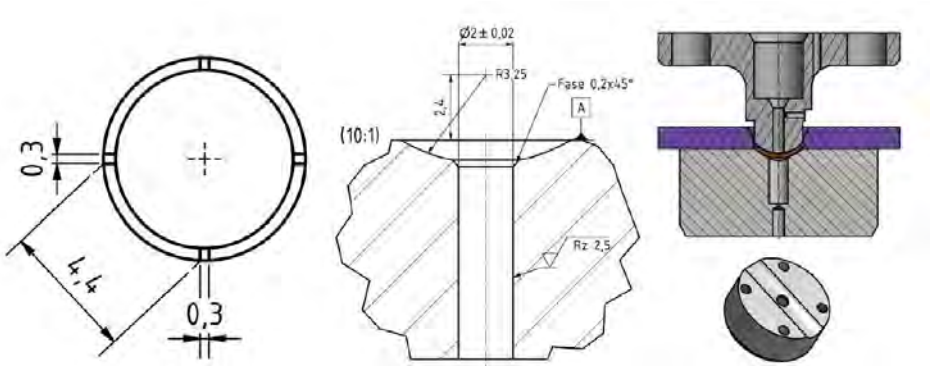

Figure 15. HZDR small punch test-setup for testing curved samples. Specimen (left), the lower die specifics (center) and a side-view of the punching configuration (right).

The tensile strength estimate R_m calculated from a flat SP test specimen is classically;

$$R'_m(F_m,u_m)=\frac{\alpha}{u_m\cdot h}\cdot F_m \qquad (1)$$

The formulation is based on and α that has to be determined for each test set-up. However, the needed parameters can be solved for ductile material with a strain hardening according to Chakrabarty 10 and Hill 11.

The estimated tensile strength R'_m is based on the Chakrabarty membrane stretch equations [1] using the force to membrane stress ratio F/σ as a function of displacement.

This equation works well with ductile materials. For ductile materials the measured d_m coincides well with the Chakrabarty predicted displacement at minimum, i.e. $d_m=1.57$ for a standard flat specimen and a test set up with 4 mm receiving hole and a ∅2.5 mm puncher.

However, in case that the material cracks at a lower displacement due to limited ductility the R'_m estimate has to be scaled according to the Chakrabarty F/σ_m curve for each individual test set-up.

$$\frac{F}{\sigma_m}=A_1\cdot A_2\cdot d+A_3\cdot d^2+A_4\cdot d^3+A_5\cdot d^4$$

The membrane stress σ_m is then converted to engineering stress by dividing it by 1+h/r as described in 17.

In addition, for a curved sample (JRC tests), a further correction factor has to be applied to take the changed force deflection response into account. This is correction is naturally not needed for the tests with test set-ups with a very small ball in relation to the inner tube curvature or for flat samples (HZDR and CIEMAT tests). In the JRC test with a 2.5

mm ball it was considered necessary. To find the corresponding displacement at maximum force (d_{mT}) for the tube, FEA simulations were performed for two materials with known tensile properties. In Figure 16 a simulation results for 3 different cladding tube dimensions (diameter, wall thickness) is shown. The prediction curve for the ∅ 6.55 (SCK•CEN) and ∅8.5 (CEA) outer diameters are relevant for this assessment.

The flat to curved sample correction is calculated for the ductile case as d_{mTube} /d_{mFlat} where d_{mFlat} is the standard specimen displacement at maximum. It is to be noted that this correction assumes that the calculated ratio is a constant over the whole displacement range.

Another source of error for the curved sample comes from the oval contact surface in the beginning of the deformation decreasing the actual pressure surface. This means that the here presented calculated R'_m are likely to be somewhat underestimated.

The calculated average αcorrelation factors for each test set-up are given for room temperature and 24%CW ductility in Table 12. Note that the CIEMAT and HZDR estimates are calculated as flat specimen.

Table 12. Test-setup specific correlation constants for flat and curved specimen.

Testing lab -set up	Chakrabarty (flat specimen) α	Average (RT) (corrected) α'
CIEMAT	0.264	0.249 [1)]
HZDR	0.255	0.231 [1)]
JRC-A (2.0 mm)	0.323	0.215 [2)]
JRC-B (2.5 mm)	0.296	0.205 [2)]
JRC-C (2.0 mm)	0.309	0.237 [3)]
JRC-D (2.5 mm)	0.286	0.224 [3)]

([1]) Assumed to be as for a flat specimen

([2]) FEA corrected for the SCK·CEN tube ($\varnothing_o$=6.55 mm, h_0=0.45 mm)

([3]) FEA corrected for the CEA tube ($\varnothing_o$=8.5 mm, h_0=0.565 mm)

It is recommended that the specimen are post-test evaluated to acquire an estimate on the axial vs. hoop strains at fracture.

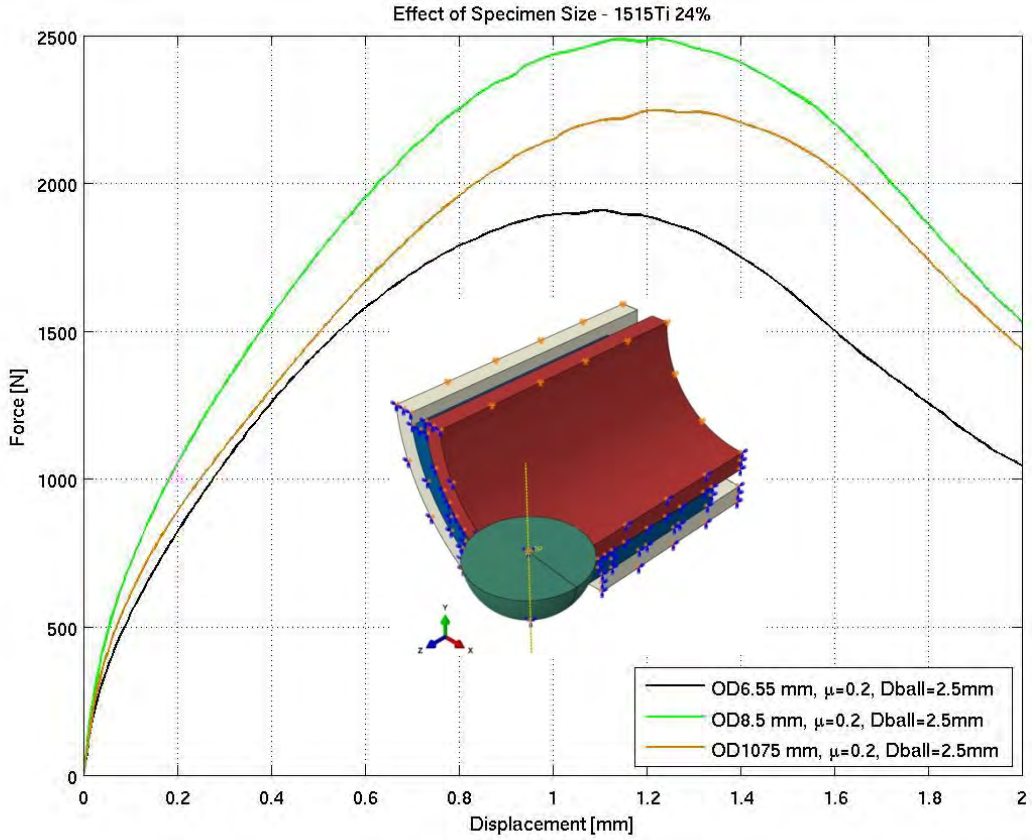

Figure 16. FEA simulations for solving the displacement correction for estimating R_m for curved specimen. Note that the h_0 is different for the different tubes.

The averages of the CIEMAT SP tests at specified temperatures are tabulated in Table 13 and the room temperature tests from HZDR and JRC are given in Table 14-Table 16.

Table 13. Average F_e (for estimating yield), F_m (for estimating R_m) forces and d_m (displacement at F_m) from the CIEMAT SP tests on SCK·CEN tube material.

CW	T (°C)	F_e	d_m	F_m
24%CW	22	75.554	0.554	504.2
	300	77.847	0.527	398.1
	500	64.883	0.537	370.6
46%CW	22	60.319	0.542	351.9
	300	72.670	0.560	486.8
	500	68.065	0.548	405.6

Table 14. Measured F_e, F_m and um from the HZDR room temperature tests on SCK·CEN tube material. Note that here the deflection from below um is measured, not the displacement of the puncher.

CW	T (°C)	F_e	u_m	F_m
24%CW	22	203.2	0.677	970.6

	22	156.1	0.665	933.6
	22	189.3	0.653	890.5
	22	240.3	0.637	910.8
	22	199.5	0.642	881.5
46%CW	22	142.9	0.550	910.8
	22	144.4	0.500	881.5
	22	170.0	0.522	890.5
	22	141.2	0.520	933.6
	22	172.9	0.540	970.6

Table 15. Measured F_m and d_m (displacement at F_m) from the JRC room temperature tests with a 2.0 mm ball and curved tube specimen for the SCK·CEN tube (JRC-A).

CW	T (°C)	d_m	F_m
24%CW	22	0.897	1630
	22	0.856	1570
	22	0.750	1560
	22	1.014	1550
	22	0.865	1620

Table 16. Measured F_e , F_m and d_m from the JRC room temperature tests with a 2.5 mm ball and curved tube specimen for the SCK·CEN tube (JRC-B).

CW	T (°C)	F_e	d_m	F_m
24%CW	22	602	1.073	2008
	22	611	0.989	1954
	22	562	1.102	2010
46%CW	22	618	1.368	2872
	22	685	1.428	2627
	22	685	1.428	2627

Table 17. Measured F_e , F_m and d_m from the JRC room temperature tests of the CEA tub (test set-ups JRC-C and D).

CW	T (°C)	F_e	d_m	F_m
22%CW (JRC-C) 2.0 mm	22	550	1.160	2010
	22	660	1.199	2030
	22	670	1.193	2000
22%CW (JRC-D) 2.5 mm	22	618	1.368	2872
	22	685	1.428	2627
	22	685	1.428	2627

All the SP tests with different test-set-up and specimen thicknesses are compared in Figures 15-20 using the simulated correction for the JRC tests. Note that for the CIEMAT and HZDR test-set up no curvature corrections have been applied. It is clear that the scatter in measured displacement / deflection cause increased scatter in the estimated R_m than what would be the case for R_m only depended on the maximum force.

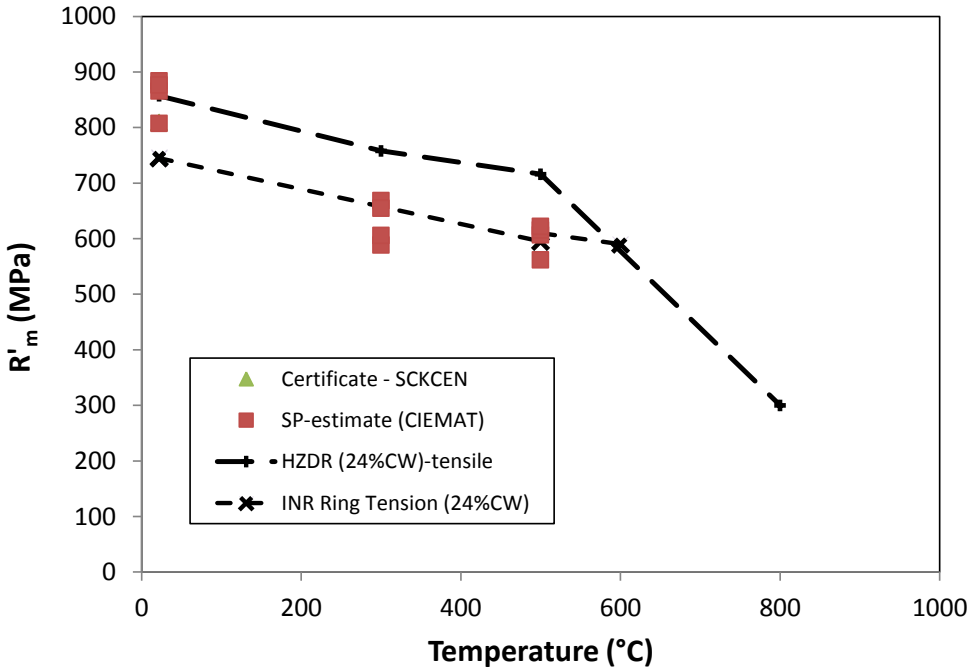

Figure 17. R_m estimates from CIEMAT 24%CW SP tests in comparison to HZDR tensile and INR hoop strength results.

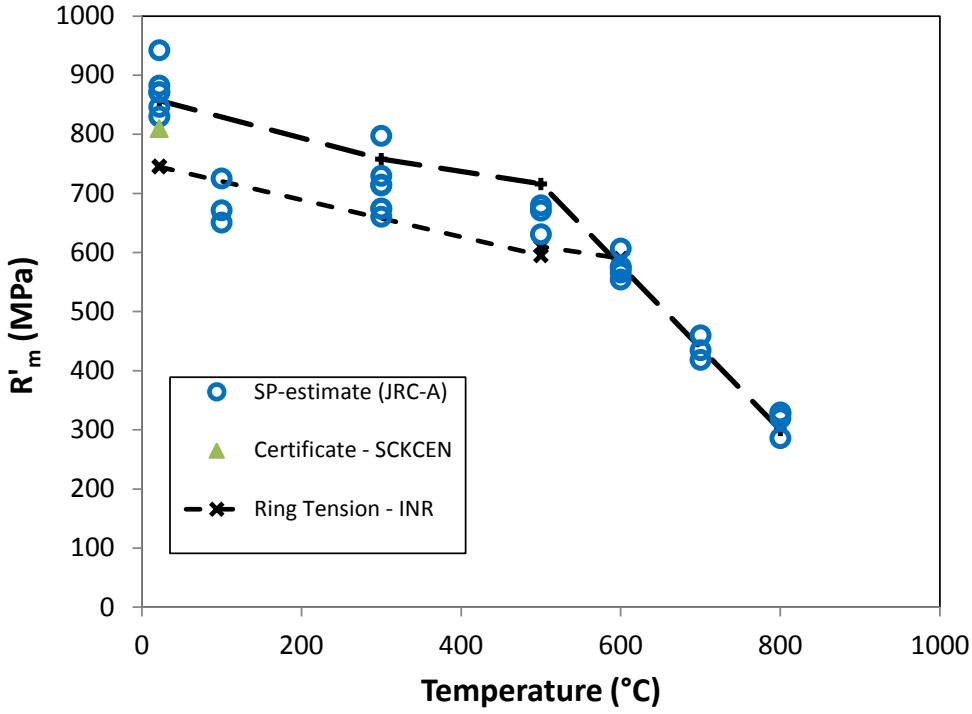

Figure 18. R_m estimates from SP (JRC-A test set-up) tests in comparison to HZDR tensile and INR hoop strength results.

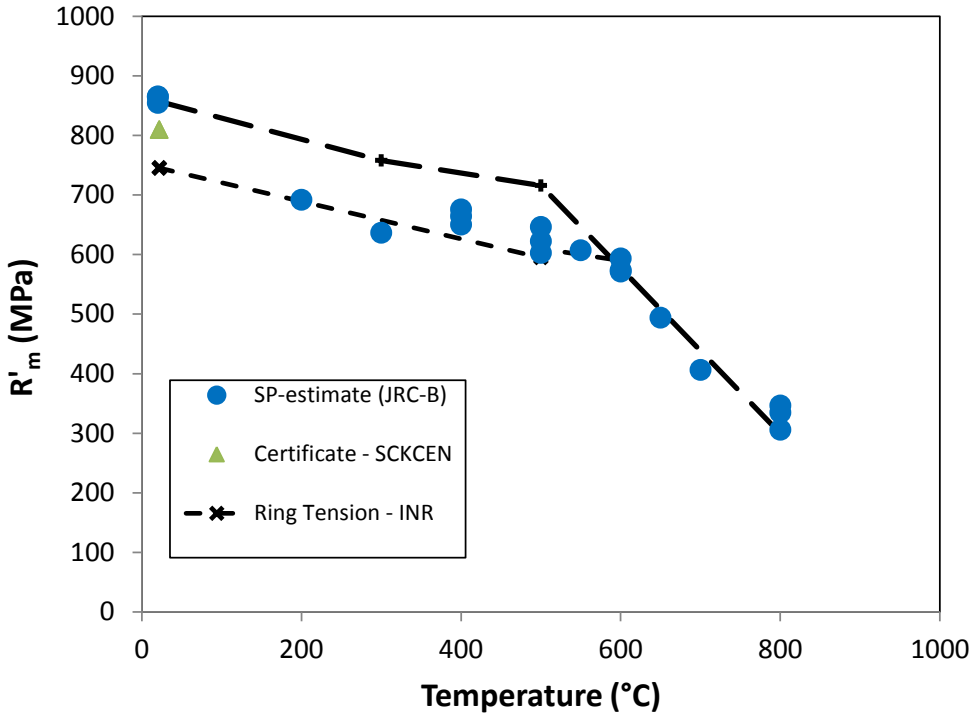

Figure 19. R_m estimates from SP (JRC-B test set-up) tests in comparison to HZDR tensile and INR hoop strength results.

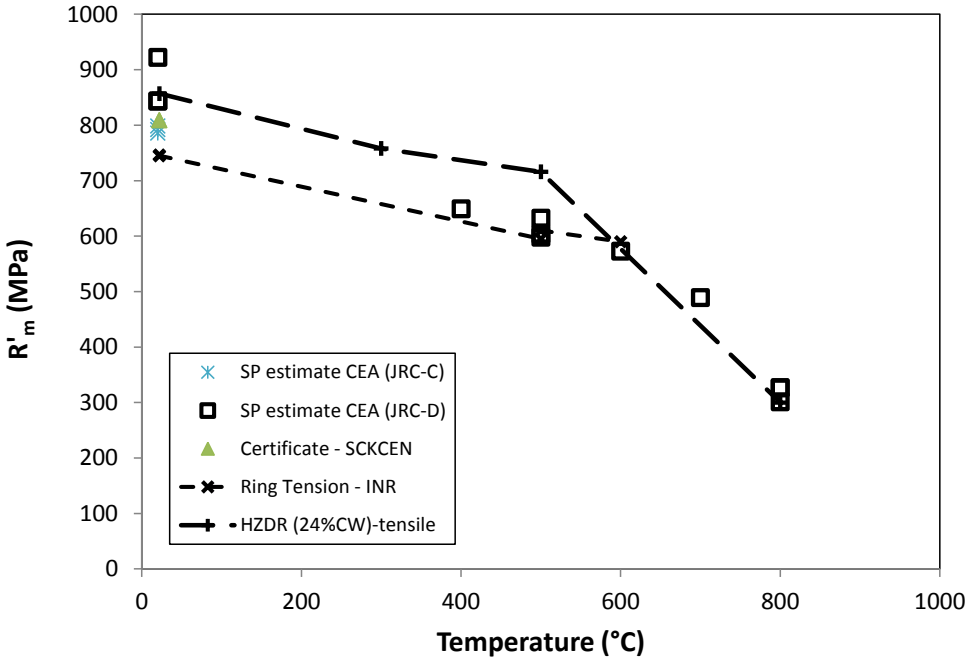

Figure 20. R_m estimates from JRC-D SP tests on the CEA tube (22%CW) in comparison to HZDR tensile and INR hoop strength results on the 24%CW tube

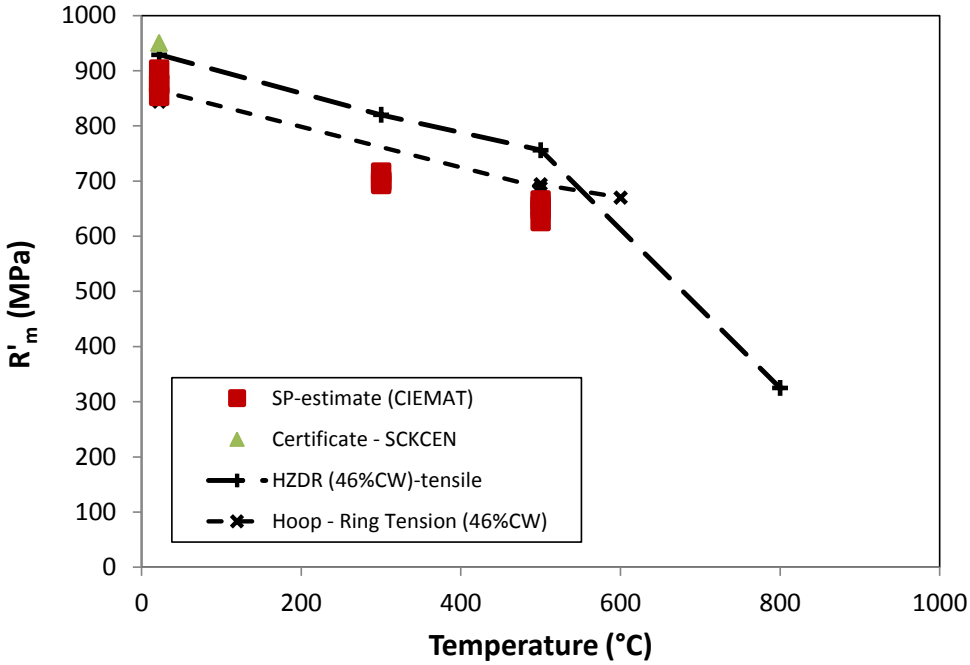

Figure 21. R_m estimates from CIEMAT 46%CW SP tests in comparison to HZDR tensile and INR hoop strength results.

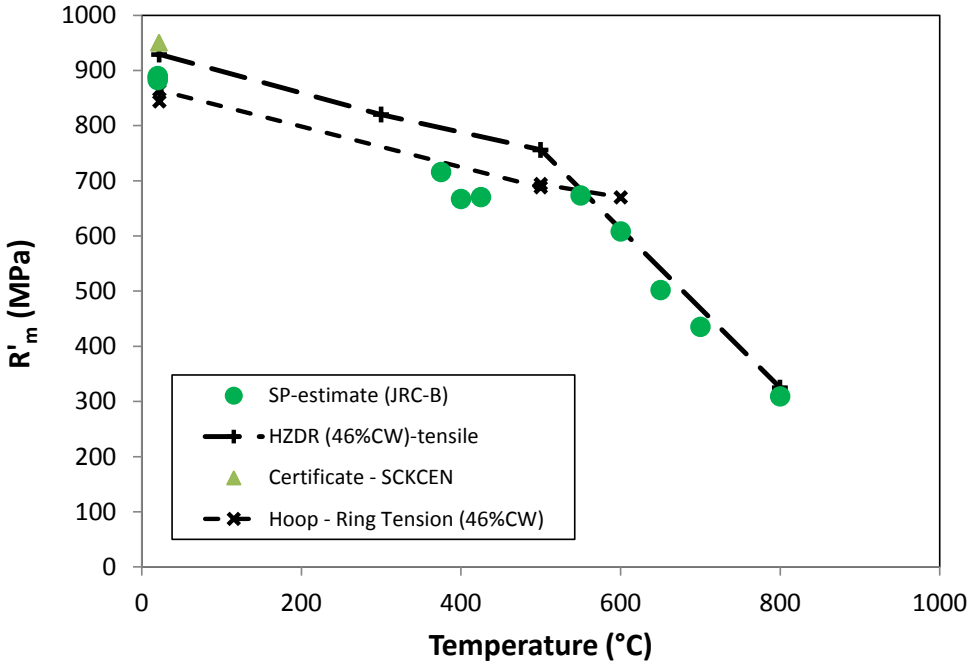

Figure 22. R_m estimates from JRC-D 46%CW SP tests in comparison to HZDR tensile and INR hoop strength results.

Note that in the assessment of the SP curved samples the following has been applied to correct for premature cracking (low ductility) and FEA correction for constraint due to specimen curvature.

An interesting trend can be found from the SP results. The room temperature estimates seem to correspond to the axial tensile results whereas the estimates for elevated temperature seem to correspond to the measured hoop properties. Also the SP results indicate a local ductility and strength minimum at temperatures 300-400°C.

4 Results on annealed and 20%CW bar material

4.1 Tensile test results on annealed and 20%CW bar material

Two uniaxial tensile tests were conducted at room temperature, one for the annealed bar and one for the 20%CW bar using an autoclave loading frame. The testing machine was chosen due to existing suitable grips for the sub-sized uniaxial specimen. The elongation of the test specimen was extracted (measured) from the cross head movement. This means that the calculated strain has to be corrected for machine compliance. Due to the rather nonlinear measured compliance it is evident that the yield strength acquired from the calculated stress-strain curve clearly contains more uncertainty than the calculated tensile strength R_m. The Young's modulus used in the determination of the Rp02 was from room temperature axial tensile tests by HZDR. The beginning of the stress-strain curves are shown in Figure 23 and the results are tabulated in Table 18. The fractured specimens are shown in comparison to the untested specimen and each other in Figure 24, Figure 25 and Figure 26.

The tensile strength of the 20%CW bar is R_m=733 MPa and the calculated yield stress R_{p02}=655 MPa. The corresponding values for the annealed bar is R_m=594 MPa and R_{p02}=248 MPa. The ratios R_{p02}/R_m for the two material states are 0.89 for the CW bar and 0.42 for the annealed bar.

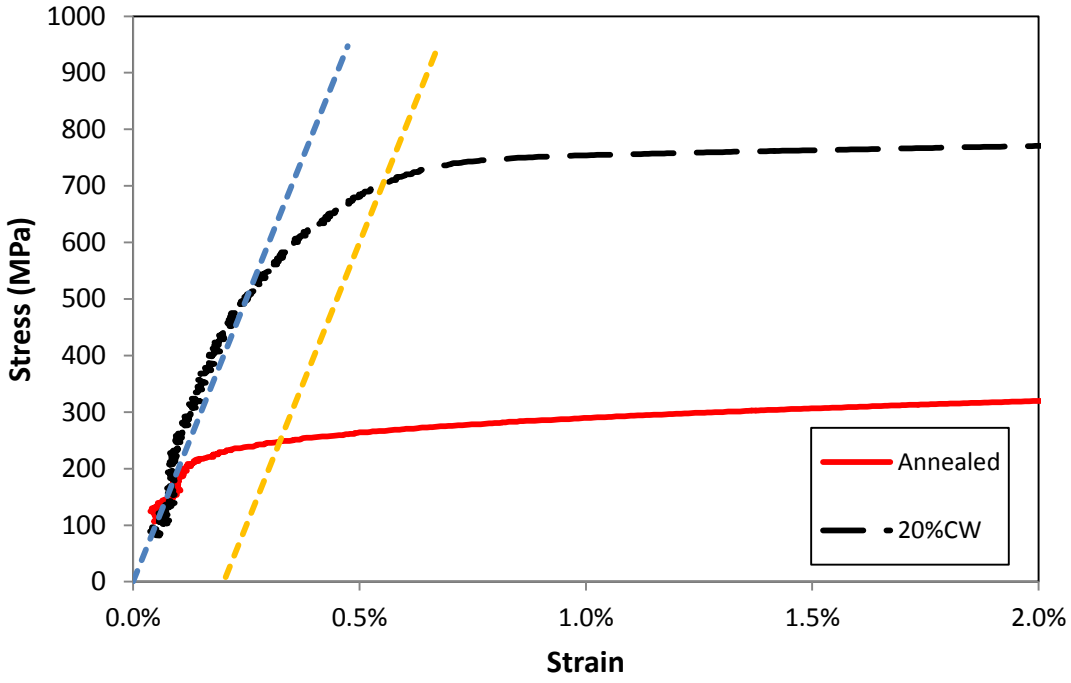

Figure 23. Tensile test curves for the annealed and 18% cold worked bar.

Table 18. Sub-sized tensile test on annealed and 20%CW bar by JRC.

	Annealed				20%CW			
Temp	$R_{p0.2}$ (MPa)	R_m (MPa)	A_g (%)	A_t (%)	$R_{p0.2}$ (MPa)	R_m (MPa)	A_g (%)	A_t (%)
RT	248	594	43	69	655	733	23	43

Figure 24. 20%CW specimen (BK), the percentage elongation after fracture A_t=43% and the reduction of Area Z=81%.

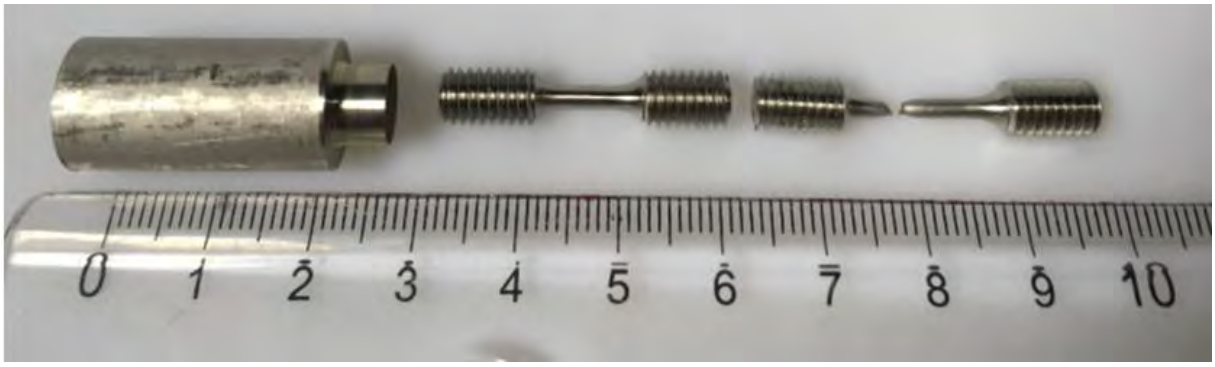

Figure 25. Annealed specimen (BL), the percentage elongation after fracture A_t=69% and the reduction of Area Z=73%.

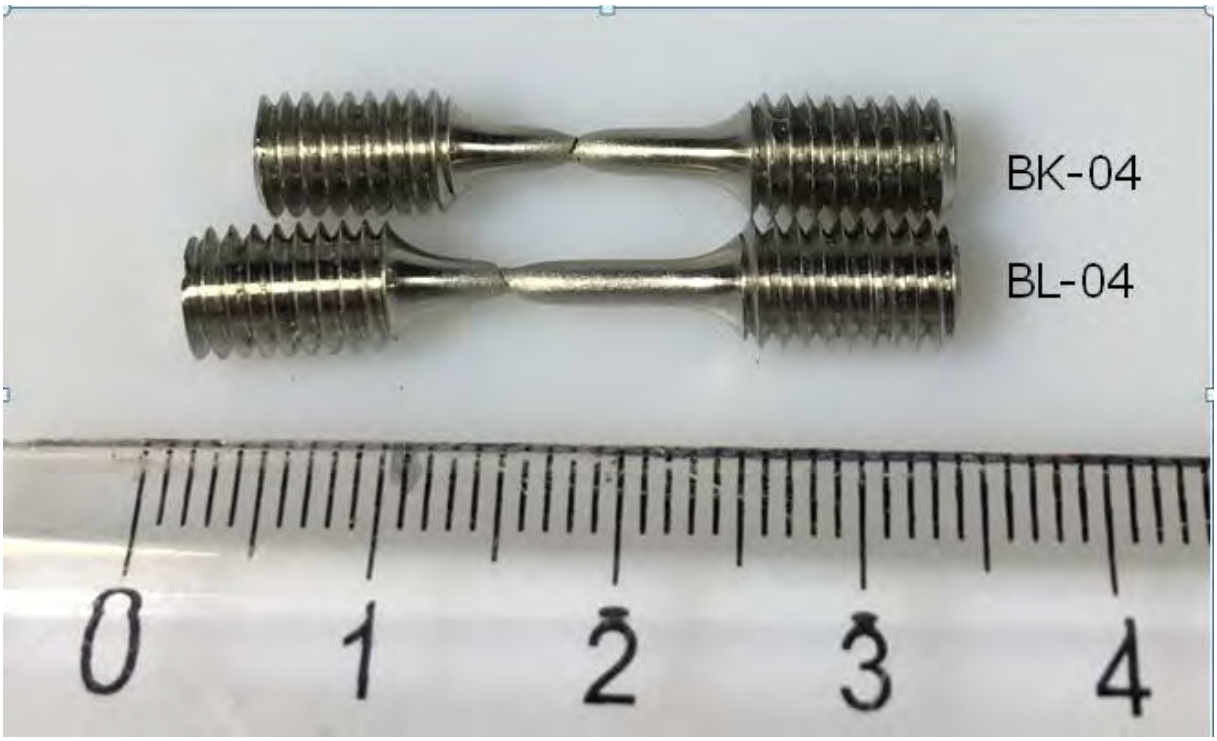

Figure 26. The difference in ductility between 20%CW (BK) and annealed specimen (BL) tested at room temperature.

The small size tensile tests described above can now be used for comparing to estimates of the tensile properties from the standard flat small punch test specimen and the curved tube specimen.

4.2 SP test results on annealed and 20%CW bar material

The small punch test for the annealed and 20%CW bar material and the annealed bar was done using the same set-up as for the curved specimen described earlier in this report. The specimens were standard flat specimen (8 mm in diameter and 0.5 mm thick). Two standard (hydraulic) testing machines were available for the test, one with deflection measurement (cryogenic test machine, CRY) and the high-temperature test set-up (HT) with only displacement measurement. The SP test results are given in Table 17 and Table 20 for 20%CW and annealed bar.

The difference between measure cross head movement and the deflection (from below) is shown in Figure 27 for both the annealed and cold worked bar from the CRY test. The distance between d_m and u_m comprises of the machine compliance and the specimen wall thinning, in this case 0.43 mm for the annealed and 0.45 mm for the 20% CW material. Both materials behave in a smooth (ductile) manner at room temperature. The estimated R'_m for annealed and 20%CW material is shown in comparison to axial and hoop tensile strength of the 24%CW tube in Figure 28.

Table 19. Measured F_m, d_m and u_m of the SP tested 20%CW bar material with a 2.5 mm ball using flat specimen. CRY=test on cryogenic test machine, HT=test on high temperature machine, n.a= not available. Note that d_m for the HT machine is compliance corrected.

CW	T (°C)	d_m / u_m	F_m
20%CW (CRY)	22	(2.02)[1)] / 1.589	2034
20%CW (HT)	22	1.616 / n.a	2047
	22	1.700 / n.a	2039
	650	1.588 / n.a	1330
	650	1.608 / n.a	1296
	800	1.548 / n.a	684

1) not compliance corrected

Table 20. Measured F_m, d_m and u_m of the SP tested annealed bar material with a 2.5 mm ball using flat specimen. CRY=test on cryogenic test machine, HT=test on high temperature machine, n.a= not available. Note that d_m for the HT machine is compliance corrected.

CW	T (°C)	d_m / u_m	F_m
annealed (CRY)	22	(2.32)[1)] / 1.870	1888
annealed (HT)	22	1.728	1981
	700	1.395	1038

1) not compliance corrected

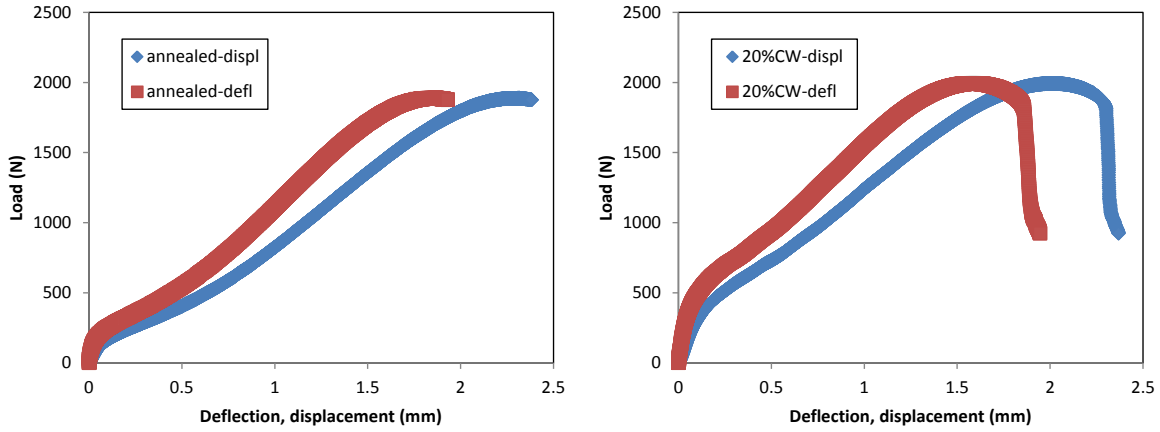

Figure 27. Comparison of load-deflection and load-displacement curves for annealed and 20%CW bar material at room temperature performed on the CRY test rig.

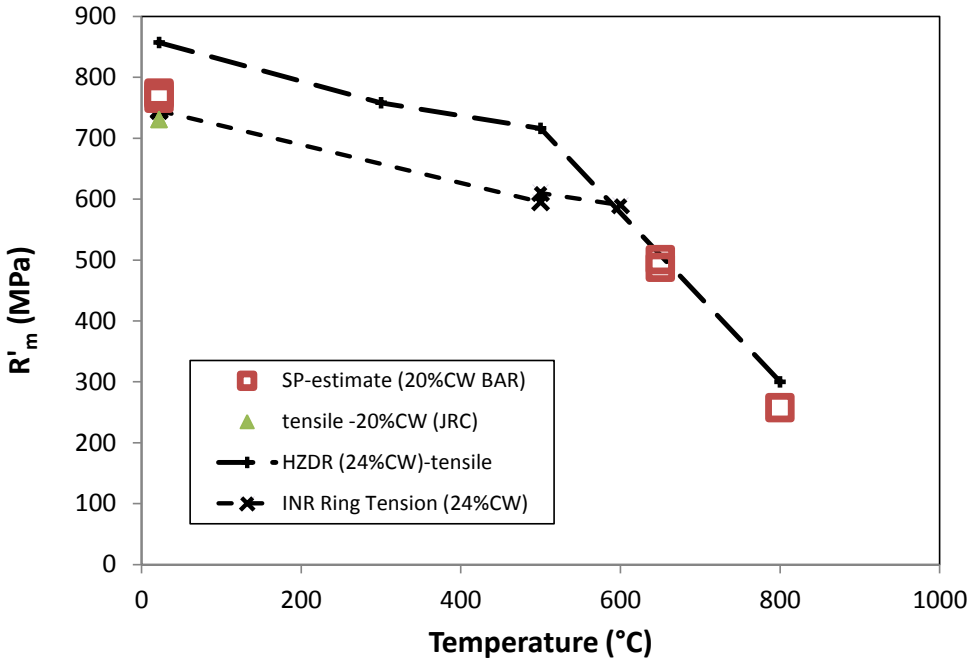

Figure 28. Comparison of estimated R_m for 20%CW bar in comparison to HZDR tensile and INR hoop strength results.

The estimated R'_m for the 20% CW are somewhat lower than the 24%CW at room temperature. However the SP test results are in-line with the single room temperature tensile test result performed on the bar. The SP estimates are 765, 771 and 774 MPa for the SP tests and the R_m of the uniaxial test was 733 MPa.

For the annealed material the room temperature R'_m estimates were 599 and 597 MPa, very close to the measure uniaxial value of 594 MPa. The SP test at 700°C does not indicate any clear difference to the cold worked material. The results are plotted in Figure 29.

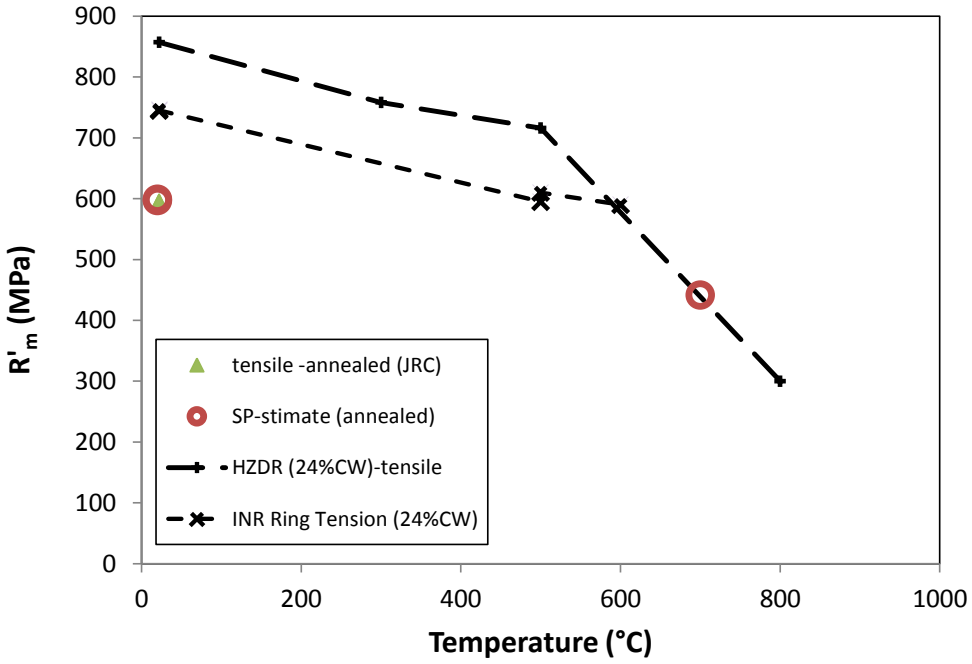

Figure 29. Comparison of estimated R'_m for annealed bar in comparison to HZDR tensile (24%CW) and INR hoop (24%CW) strength results.

5 SPC (creep) testing on cold worked 1515Ti tubes and bars

The results on the SPC creep tests are presented in Table 21. In Figure 31 the SPC test results are presented converted to normalized stress to make it possible to compare with expected uniaxial creep test results. The presented expected creep strengths are based on the hoop stress of internal pressure burst made available by SCK·CEN.

Table 21. SPC creep test results for 24%CW, 20%CW bar and annealed bar.

Specimen type	h_0 (mm)	d (mm)	D (mm)	Temp °C	Force (N)	t_r (h)
24%CW tube	0.45	2	4	500	1000	68
24%CW tube	0.45	2	4	600	900	0.13
24%CW tube	0.45	2	4	600	850	0.43
24%CW tube	0.45	2	4	600	800	0.7
24%CW tube	0.45	2	4	600	750	2.33
24%CW tube	0.45	2	4	600	700	2.77
24%CW tube	0.45	2.5	4	600	700	2.35
24%CW tube	0.45	2.5	4	600	550	4.61
24%CW tube	0.45	2.5	4	600	400	22.33
24%CW tube	0.45	2.5	4	650	550	3.12
20%CW bar	0.488	2.5	4	650	400	5.05
20%CW bar	0.498	2.5	4	650	400	19.82
Annealed	0.488	2.5	4	650	400	140[1)]

1) Interrupted

The conversion of SPC force F_{SPC} (N) to corresponding (converted) creep stress σ' (MPa) is here calculated using the classical CoP 14 relationship for the load over stress ratio F/σ;

$$F_{SPC}/\sigma' = 3.33 \cdot k_{SP} \cdot R^{-0.2} \cdot r^{1.2} \cdot h_0 \qquad \text{(X)}$$

where R is the radius of the receiving hole, r the radius of the puncher or ceramic ball, h_0 the specimen thickness and k_{SP} is a non-dimensional SP ductility parameter. The default value of k_{SP} =1. This value has also been used here. It is to be remembered that it has been shown that the k_{SP} parameter deviates from unity for a number of materials and especially for longer test durations (low forces) 18.

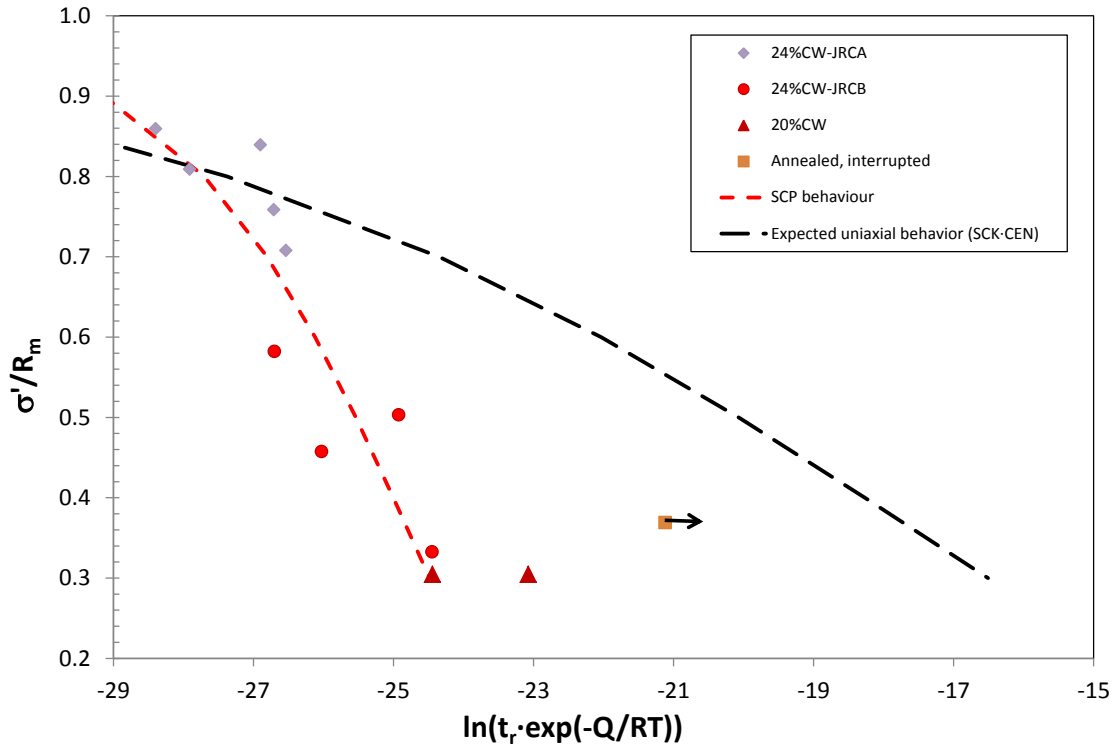

Figure 30. SPC creep test results presented in Wilshire plot form, with normalized (converted) stress over the tensile strength at specified temperature.

In Figure 31 the difference in failure for a SP (tensile) test and a SPC (creep) test. It can be seen that the for the interrupted SPC test the specimen start cracking at a very ealy stage of the test. The same was also found for the cold worked bar material (see Figure 33).

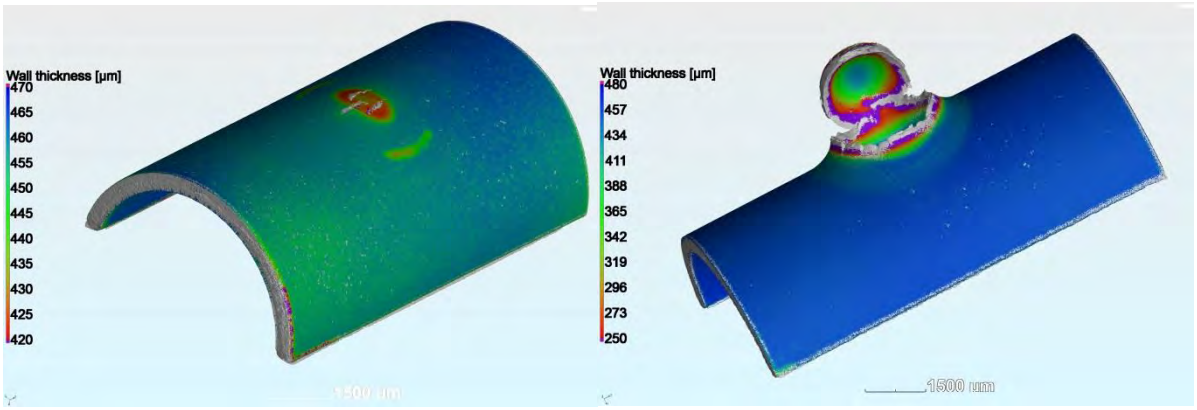

A B

Figure 31. A) AT-063 (SCK·CEN) cracked SPC specimen interrupted after loading at 600°C / 400N with estimated $\ln(h_0/h_f)$~6-9%, B) Specimen AT-054 tested at 600°C as "tensile" SP test with F_m=1296N and $\ln(h_0/h_f)$~50%.

Two SCP creep tests were conducted on 20%CW bar material. Both tests were performed at 650°C and 400N. The first test (BK-05) was tested until fracture and the second test was interrupted at about half life. The CT scanned samples are shown in Figure 32 and

Figure 33 correspondingly. It can be seen that the specimen are performing in a creep-brittle manner as was found for the curved 24%CW test samples described above.

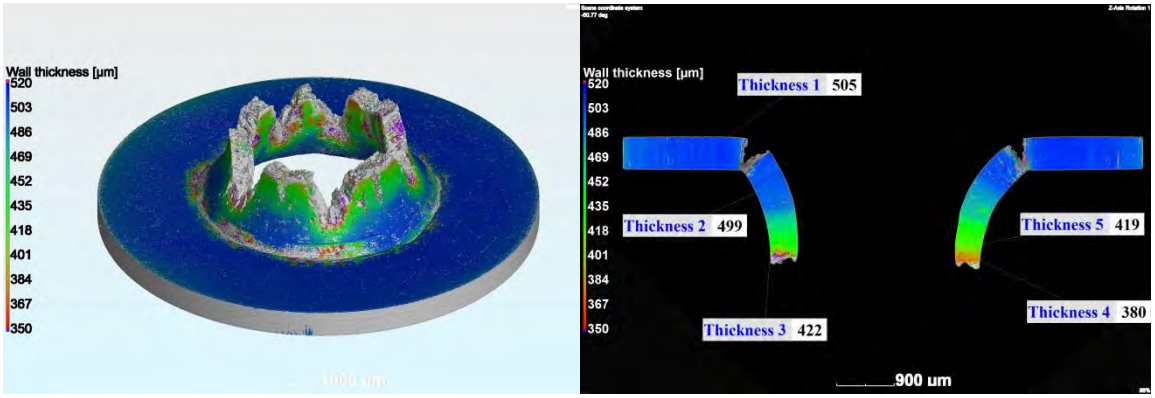

Figure 32. Specimen BK-05 (20%CW bar) Tested at 650°C / 400N, final failure after 20h. Estimated strain at fracture, $\ln(h_0/h_f)$=17.2%

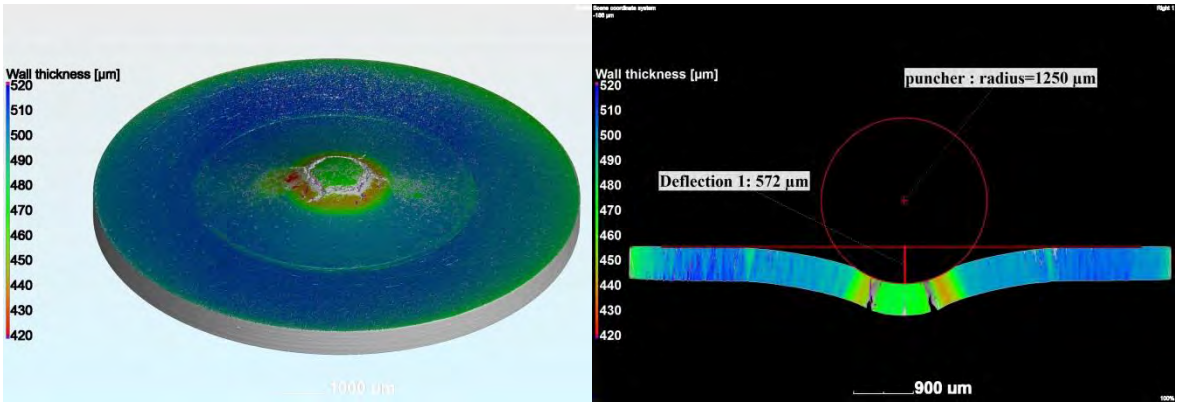

Figure 33. Specimen BK-06 (20%CW bar) interruptred after estimated half life (8.5h) tested at 650°C / 400N. Estimated strain at interruption, $\ln(h_0/h_f)$=12%

The unexpectedly short rupture times, the low ductility failures and the early cracking of the CW 1515Ti indicate that the SPC technique is not an optimal technique for determining the sought creep properties.

6 Discussion

The results acquired from the different test methodologies and testing labs give an excellent opportunity to compare the robustness of estimates and scatter. The further generation of data and further analysis of the TASTE data will hopefully continue in the frame of EERA JPNM pilot projects.

The standard uniaxial type test performed on machined and non-machined test tubes is naturally the basis for comparing tensile yield stress and ultimate tensile strength. These properties are naturally the properties for the axial direction.

A second important test for comparison to the more innovative and less material consuming tests is the ring tension tests. This test gives estimates on the strength properties in the hoop direction. However the simplified methodology applied in the TASTE assessment does not attempt to measure yield stress and the calculated tensile strength (R_m) does not take into account bending and friction stresses (see Appendix D).

The miniature tests with sample sizes retrievable in both the axial and hoop direction are naturally very interesting. In TASTE the amount of test performed with this technique was regrettably not sufficient to determine the accuracy of prediction or data scatter.

There were no internal pressure tests performed in TASTE for the 15-15Ti. Thus the "standard" test with the anticipated service stress state (biaxiality ratio: ~ axial 2 / hoop 1) was not included in the testing.

The SP test has shown promise in estimating the material properties with a more pronounced biaxiality (biaxiality ratio: ~ axial 1 / hoop 1). The estimates seem robust and seemingly follow the weaker direction material properties.

A comparison of the 1515Ti results for the 24%CW tubes are shown in Figure 34 and the ration 24%CW over 46%CW tensile strength in Figure 35.

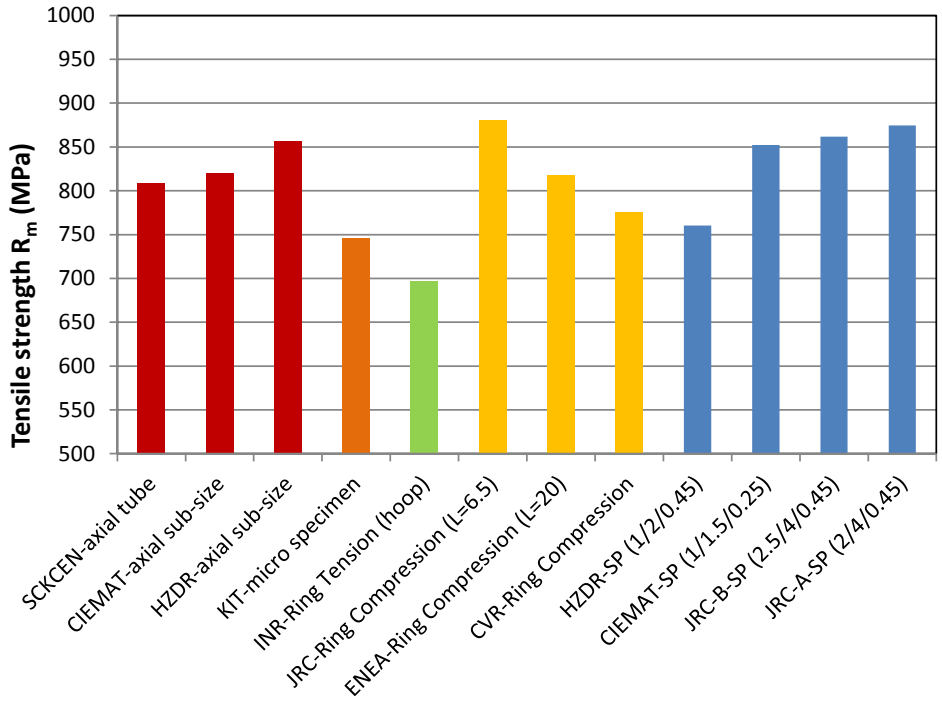

Figure 34. Comparison of measured and the estimated tensile strength R_m at room temperature for all test types assessed. Note that the RC tests were calibrated at a nominal length of 20 mm. (see Appendix E).

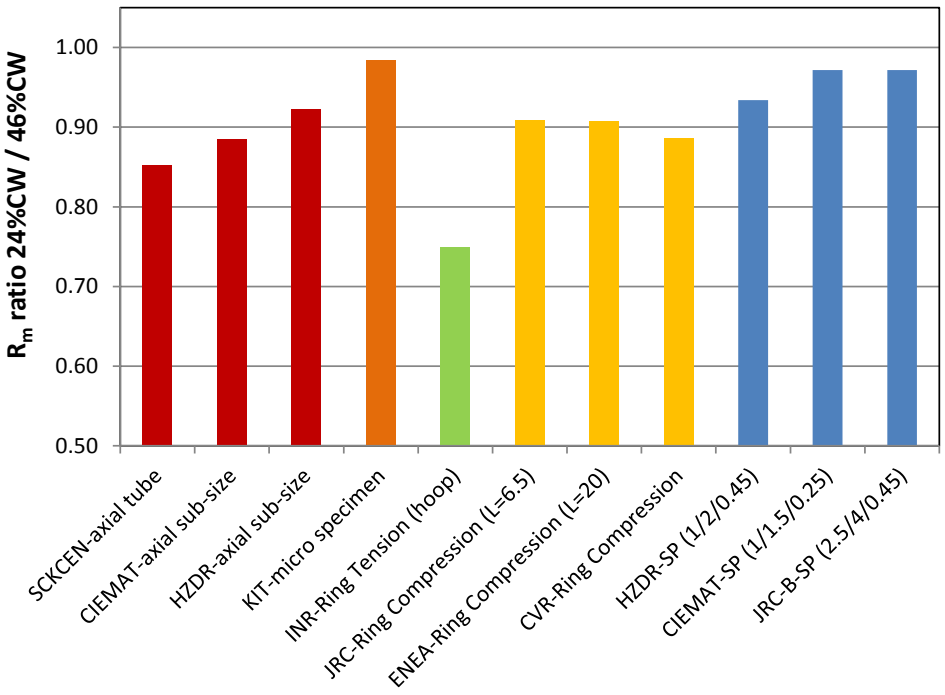

Figure 35. Comparison of strength ratio between the 24%CW and the 46%CW estimated tensile strengths R_m at room temperature for all test types assessed.

7 Conclusions and recommendations

The data assessments on the different test types in the TASTE project has lead to the following conclusions and recommendations regarding the material properties of 1515-Ti.

The ultimate tensile strength of 24%CW and 46%CW cold work has been estimated in the temperature range RT-800°C

The estimates from the different methods give the roughly the tensile strength ratio between the different grades of cold work, i.e. $R_{m\text{-}24\%CW}/R_{m\text{-}46\%CW}$ = 0.91 in average at room temperature.

The yield properties are difficult to extract from the RT, RC and SP tests. The SP correlation to the "yield force" F_e will be attempted in future work.

The SPC creep tests were not able to determine the creep properties of 15-15Ti.

Recommendations for future work:

1. The applicability of the promising test techniques for hot-cell testing;

- Ring Tensile; challenges: extraction of yield estimate, bending and friction
- Ring compression: extraction of yield estimate, calibration and repeatability of the K_{UTS} for pre-defined tube sizes, definition of collapse load
- SP for curved samples, optimize best test set-up for minim of specimen machining and robust estimates; extraction of yield estimate
- Include other miniature test techniques for creep property determination; suggested technique indentation creep

References

1. Bergmann, H-J. Dietz, D. Ehrlich, K., Mühling, G. Schirra, M. Entwicklung des Werkstoffs X10CrNiMoTiB 1515 als Strukturmaterial für Brennelemente. Wissenschaftliche Berichte FZKA 6864, Forschungszentrum Karlsruhe GmbH, 2003.
2. Holmström, S. et. Al., Test methodologies for determining high temperature material properties of thin walled tubes, EUR 28642 EN, doi: 10.2760/702821.
3. Delville, R., et al., R&D programme for the fuel qualification of the research fast reactor MYRRHA in DESIGN, MANUFACTURING AND IRRADIATION BEHAVIOUR OF FAST REACTOR FUEL Obninsk, Russian Federation, 30 May - 03 June, 2011. IAEA.
4. Delville, R., Stergar, E., and Verwerft, M., Results of a new production of nuclear-grade 1.4970 15-15Ti stainless steel fuel cladding tubes for GEN IV reactors in 22nd International Conference on Nuclear Engineering ICONE22. Prague, Czech Republic July 7-11, 2014. ASME.
5. Fissolo, A., Levy, J-L,. Seran, A., Maillard, A. Royer, J., Raboulle, O. Tensile Properties of Neutron Itrradiated 316Ti and 1515Ti steels. Proceedings of the 16th Symposium on Effects of Radiation on Materials, Denver, Colorado, USA, 1992.
6. International Standard ISO 6892-1:2016, Metallic materials-Tensile testing, Part1: Method of test at room temperature.
7. International Standard ISO 6892-2:2011, Metallic materials-Tensile testing, Part2: Method of test at elevated temperature.
8. Altstadt E., Houska M., Mechanical Properties of 15-15 Ti based on small specimen testing. HZDR report for TASTE, 2016.
9. Radu V., Nitu A, Pitigoi V., Analyses of the Ring Tension Tests performed on the 15-15Ti tube specimens, RATEN ICN status report for TASTE, 2016.
10. Chakrabarty, J., theory of stretch forming over hemispherical punch heads, International Journal of Mechanical Sciences, Volume 12, Issue 4, pp. 315-325, 1970
11. Hill, R. Phil.Mag. 41, 1333, 1950.
12. Cristalli C., Ring Compression Tests at room temperature to predict YS and UTS, ENEA status report for TASTE, 2016.
13. International Standard ISO 204:2009, Metallic materials — Uniaxial creep testing in tension — Method of test.
14. CEN Workshop Agreement CWA 15627: Small Punch Test Method for Metallic Materials: European Committee for Standardization, CWA 15627: 2007
15. E. Altstadt, H. Ge, V. Kuksenko, M. Serrano, M. Houska, M. Lasan, M. Bruchhausen, J.-M. Lapetite, Y. Dai, Critical evaluation of the small punch test as a screening procedure for mechanical properties, Journal of Nuclear Materials 472 (2016) 186-195, doi:10.1016/j.jnucmat.2015.07.029
16. T.E. García, C. Rodríguez, F.J. Belzunce, and C. Suárez, Estimation of the mechanical properties of metallic materials by means of the small punch test. Journal of Alloys and Compounds 582:708−717, 2014.
17. S. Holmström, I. Simonovski, S. Ripplinger, E. Altstadt, R. delville, M. Serrano, V. Radu, Tensile and creep property determination of 15-15Ti fuel cladding steel by small punch testing, International Conference on Life Management and Maintenance for Power Plants, VTT TECHNOLOGY 261, http://www.vtt.fi/inf/pdf/technology/2016/T261.pdf, pp. 293-305, 2016.

18. Holmström, S, et Al. Small punch creep testing for material characterization and life time prediction, 10th Liege Conference: Proc. Materials for Advanced Power Engineering 2014, ISSN 1866-1793. (2014). 627-635

19. B. Wilshire, P.J. Scharning, Extrapolation of creep life data for 1Cr− 0.5Mo steel, International Journal of Pressure Vessels and Piping 85 (2008) 739− 743

20. ABAQUS 6.14-2, Dassault Systemes, 2015

Appendix A

Microstructural analysis of 15-15Ti stabilized stainless steels

CV/REZ Report by H-K Namburi, P. Halodová, P. Bublíková and R. Delville

Centrum výzkumu Řež s.r.o.
Research Centre Rez

Ev. č.: CVR 1543
Department 8580

1/2017

Joint Programme on Nuclear Materials Sub-programme on Support to ESNII (SP1)

Testing and ASsessment methodologies for material characterization of thin-walled cladding TubEs (TASTE)

MICROSTRUCTURAL EVALUATION OF NUCLEAR GRADE TITANIUM STABILIZED STAINLESS STEEL FUEL CLADDINGS

Authors: Hygreeva Kiran Namburi (CVR)
Patricie Halodová (CVR)
Petra Bublíková (CVR)
Rémi Delville (SCK-CEN)

Abstract

In this work, recently produced nuclear grade stainless steel cladding material DIN 1.4970, cold worked at 24 % and 46 % microstructural analysis was performed. In both materials, microscopic investigations revealed the presence of Ti-(C,N) precipitates at the sub-micrometre range and a few larger precipitates up to several microns. Elongated stringer-like TiC precipitates in the tube drawing direction were also revealed. Grain size was determined and a well-defined substructure was observed in Field Emission Gun Scanning Electron microscopy (FEG-SEM) and High Resolution Transmission Electron Microscopy (HR-STEM) with characteristic features as MC precipitates, twins, micro-twins, slip bands. No significant microstructural variance between the two cold worked materials was observed.

1. Introduction

Ti-stabilized austenitic stainless steels are candidate material for nuclear grade fuel cladding for Gen IV fast reactors in Europe [1]. Ti-stabilized austenitic stainless steel with defined alloying element specifications and strict manufacturing routes showed superior resistance to void swelling and creep strength than other stainless steels [2-4]. Addition of Ti as stabilizing element to austenitic steels is advantageous as it forms fine precipitates of TiC dislocations that enables to improve the resistance to void swelling and creep strength [5-7].

Current study is focused on microstructural examination of recently produced DIN 1.4970Ti-stabilizedstainless steel by Sandvik for SCK-CEN with two different cold worked levels. The aim of this study is to investigate the pristine material microstructure and determine variations introduced by different cold-work level.

2. Material history and Experimental

The material used in this work is nuclear-grade austenitic steel cladding tubes manufactured by Sandvik for SCK•CEN at two Cold Worked (CW) level of 24 % and 46 % introduced during the last cold-drawing step. Tubes have an external diameter of tubes as 6.55 mm and a wall thickness of 0.45 mm. The chemical composition in wt. % is shown in Table 1.

Tranversal cross-sections along the(Radial-Circumferential (RC) plane and longitudinal cross-section along the Radial-Axial (RA) plane were prepared for analysis. Standard metallographic steps were implemented to prepare the samples for microstructural analysis by Light Optical microscopy (LOM), Field Emission Gun Scanning Electron Microscopy (FEG-SEM) with EDX detector and Transmission Electron Microscopy (TEM).

3. Results and Discussion

3.1 Light Optical Microscopy

Optical micrographs of the 24 % and 46 % CW material in RC and RA planes, revealed grain boundaries, precipitates, deformation twins and slip bands. Fig. 1-2 corresponds to 24% and 46 % CW respectively, in RC and RA planes of the samples. Images taken at higher magnifications clearly reveals the details of grain boundaries, slips and precipitates (dark spots).

Squared or platelet-like coarse precipitates usually located at grain boundaries and homogeneously distributed intra-granular finer precipitates were observed throughout the cross-sections. . In both the specimens, in RC plane (traversal cross sections) the precipitates are coarse and fine. Whereas in the RA plane (longitudinal cross section) of both the specimens, elongated inclusions with the fine and coarse precipitates were identified, as visible in Fig. 1 (B) and 2 (B). Average grain size estimated in transverse and longitudinal planes is 9.5 µm.

3.2 Scanning Electron Microscopy

FEG-SEM with EDX (Energy-Dispersive X-ray spectroscopy) detector was used to perform the detailed study of microstructure at higher magnification, to determine the nature of precipitates morphology, sizes and qualitative chemical analysis. Fig. 3A and 3B corresponds to the 24 % cold worked specimen in in RC and RA planes respectively. While the Fig. 4A and 4B corresponds to the 46% cold worked specimen in RC and RA planes. -SE and BSE mode combined with EDX were used to resolve the nature of precipitates. From the

SEM observations the precipitates can be divided into two groups in terms of their formation site (directly at grain boundaries or within the grain boundaries) and size (fine, coarse or elongated) as illustrated in Figure 3B. Based on SEM observations no significant difference between the 24 % and 46 % CW specimens are observed and is consistent with already reported microstructure for 15-15Ti [11-15].

Firstly, coarse precipitates (pointed as 1, in Fig. 3(A-B) and 4(A-B)) are formed on the grain boundaries and are of either squared or triangular shaped with round edges. They have mostly size range of 2-5 μm. The second type of precipitates are finer (nano-precipitates, bright dots) and observed as intergranular sizing few tens to hundreds nanometers in size. They are pointed as 2, in the Fig. 3 (A-B) and 4 (A-B). Some of these nano-precipitates (pointed as 3, see Fig.3 and 4) are located on the straight lines within in each grain.

These straight lines are deformed twin boundaries (pointed as 4 on images) originated from cold-drawing that provides high energy nucleation sites for precipitates. Several slip bands with characteristic contrast are visible with in the grains in Fig. 3 and 4. The major microstructural difference noticed between the RC and RA planes of the specimens is the elongated precipitates (mostly TiC, broken due to cold drawing) that are present in RA planes (pointed as 5 in Fig. 4B). These elongated inclusions are frequently observed on RA planes in the specimen's longitudinal direction.

The spectra showing variation of intensity with energy taken from the precipitates are presented in Fig.5. EDX analysis in SEM with a focused electron beam determined the precipitates with chemical composition as Ti-(C,N).

Furthermore EBSD (Electron Back Scattered Diffraction) analysis was performed in transverse and longitudinal directions to analyse the structure of alloys. The EBSD maps and color key for crystallographic direction are shown in Fig. 6 (A-B). The color reveals the grains orientation in specific direction. The noticeable difference is that in 24 % CW specimens the grains are more equiaxed, whereas in 46 % specimens grains are more elongated in transverse direction due to higher deformation caused by cold rolling.

3.3 Transmission Electron Microscopy Analysis

Typical overview of microstructural details from 24 % and 46 % CW Ti-stabilized stainless steel are shown in Fig. 7-8. Most obvious features are deformation twins and a dense network of entangled dislocation introduced by cold-drawing. - Particles of Ti-(C, N) are between 50 - 200 nm in size, shown in Fig. 7B and 8B.

4. Conclusions

The present work covered the detailed microstructural analysis of recently produced 15-15 Ti-stabilized stainless steel used as nuclear grade cladding tube material for sodium cooled fast reactors. Analysis included materials from two cold worked conditions i.e. 24 % and 46 % CW. No major differences were observed in the either of the materials. In both the materials, microstructural features were similar and are representative of the reference standard, DIN 1.4970.

Besides the above general observations, the following conclusions can be drawn from the current study:

1. Visual observations by optical microscopy technique showed that the precipitates are present in large areal fraction and in different sites.
2. SEM observations revealed the nature of the precipitates more in detail with respect to their formation sites. In particular coarse precipitates were formed on the grain boundaries and were of few micrometers in size with either squared or triangle shape having round edges.
3. The second type of precipitates are finer (nano-precipitates), ranging between few tens up to hundreds nanometers in size. Some of these nano-precipitates were located on the twin boundary.
4. Numerous twin boundaries were observed, certainly originated due to deformation by cold-drawing.
5. EDX analysis showed precipitates are of type Ti(C,N).
6. EBSD analysis, showed elongated grains in 46 % CW specimens in comparison to 24 % CW specimens.
7. TEM characterization revealed the shape and size of the nano-precipitates. Deformation twins and slip bands were another type of microstructural features observed in TEM inspections.

Acknowledgments

The authors would like to thank Ondrej Libera for his help with optical microscopy. The presented work was financially supported by the Ministry of Education, Youth and Sport Czech Republic (National Programme of Sustainability II) Project LQ1603 (Research for SUSEN“).

References

[1] H.-J. Bergmann, W. Dietz, K. Ehrlich, G. Muhling, M. Schirra, Forschungszentrum Karlsruhe, Report FZKA- 6864, 2003.
[2] S. Venkadesan, A.K. Bhaduri, P. Rodriguez, K.A. Padmanabhan, J. Nucl. Mater.186 (1992) 177–184.
[3] D.L. Smith, J. Nucl. Mater. 122&123 (1984) 51–65.
[4] Y. Tateishi, J. Nucl. Sci. Technol. 26 (1989) 132–136.
[5] Kesternich, J. Rothaut, J. Nucl. Mater. 103&104 (1981) 845–852.
[6] Todd, J.A. and Ren, J.-C., The effect of cold work on the precipitation kinetics of an advanced austenitic steel.Materials Science and Engineering: A,117 (1989), 235-245.
[7] S. Latha, M.D. Mathew, P. Parameswaran, K. Bhanu Sankara Rao, S.L. Mannan, Int. J. Press. Vess. Pip. 85 (2008) 866–870.
[8] Garner, F.A., Hamilton, M.L., Eiholzer, C.R., Toloczko, M.B., and Kumar, A.S., Influence of cold work on the irradiation creep and creep-rupture of titanium-modified

austenitic stainless steel, in Effects of Radiation on Materials: 16th International 5 Copyright 2014 by ASME Symposium, A.S. Kumar, et al., Editors. 1994. 696-713.

[9] Gilbert, E.R. and Garner, F.A., The influence of cold-work level on the irradiation creep and swelling of AISI 316 stainless steel irradiated as pressurized tubes in the EBR-II fast reactor .Journal of Nuclear Materials, 367(2007) 954-959.

[10] Klueh, R.L. and Maziasz, P.J., Effect of cold work on tensile behavior of irradiated type 316 stainless steel. 1986. Medium: ED; Size: Pages: 35.

[11] Remi Delville et. Al. RESULTS OF A NEW PRODUCTION OF NUCLEAR-GRADE 1.4970 '15-15TI' stainless steel fuel cladding tubes for Gen VI reactors Proceedings of the 2014 22nd International Conference on Nuclear Engineering ICONE22, July 7-11, 2014, Prague, Czech Republic

Table 1: Chemical composition of nuclear grade 15-15 Ti-stabilized stainless steel in wt %.

C	Si	Mn	P	S	Cr	Ni	Co	Mo
0.10	0.56	1.83	0.013	<0.001	15.08	15.04	0.02	1.21
B	**N**	**Ti**	**V**	**Ta**	**Cu**	**Ca**	**Fe**	
0.0028	0.011	0.49	0.034	<0.005	0.026	<0.010	Bal.	

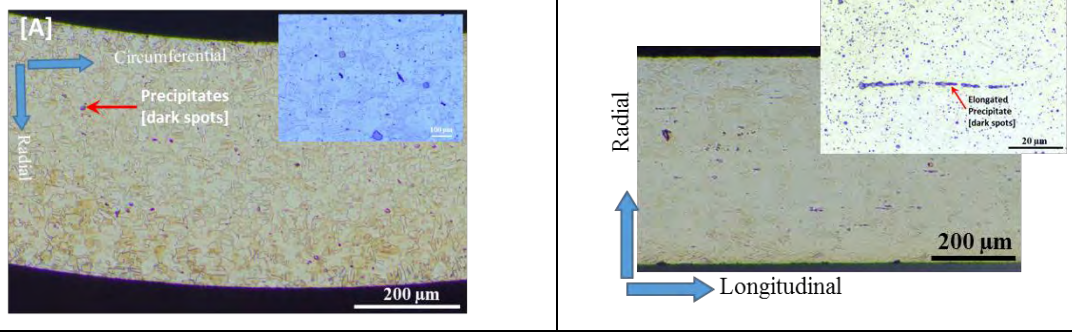

Fig. 1: Details of microstructure of 24 % CW specimen in **[A]** RC plane (transversal cross section) and **[B]** RA plane (longitudinal cross section). Light Optical Microscopy image.

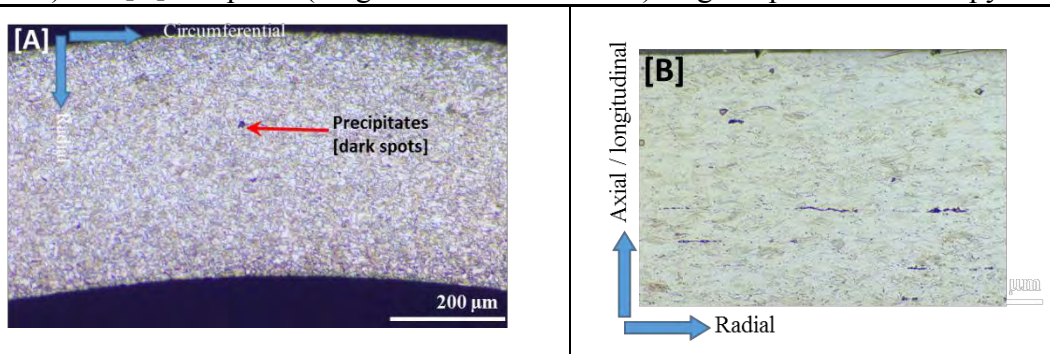

Fig. 2: Details of microstructure of 46 % CW specimen in **[A]** RC plane (transversal cross section) and **[B]** RA plane (longitudinal cross section). Light Optical Microscopy image.

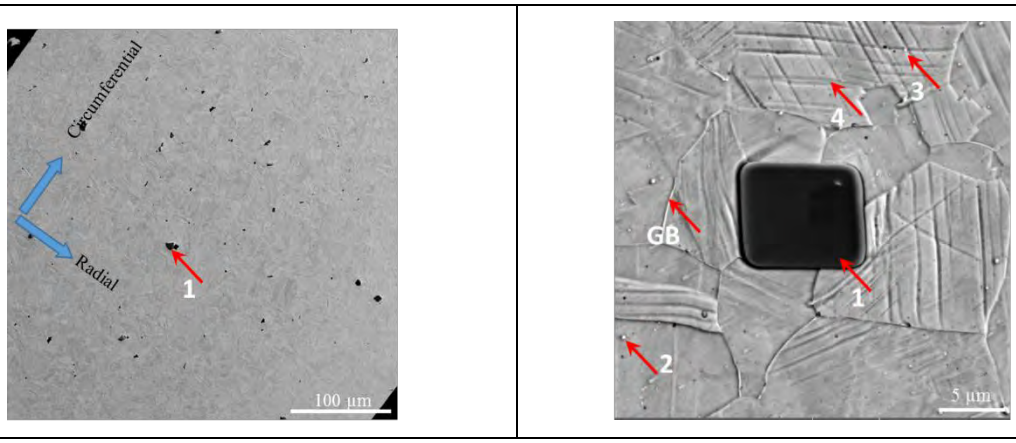

Fig. 3A: Details of microstructure of 24 % CW specimen in (A) RC plane (transversal cross section). GB – Grain Boundary. Scanning Electron Microscopy image.

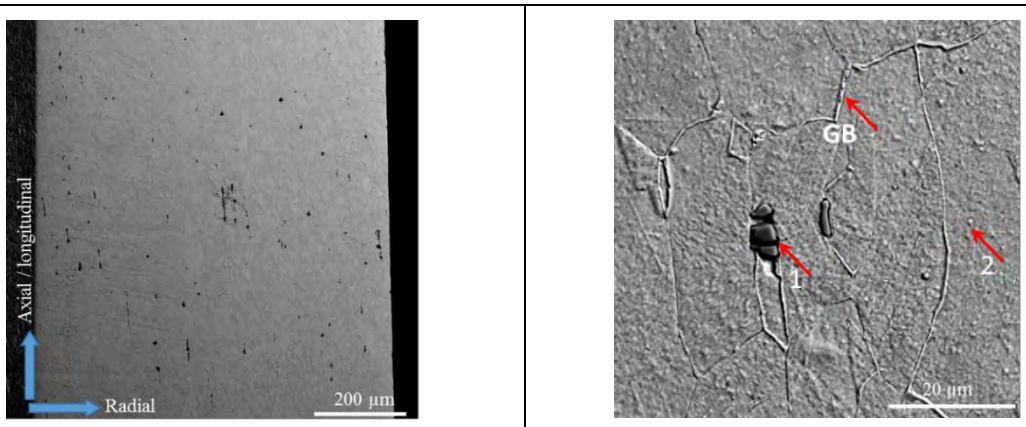

Fig. 3B: Details of microstructure of 24 % CW specimen in RA plane (longitudinal cross section). GB – Grain Boundary. Scanning Electron Microscopy image.

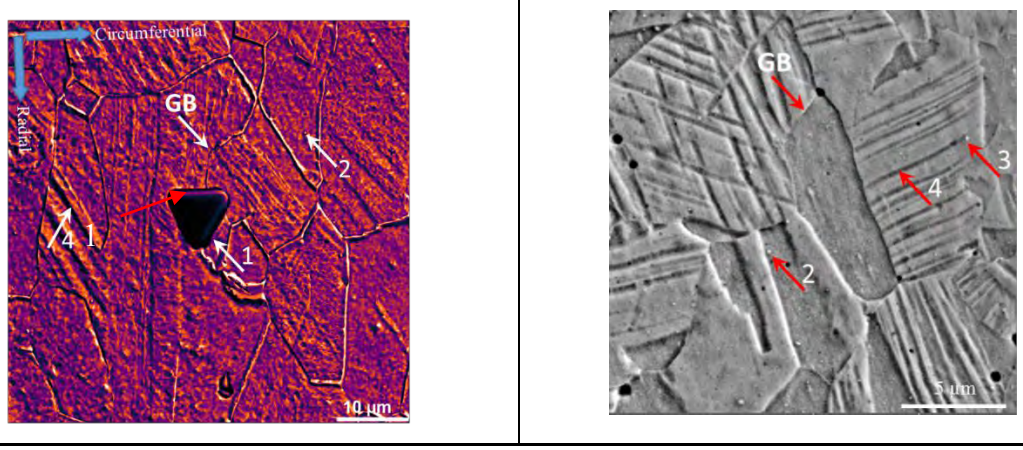

Fig. 4A: SEM micrograph with details of microstructure from 46 % CW specimen in (A) RC plane (transversal cross section). GB – Grain Boundary.

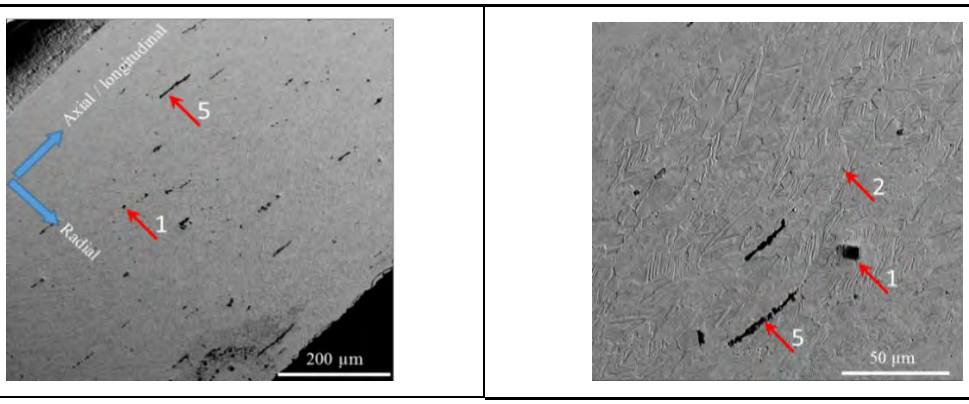

Fig. 4B: Details in microstructure of 46 % CW specimen in RA plane (longitudinal cross section). Scanning Electron Microscopy image in SE and BSE mode.

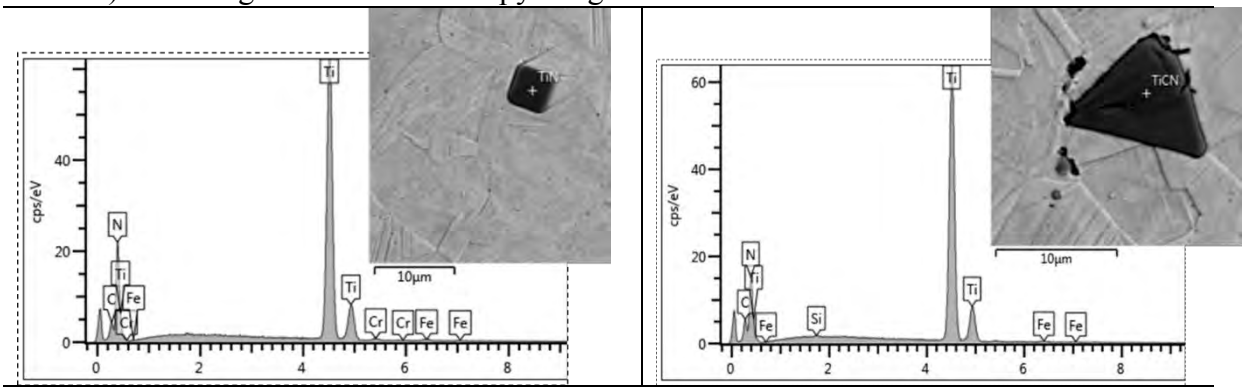

Fig. 5: SEM-EDX Spectra confirming Ti(C,N) type precipitates

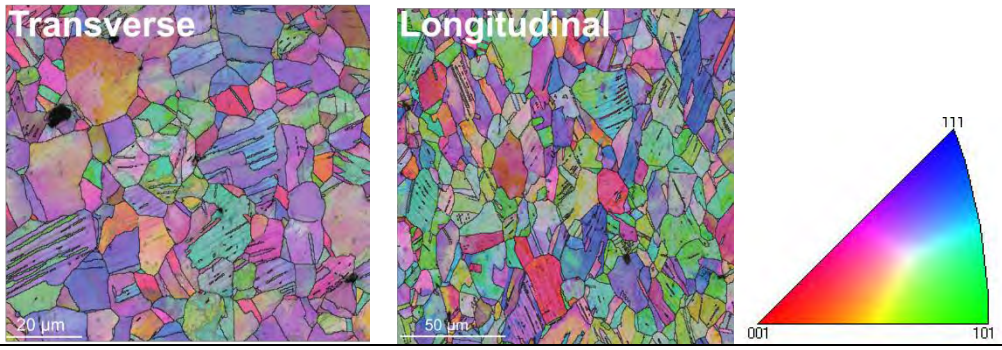

Fig. 6A: EBSD orientation distribution maps and color key for crystallographic direction of 24 % CW specimen in RC plane ((transversal cross section) and RA plane (longitudinal cross section).

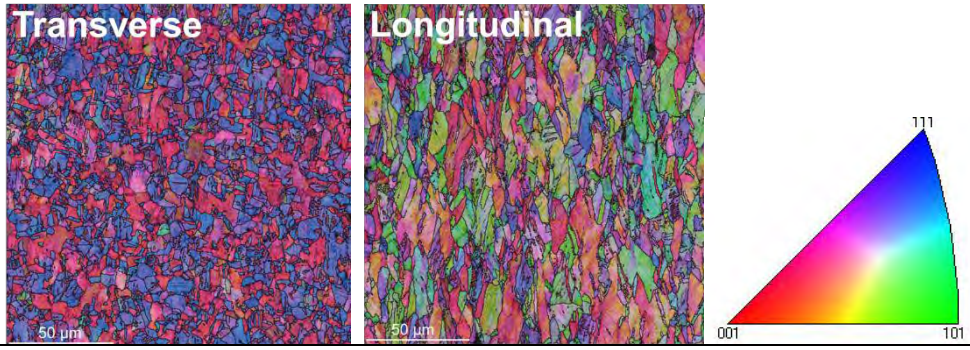

Fig. 6B: EBSD orientation distribution maps 46 % CW specimen in RC plane ((transversal cross section) and RA plane (longitudinal cross section).

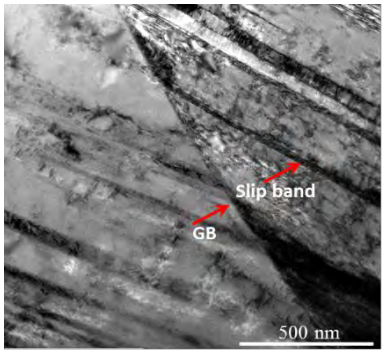

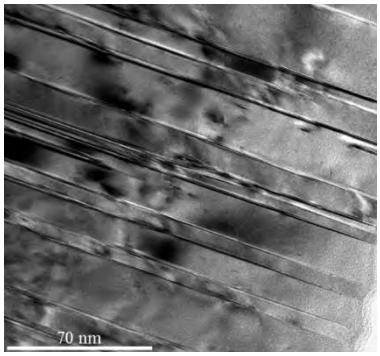

Fig. 7A: Details of deformation twins and dislocations from 24 % cold worked specimen in bright and dark field imaging mode. GB – Grain Boundary. Transmission Electron Microscopy.

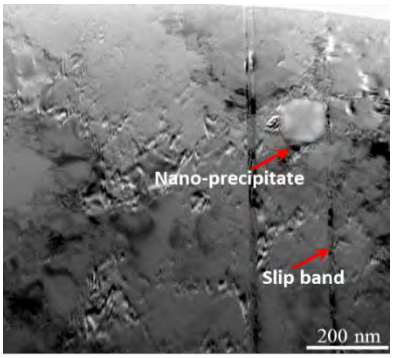

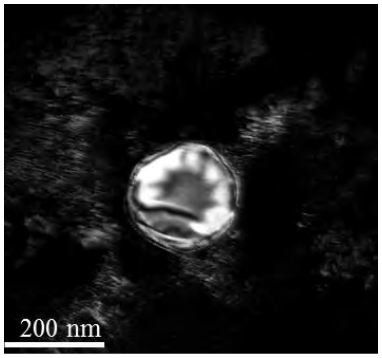

Fig. 7B: Details of TiC precipitates in 24 % CW specimen with slight faceting and dislocations. Transmission Electron Microscopy.

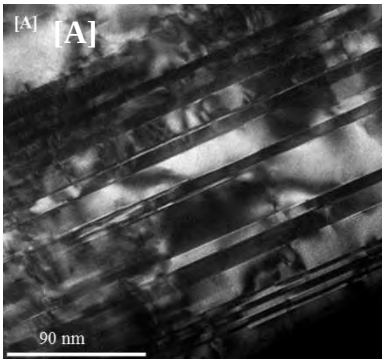

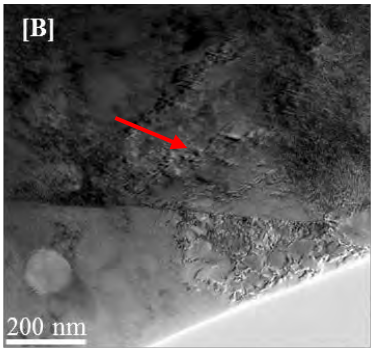

Fig. 8 (A,B): Details in 46 % CW specimen showing dark field images of slip bands and dislocations from cold working [A] & TiC precipitate in dislocation network [B]. Transmission Electron Microscopy.

Appendix B

Mechanical Properties of 15-15 Ti based on small specimen testing

HZDR report by E. Altstadt and M. Houska

HZDR
HELMHOLTZ ZENTRUM DRESDEN ROSSENDORF

Institute of Ion Beam Physics and Materials Research
Structural Materials Division

Report FWIK-F-03/2016-Rev.1

E. Altstadt and M. Houska

Mechanical Properties of 15-15 Ti based on small specimen testing

Contribution to the EERA-JPNM pilot project:
Testing and assessment methodologies for material characterization of thin-walled cladding tubes (TASTE)

Released: June 21, 2016

1 Introduction

The integrity of the fuel cladding in present and future nuclear fuel concepts is critical for the safe performance of the power plants. Within the EERA-JPNM pilot project TASTE, the material performance and mechanical properties of thin walled fuel cladding tubes are evaluated through a number of testing techniques and evaluation methodologies.
In this report, tensile tests based on specimens manufactured from thin-walled 15-15 Ti tubes and small punch test with curved specimens are presented.

2 Experimental

2.1 Material

HZDR received 15-15 Ti tubes 6.55 mm x 5.65 mm in two conditions: 24% and 46% cold worked, each of 200 mm length. The specifications of the pipes are given in [1,2]. The chemical composition is listed in Table 1. The cross sections of our specimens were calculated based on a thickness of 0.45 mm.

Table 1: Chemical composition of the tubes [1,2]

Tube	C	Si	Mn	P	Cr	Ni	Mo	Ti	Cu
24% CW	0.096	0.57	1.86	0.013	15.06	15.05	1.21	0.44	0.026
46% CW	0.10	0.57	1.89	0.013	15.09	15.05	1.21	0.44	0.027

The tensile properties are specified as follows (Table 2):

Table 2: Mechanical properties at room temperature [1,2]

Tube	Yield stress (YS) $R_{p0.2}$ (MPa)	Ultimate tensile stress (UTS) R_m (MPa)	Total elongation A_t (%)
24% CW	691	809	25.4
46% CW	926	950	10.3

2.2 Tensile tests

The tensile specimens were cut from the tubes by electrical discharging machining (EDM) as shown in Figure 1. The detailed geometry is shown in Figure 2. The cross section of the gauge region is 1.24 mm^2. A special loading component was developed consisting of a convex and a concave clamping claw (Figure 3). The geometry was chosen such that the loading axis coincides with the centre of area of the cross section of the specimen gauge in order to minimize bending effects.

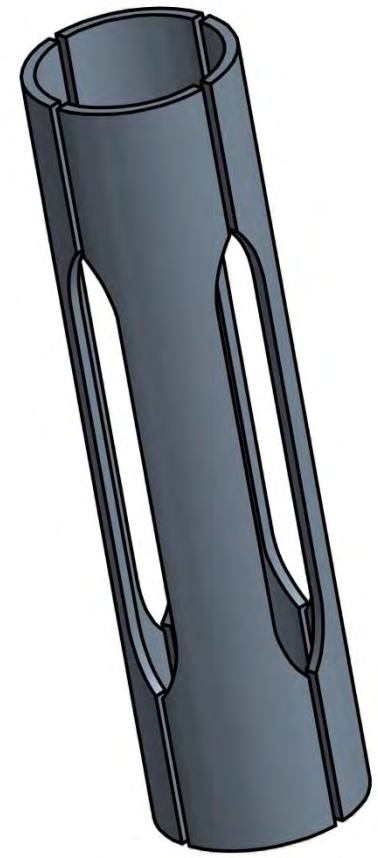

Figure 1: Cutting scheme for mini tensile tube specimens

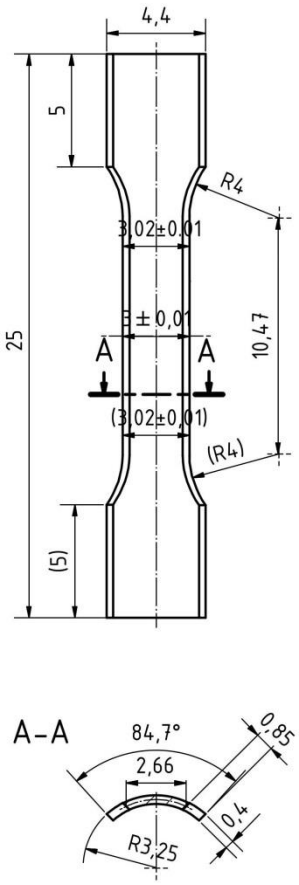

Figure 2: Detailed geometry of mini tensile tube specimens

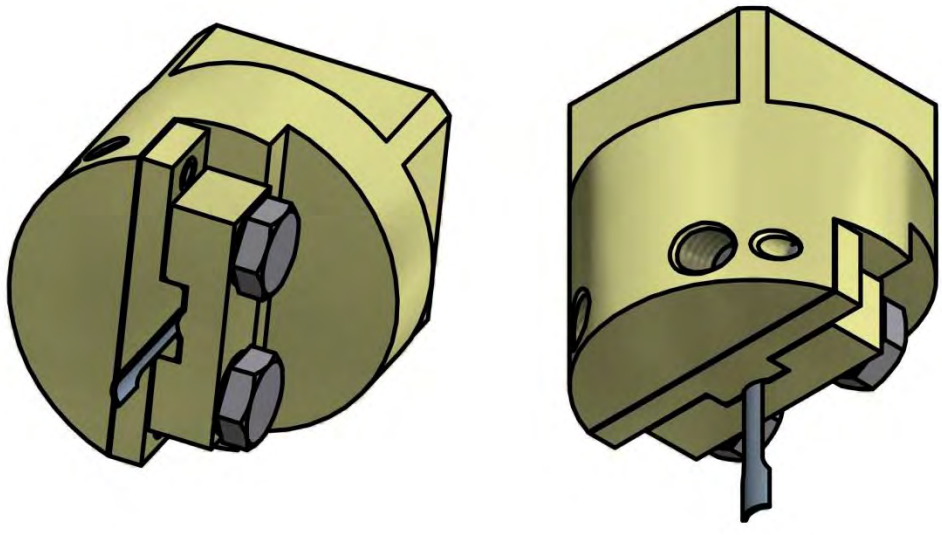

Figure 3: Clamping device for mini tensile tube specimens

Tensile tests were performed for both materials at room temperature, 300 °C, 500 °C and 800 °C. A 10 kN INSPECT DESK testing machine was used. The strain rate was about 10^{-4}/s. The elongation was measured by a LASER SPECKLE 1C extensometer. Table 3 gives an overview of the valid tests. In some tests at 800 °C, a slipping of the specimen relative to the

clamping claws was observed, most probably due to thermal expansion of the clamping screws. Those tests were rejected.

Table 3: Test temperatures and number of valid tensile tests

Test temperature	Number of valid tests 24% CW	Number of valid tests 46% CW
23 °C	3	3
300 °C	4	3
500 °C	3	4
800 °C	2	2

2.3 Small punch tests

The curved SPT specimens were cut from the tube by EDM without any further finishing. The geometry is 4.4 mm x 4.4 mm x 0.45 mm. An adapted test device with a concave lower die and a convex downholder was developed (Figure 4). The diameter of the receiving hole is 2 mm and the diameter of the hemispherical puncher is 1 mm.

Small punch tests were performed in the temperature range from -193 °C up to +22 °C for both materials (15 tests for 24% CW, 14 tests for 46% CW). The loading rate was 0.5 mm/min (puncher displacement).

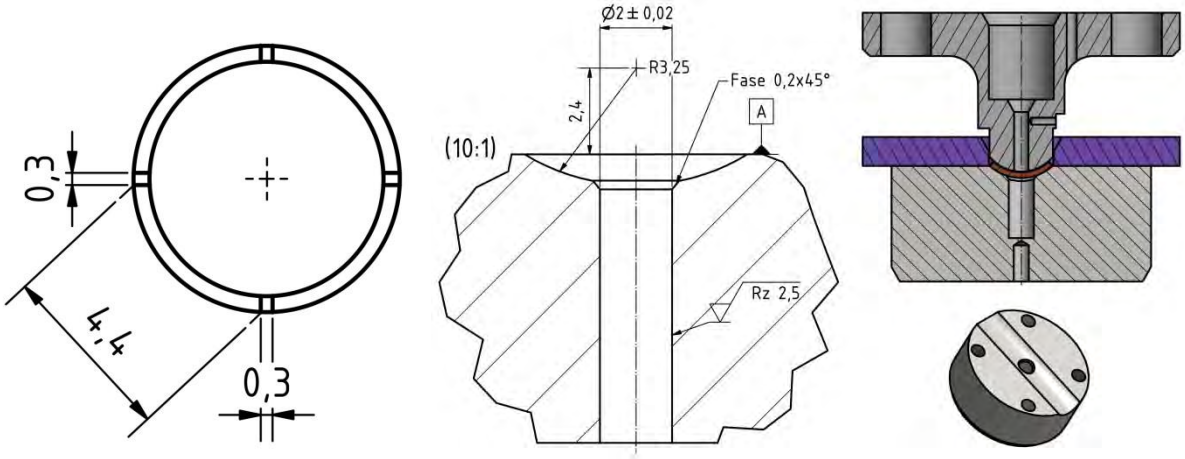

Figure 4: Small punch test specimens (left) and lower die geometry (right)

3 Results

3.1 Tensile tests

The results are based on averaged stress-strain curves, calculated from the available valid single test curves for a given temperature (cf. Table 3). Prior to the averaging, the single test curves were corrected in such a way that the linear-elastic slope agrees with the expected elasticity modulus. The underlying equation is:

$$\bar{\varepsilon}_{corr} = \bar{\varepsilon}_{meas} - \left(\frac{1}{E_{meas}} - \frac{1}{E(T)} \right) \cdot \bar{\sigma}_{meas} \qquad \textbf{Eq 1}$$

where the overbar indicates nominal stress and strain. E_{meas} is the linear-elastic slope of the measured data (obtained by linear regression) and E(T) is the target elasticity module at the test temperature. For 15-15 Ti, the following correlation for the elasticity module is available in [3]:

$$\frac{E(T)}{MPa} = 202700 - 81.6 \cdot \left(\frac{T}{°C}\right) \qquad \textbf{Eq 2}$$

which is valid from room temperature up to 800°C. The results of the tensile tests are summarized in Figure 5. The tensile properties are listed in Table 4. The comparison of the stress-strain curves for 24% and 46% CW is shown in Figure 6.

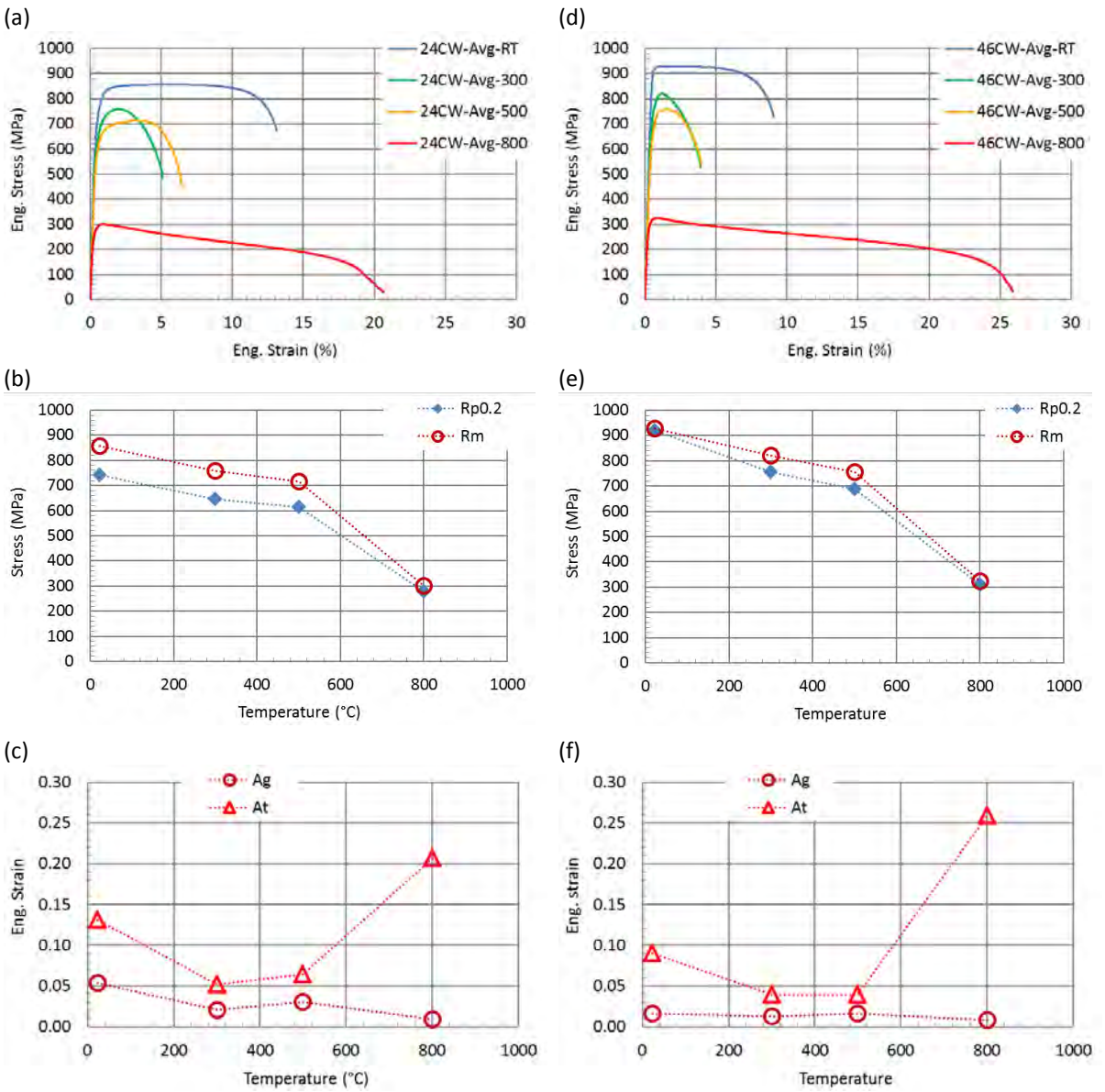

Figure 5: Tensile results for the 24% CW tube (a-c) and the 46% CW tube (d-f): averaged stress-strain curves for different temperature (a, d); dependence of $R_{p0.2}$ and R_m on temperature (b, e); dependence of A_g and A_t on temperature (c, f)

Table 4: Tensile properties of 15-15 Ti tubes measured by mini tensile tube specimens

	15-15 Ti 24% CW				15-15 Ti 46% CW			
T (°C)	$R_{p0.2}$ (MPa)	R_m (MPa)	A_g (%)	A_t (%)	$R_{p0.2}$ (MPa)	R_m (MPa)	A_g (%)	A_t (%)
RT	740	857	5.4	13.1	918	929	1.6	9.0
300 °C	646	758	2.0	5.1	754	820	1.2	3.9
500 °C	613	716	3.1	6.4	689	756	1.7	3.9
800 °C	278	300	0.9	20.7	311	325	0.8	25.9

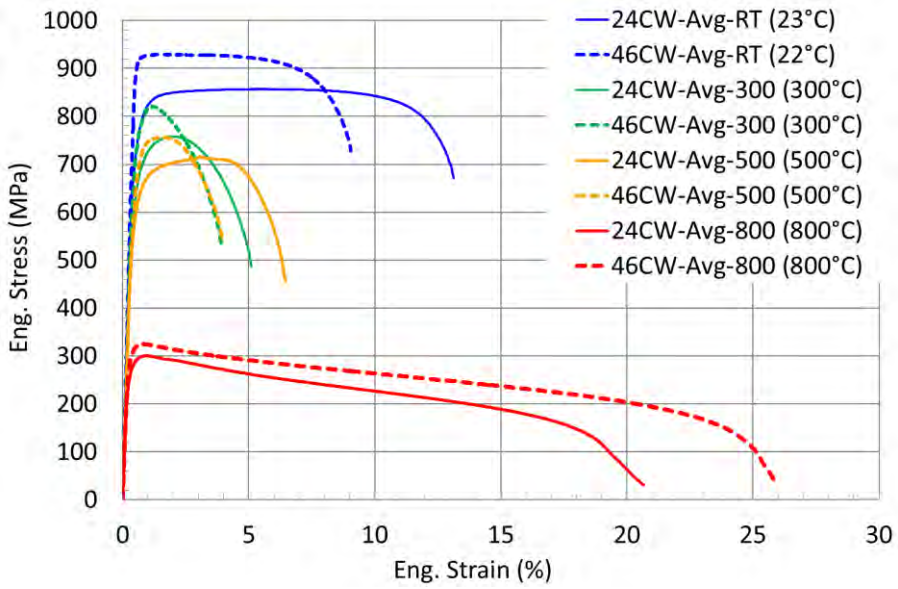

Figure 6: Comparison of averaged stress-strain curves at different temperatures; solid lines: 24% CW, dashed lines: 46% CW

3.2 Small punch tests

Figure 7 shows the averaged load-displacement curves at RT obtained from SP tests with curved specimens for 24% CW and 46% CW. These curves are convex in the whole displacement range. The displacement at maximum load u_m is significantly smaller for 46% CW, while the maximum loads F_m are about the same for 24% and 46% CW.

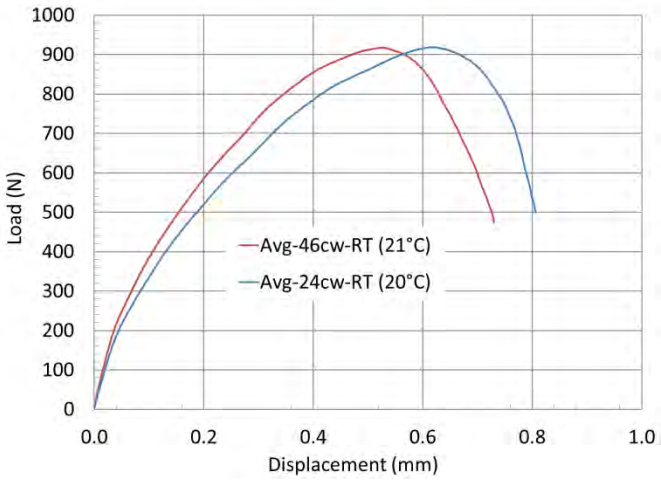

Figure 7: Averaged load-displacement curves at RT for 24% CW and 46% CW

Figure 8 shows the load-displacement curves at different temperatures for 24% CW. As a general trend, it can be seen that u_m and F_m are both decreasing with increasing temperature. The same is true for 46% CW but not shown here.

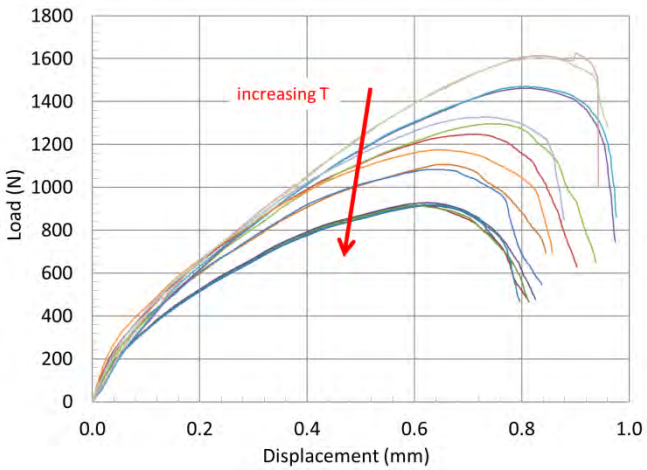

Figure 8: Load-displacement curves at different temperatures for 24% CW

The total SP energies are shown versus temperature in Figure 9. The energies are the calculated areas under the load-displacement curves from u = 0 up to u = u_m [4]. The trend curve for 46% CW lies below the curve for 24% CW and exhibits a larger scatter.

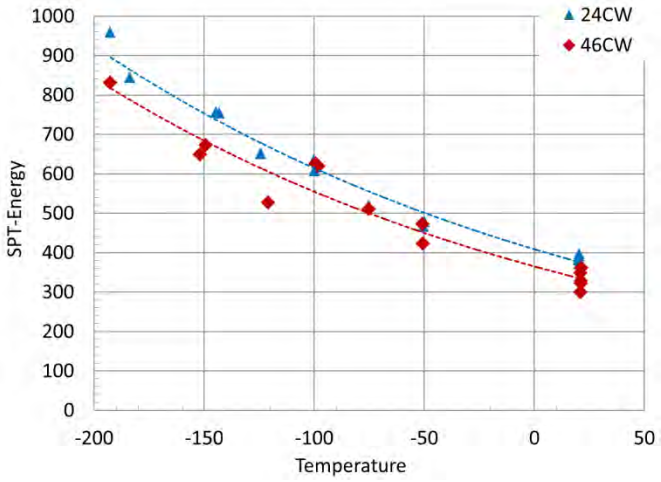

Figure 9: Total SP energy (up to u_m) versus temperature for 24% and 46% CW

4 Discussion

The comparison of tensile properties at room temperature (Table 4) gives higher YS and UTS and lower A_t as compared to standard tensile tests (Table 2). The causes for this deviation are not clear, as the exact geometry and the method of extraction of the specimens are not specified in [1,2]. Tolerances in the wall thickness of our tensile specimens may also be responsible. Higher test temperatures lead to lower A_g values (i.e. earlier necking). The total elongation (fracture strain) appears to have a minimum between 300 °C and 500 °C. A higher amount of cold working leads to higher YS and UTS. The ratio UTS/YS decreases with increasing cold working. Higher cold working also leads to a reduction of ductility (total elongation). This is not the case for T = 800 °C.

The SPT load-displacement curves are convex in the whole displacement range – unlike the curves obtained with plane specimens. This is due to the fact that the deformation is characterised by drawing mode right from the beginning of the test. The initial bending mode is absent. As consequence of the shape of the curves, it is not feasible to determine an

elastic-plastic transition load by bi-linear interpolation [4]. As for the properties of 15-15 Ti, it is interesting to note that there is no brittle behaviour at low temperatures. On the contrary, the displacement at maximum load u_m is increasing with decreasing temperatures. Consequently, there is no ductile to brittle transition as the SP energies continuously increase with decreasing temperature.

In future investigations, tensile tests at low temperatures $T < 0$ °C and SP tests at high temperatures are needed to correlate the features of SP load-displacement curves with tensile properties.

5 Conclusions

Tensile testing and small punch testing with specimens directly cut from thin-walled tubes is feasible. The detailed understanding of the results has to be further developed. Finite element analyses are expected to be helpful.

6 References

[1] Delville R., Specifications DIN 1.4970 24% cw cladding tubes, SCK •CEN-R-5686, May 2014

[2] Delville R., Specifications DIN 1.4970 46% cw cladding tubes, SCK •CEN-R-5687, May 2014

[3] Luzzi L., Lorenzi S., Pizzocri D., Rozzia D., Aly A., Del Nevo A., Modelling and analysis of nuclear fuel pin behavior of innovative lead cooled FBR, ENEA report ADPFISS-LP2-054, Sep 2014

[4] E. Altstadt, H.E. Ge, V. Kuksenko, M. Serrano, M. Houska, M. Lasan, et al., Critical evaluation of the small punch test as a screening procedure for mechanical properties, J. Nucl. Mater. (2015). doi:10.1016/j.jnucmat.2015.07.029

Appendix: Averaging of tensile curves and SPT load-displacement curves

1. Calculate path lengths of the curves $y^j(x^j)$:

$$s_n^j = \sum_{i=2}^{n} \sqrt{\left(y_i^j - y_{i-1}^j\right)^2 + \left(x_i^j - x_{i-1}^j\right)^2} \; ; \quad s_1^j = 0$$

j: curve index (j = 1 … nc); n, i: sample index; n = 1 … N^j; N^j – number of samples of curve j

2. Calculate relative path lengths:

$$\xi_n^j = s_n^j / s_{N^j}^j$$

3. Average points of the same relative path length:

$$\bar{x}(\xi) = \left\langle x^j(\xi) \right\rangle ; \quad \bar{y}(\xi) = \left\langle y^j(\xi) \right\rangle ; \quad j = 1 \ldots nc ; \quad \xi = 0 \ldots 1$$

$\langle \; \rangle$ - arithmetic mean

The above procedure is separately applied section by section.

For tensile tests (see Figure 10):

- $x \equiv \bar{\varepsilon}^{total}$; $y \equiv \bar{\sigma}$
- Section 1: $0 \le \bar{\varepsilon}^j \le \bar{\varepsilon}_{0.2}^j$
- Section 2: $\bar{\varepsilon}_{0.2}^j \le \bar{\varepsilon}^j \le \bar{\varepsilon}_{uni}^j$
- Section 3: $\bar{\varepsilon}_{uni}^j \le \bar{\varepsilon}^j \le \bar{\varepsilon}_{frac}^j$

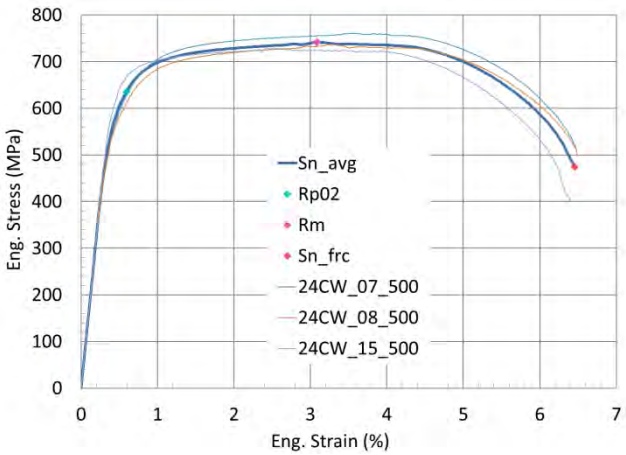

Figure 10: Average tensile curve at 500 °C for 24% CW

For SP tests:

- $x \equiv u$; $y \equiv F$
- Section 1: $0 \le u^j \le u_m^j$ (beginning until maximum load point)
- Section 2: $u_m^j < u^j \le u_{end}^j$ (maximum load point until last point)

Appendix C

CIEMAT results by Marta Serrano (Power Point presentation)

TASTE PP
CIEMAT tests on 15-15Ti cladding tubes

Marta Serrano
CIEMAT

www.eera-set.eu

Contents

- Results presented at AMPT 2015
  - M. Serrano Garcia, D. Sanchez Avila, D. Rémi, “Evaluation of the mechanical behavior by small punch tests for Titanium stabilized 1.4970 “15-15Ti” stainless steel cladding” AMPT 2015 - NS 1 - New steels for applications under extreme conditions: steels for energy applications, Madrid 14-17 December 2015
- Partially included in:
  - David Sanchez Davila, “Estudio de materiales candidatos para vainas de combustible de los reactores nucleares de IV generación” Master Thesis, Universidad Carlos III de Madrid, Jul 2015

www.eera-set.eu

Objective

- Characterization of cladding tubes:
  - 15-15Ti with different cold work levels
  - Small Punch tests
  - Correlation with tensile tests

Material

- Two 15-15Ti Cladding tubes received from SCK CEN
  - DIN 1.4970 24% cw – Tube 699
  - DIN 1.4970 46% cw – Tube 29
  - Outside diameter 6.55+0.03/-0.05 mm
  - Inside diameter 5.65+/-0.03 mm
  - Wall thickness ≥ 0.45 mm

Wt%	C	Si	Mn	P	S	Cr	Ni	Co	Mo	N	Ti	V	Cu
24CW	0.096	0.570	1.860	0.013	<0.001	15.060	15.050	0.020	1.210	0.011	0.440	0.034	0.026
46CW	0.100	0.570	1.890	0.013	<0.001	15.090	15.050	0.019	1.210	0.009	0.440	0.034	0.027

Room temperatue	YS (MPa)	UTS (Mpa)	A (k=5.65) %
24CW	691	809	25.4
46CW	926	950	10.3

Small Punch tests

- 3 mm diameter, 0.250 mm thickness
  - RT, 300ºC and 500ºC
  - 0.3 mm/min
  - Specimen disc deflection

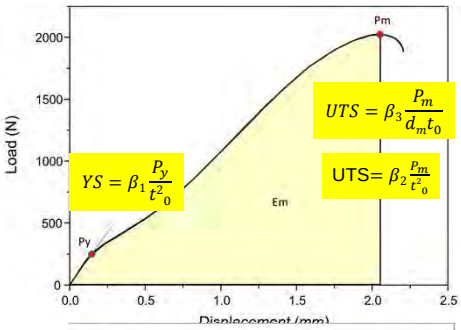

Biaxial

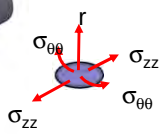

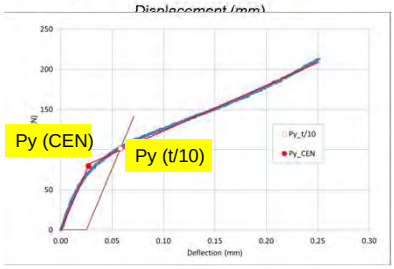

CEN CWA 15627:2006 Part B: A Code of Practice for Small Punch Testing for Tensile and Fracture Behaviou

Tensile tests

- Uniaxial tensile specimens were machined from the tube
  - Gage length = 18 mm
  - 1x10^{-4} mm/mm/s
  - RT, 300ºC and 500ºC

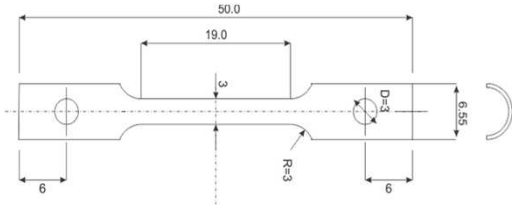

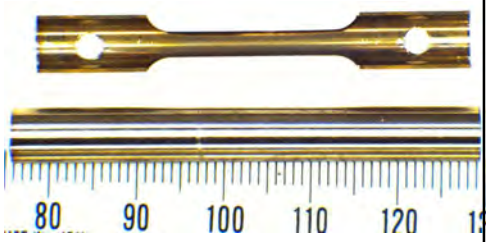

www.eera-set.eu

Tensile tests

- Higher CW level -> higher YS and UTS

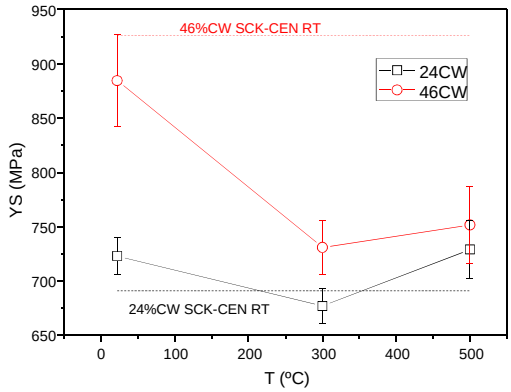

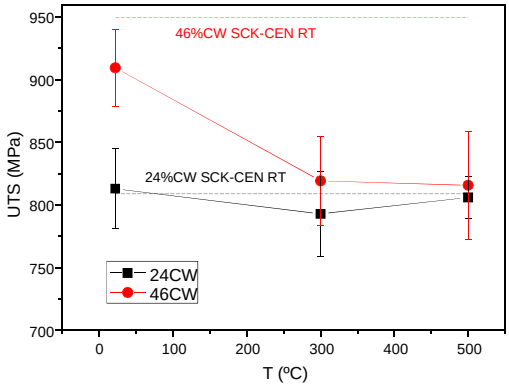

Small Punch tests

15-15Ti **24%CW** Cladding tube

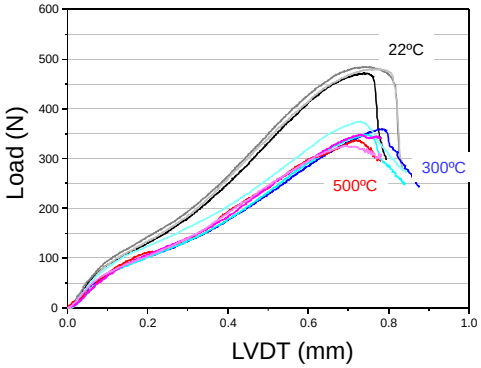

15-15Ti **46%CW** Cladding tube

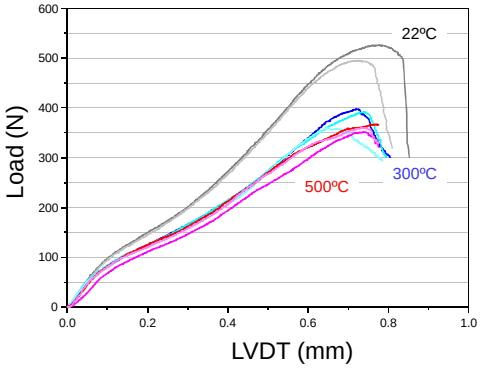

Small Punch tests

- Higher CW -> Higher strength

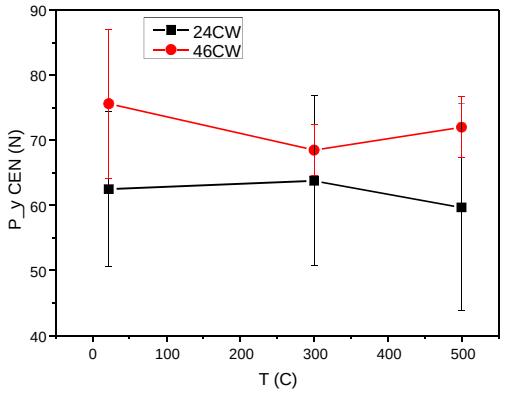

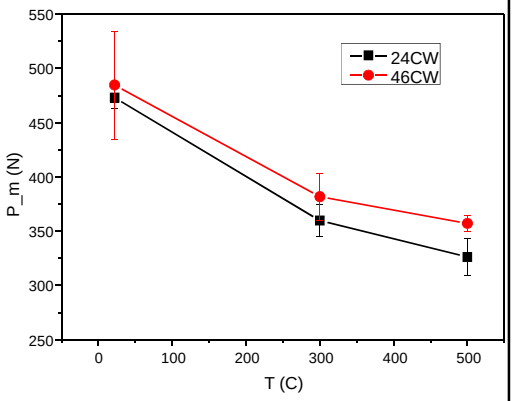

Small Punch tests

- Calculation of Py
  - CEN procedure
  - Offset t/10 -> Overestimation around 30%

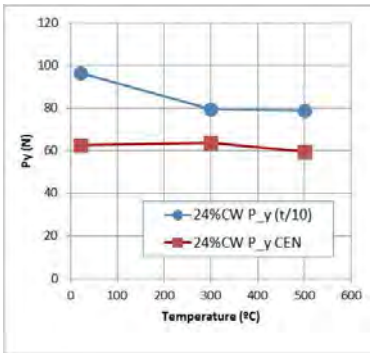

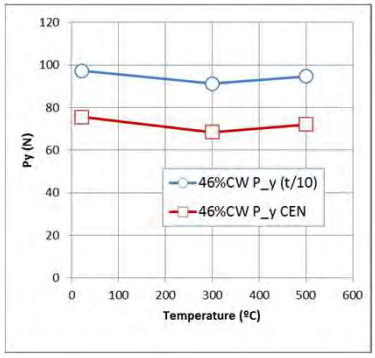

www.eera-set.eu

Small Punch tests - Correlation with tensile tests

- Correlation of Py with yield strength is better when the Py value is calculated by the t/10 offset method

$$YS = \beta_1 \frac{P_y}{t^2_0}$$

β_1=0.476 (CWA CEN)

Py calculated at t/10 -> β_1=0.520

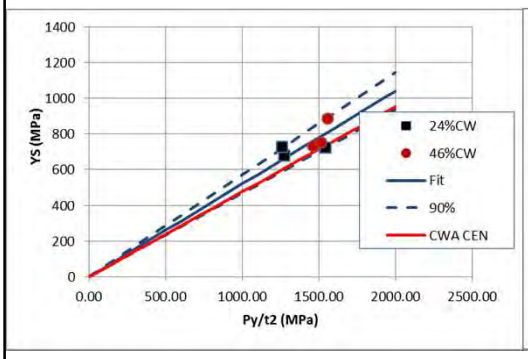

Py calculated by CEN proc. -> β_1=0.679

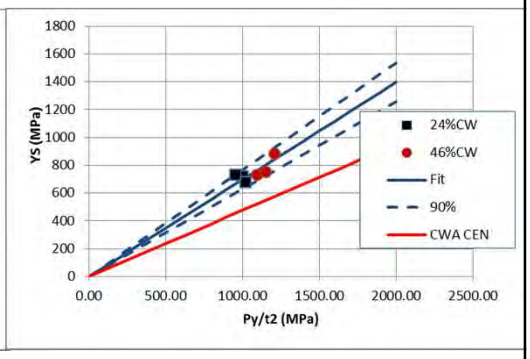

Small Punch tests - Correlation with tensile tests

- *UTS-Pmax*
  - P_{max} region does not represent necking zone (as UTS in tensile properties) and that necking starts earlier to P_{max}
  - Good correlation with Pm/(dm*t)

$$UTS = \beta_3 \frac{P_m}{t_0^2}$$

β_2= 276 (this results)
β_2=277 (T.E Garcia et al)

$$UTS = \beta_2 \frac{P_m}{d_m t_0}$$

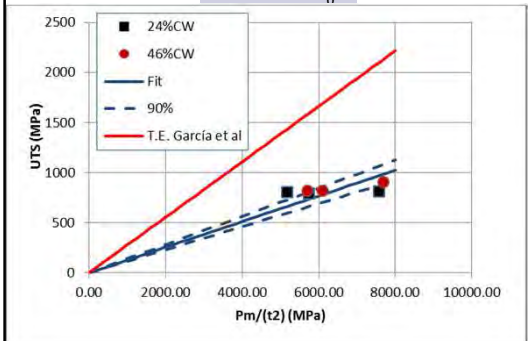

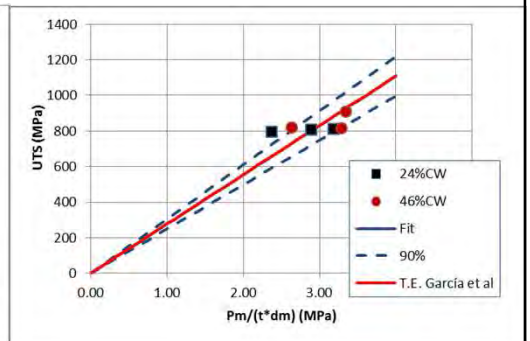

T.E. García et al. / Journal of Alloys and Compounds 582 (2014) 708–717

Summary

- Small punch tests were performed with 3 mm diameter – 0.25 mm thickness specimens mechanised from the thin-walled tube
  - Higher CW values -> higher Py and Pm
  - The correlation of tensile and small punch at yield depends on the calculation method
  - For Yield Strength: the correlation is better when the Py value is calculated with the t/10 offset
  - For UTS, the correlation is better with Pm/(dm*t)

Next steps

- Fractographic analysis of the broken specimens
- Small punch with the 15-15Ti bars

Appendix D

Analyses of the Ring Tension Tests Performed on the 15-15Ti tube specimens.

RATEN ICN Pitesti report by V. Radu, A. Nitu and V. Pitigoi

Analyses of the Ring Tension Tests performed on the 15-15Ti tube specimens

-Status report on the EERA JPNM Pilot project TASTE-

Vasile RADU
Alexandru NITU
Vasile PITIGOI

RATEN ICN Pitesti, Romania

Abstract

RATEN ICN performed the ring tension tests on the 15-15Ti specimens in the framework of EERA JPNM Pilot project TASTE. The ring tension test is a test for determining material properties only in the hoop direction of a tube. The hoop direction properties are needed for tubular structural components which are known to have anisotropic mechanical properties due to the fabrication process. The paper presents the experimental procedure, the ring tension test methodology, the experimental results at various temperatures and the analyses of results.

Introduction

The ring tensile/tension test (RTT) [1, 2] and its variant, the ring hoop tension test (RHTT) [3, 4], are the non-conventional tests that use a ring specimen to obtain the hoop tensile properties of tube-shaped structures.

The experimental ring tension test (RTT) is designed for the mechanical characterization of the thin-walled cladding tubes. Actually, the ring tension test is a test for determining material properties only in the hoop direction. The hoop direction properties are needed for tubular structural components which are known to have anisotropic mechanical properties due to the fabrication process.

Tensile test is performed by applying a tensile force to the inside of the ring. The main shortcomings of this test are the bending deformation due to specimen curvilinear shape and the impact of friction between inserts and test material. The radial displacement is induced by a moving a plug into half-cylinders and friction is therefore an issue. To minimize the friction coefficient between the outer surface of the half mandrels and the inner surface of the specimen, some lubrication such as vacuum grease or Teflon have been used by some testing laboratories.

Some advantages of the ring tension test are:

- it is used to determine the mechanical properties in the hoop direction of a tube-shaped structures;
- requirement of smaller specimen volume;
- easier specimen preparation;
- and easier specimen setup in the test apparatus (especially in the test of irradiated fuel cladding).

Experimental procedure

Material and specimens

In the TASTE PP are available three lots of 15-15Ti in tube forms. First two lots are provided by SCK CEN, and the tubes have the following geometric characteristics:

- Inner diameter of 5.65 mm;
- Outer diameter 6.55 mm.

The tube samples have a different cold-work treatment: first one is 24% CW and the second one is 46% CW.

The third lot of 15-15 Ti is provided by CEA and these tubes have:

- Inner diameter of 8. 5 mm;
- Outer diameter of 7.37 mm.

The 15-15Ti tubes from CEA have a 22% of CW.

In this report are discussed the experimental results that have been obtained in the ring tension tests performed on the SCK CEN tubes (15-15 Ti with both 24% CW and 46% CW).

The chemical composition and geometric characteristics for 15-15Ti with 24% CW are displayed in Figure 1, and some mechanical properties are shown in Figure 2 [5].

Chemical composition :

Results chemical analysis (wt. %)	C	Si	Mn	P	S	Cr	Ni	Co	Mo	B	N
Required	0.08 0.12	0.5 0.7	1.0 2.0	<0.015	<0.015	14.5 15.5	14.5 15.5	<0.03	1.0 1.4	0.003 0.008	<0.015
Measured	**0.096**	**0.57**	**1.86**	**0.013**	**<0.001**	**15.06**	**15.05**	**0.02**	**1.21**	**0.0025[1] 0.0031[2]**	**0.011**

Results chemical analysis (wt. %)	Ti	V	Ta	Cu	Ca	Fe
Required	0.33 0.55	<0.05	<0.02	<0.05	<0.03	bal
Measured	**0.44**	**0.034**	**<0.005**	**0.026**	**0.017**	**bal**

[1]Results of first ICP measure at Sandvik; [2]Results of second ICP measure at Aubert&Duval after erosion of 75µm external tube layer

Dimensional control :

Dimensional control	∅ *outside*	∅ *inside*	*Wall thickness*	*Ovality*
Required	6.55 +0.03/-0.05 mm	5.65 +/-0.03 mm	≥ 0.45 mm	<0.04 mm
Values	*Conform*	*Conform*	*Conform*	*Conform*

Figure 1.Chemical composition and dimensional control for 15-15 Ti, 24% CW (SCK CEN) [5]

Mechanical test at room temperature after final cold-working:

Average value of 3 tensile tests on batch

	UTS	YS	Total elongation
	Rm (MPa)	*Rp0.2 (MPa)*	*A (%) (over 5.65√So)*
Results	809 MPa	691 MPa	25.4%

Figure 2. Mechanical properties for 15-15Ti, 24% CW (SCK CEN) [5]

The chemical composition and geometric characteristics for 15-15Ti with 46% CW are displayed in Figure 3, and some mechanical properties are shown in Figure 4 [6].

Chemical composition :

Results chemical analysis (wt. %)	C	Si	Mn	P	S	Cr	Ni	Co	Mo	B	N
Required	0.08 0.12	0.5 0.7	1.0 2.0	<0.015	<0.015	14.5 15.5	14.5 15.5	<0.03	1.0 1.4	0.003 0.008	<0.015
Measured	**0.10**	**0.57**	**1.89**	**0.013**	**<0.001**	**15.09**	**15.05**	**0.019**	**1.21**	**0.0038**	**0.009**

Results chemical analysis (wt. %)	Ti	V	Ta	Cu	Ca	Fe
Required	0.33 0.55	<0.05	<0.02	<0.05	<0.03	bal
Measured	**0.44**	**0.034**	**<0.005**	**0.027**	**0.010**	**bal**

[1]Results of first ICP measure at Sandvik; [2]Results of second ICP measure at Aubert&Duval after erosion of 75µm external tube layer

Dimensional control :

Dimensional control	*∅ outside*	*∅ inside*	*Wall thickness*	*Ovality*
Required	**6.55+0.03/-0.05 mm**	**5.65+/-0.03 mm**	**≥ 0.45 mm**	**<0.04 mm**
Values	*Conform*	*Conform*	*Conform*	*Conform*

Figure 3. Chemical composition and dimensional control for 15-15Ti, 46% CW (SCK CEN) [6]

Mechanical test at room temperature after final cold-working:

Average value of 3 tensile tests on batch

	UTS	YS	Total elongation
	Rm (MPa)	*Rp0.2 (MPa)*	*A (%) (over 5.65√So)*
Results	950 MPa	926 MPa	10.3%

Figure 4. Mechanical properties for 15-15Ti, 46% CW (SCK CEN) [6]

The samples used for the ring tension tests were debited by turning 15-15Ti tube. The ring width is of 5 mm and its length is of 5 mm. They were processed with two symmetrically

distributed narrowing sections (Figure 5 (a)). The loading scheme versus gauged sections is displayed in Figure 5 (b).

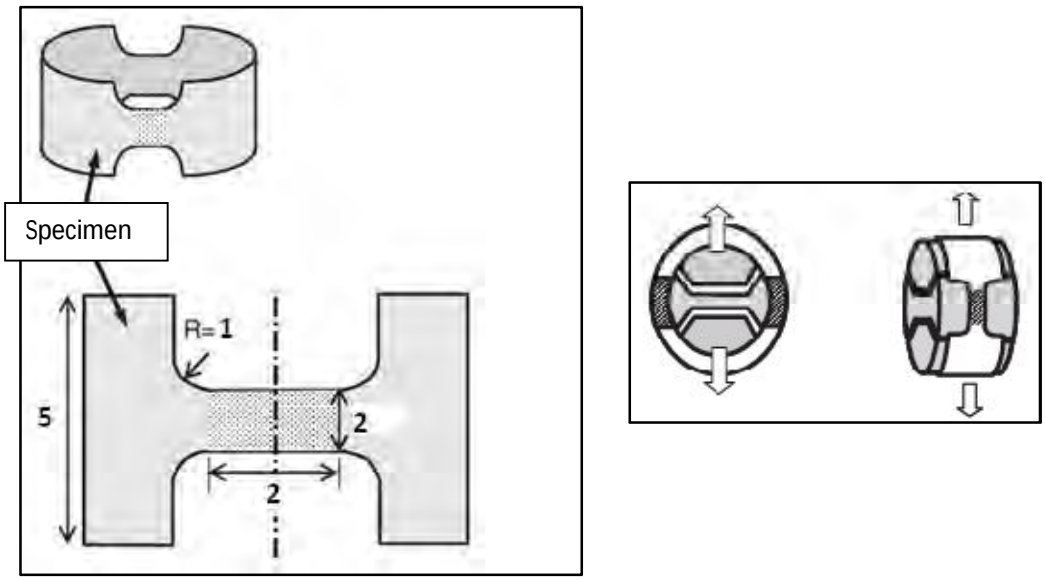

(a) (b)

Figure 5. The specimen sketch with dimensions in mm (a) and the direction of loading (b)

A picture of final shape of the ring tension test is shown in Figure 6, and for comparison purpose, a similar specimen prepared from Zircaloy-4 cladding tube is showed.

Figure 6. The Ti-Ti15 (24%CW) specimen vs. Zy-4 specimen for ring tension test

Ring tension tests

The ring tension tests were performed at room temperature, 500°C and 600°C, respectively, with a slow deformation rate about 0.017mm/s. A Teflon tape has been used between ring specimen and gripping system to reduce the friction coefficient. The ring tension device (Figure 7) is positioned in the Walter+Bai Static & Dynamic Materials Testing System 30KN (Figure 8).

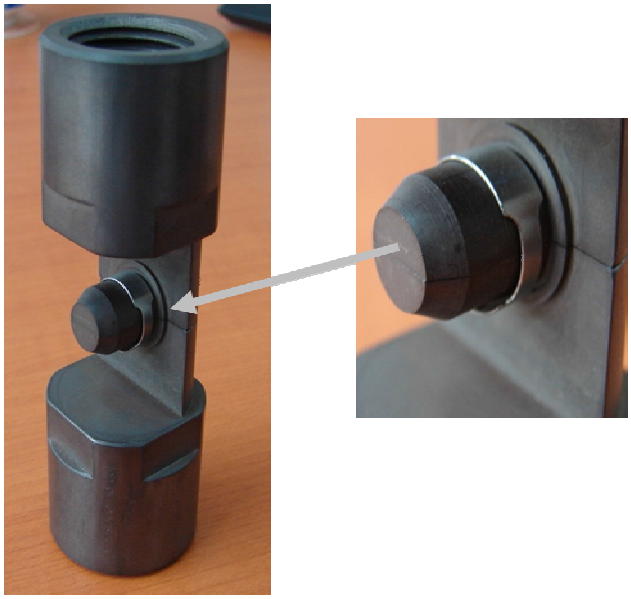

Figure 7. Ring tension device (loading grips and specimen)

Figure 8. The testing facilities (Walter Bai Testing System and acquisition system)

Suitable software for data acquisition and processing is used to obtain simultaneously information about the experiment temperature and stress versus displacement during the ring tension test, as well.

Results and discussion

Typical assessment procedure

The results obtained in the ring tension experimental tests allow obtaining of the tubes mechanical parameters (yield stress, UTS) in the circumferential direction. A quick and accurate

assessment of the hoop constitutive behavior of a tested material in the ring tension test is performed by processing the experimental force-elongation data in the same way as for the uniaxial tests. The simplest assessment of the load-deformation data to give indicative values for the tensile strength and yield is by assuming a nominal engineering stress as:

$$\sigma = \frac{F}{2 \cdot A_0} \tag{1}$$

where A_0 is the area of the thinned sections of the ring sample.

The stress does not take into account bending and stress distribution. The strain is calculated without corrections for bending.

Experimental results for temperature T_{cam} and 500 ℃

The primary experimental results from ring tensile test are represented by the curves of hoop stress versus deformation. These can be seen in Figure 9 for 15-15Ti 24%CW specimens at room temperature and 500°C, and Figure 9 for 15-15Ti 46%CW specimens at the same temperatures.

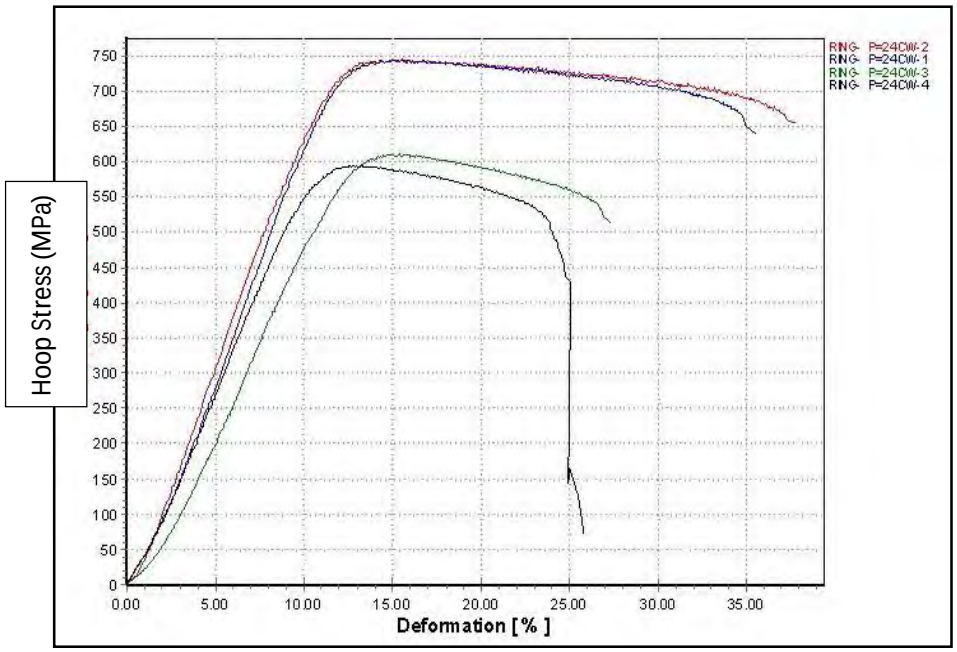

Figure 9. Hoop stress vs. deformation curves in the ring tension tests on 15-15 Ti 24%CW specimens

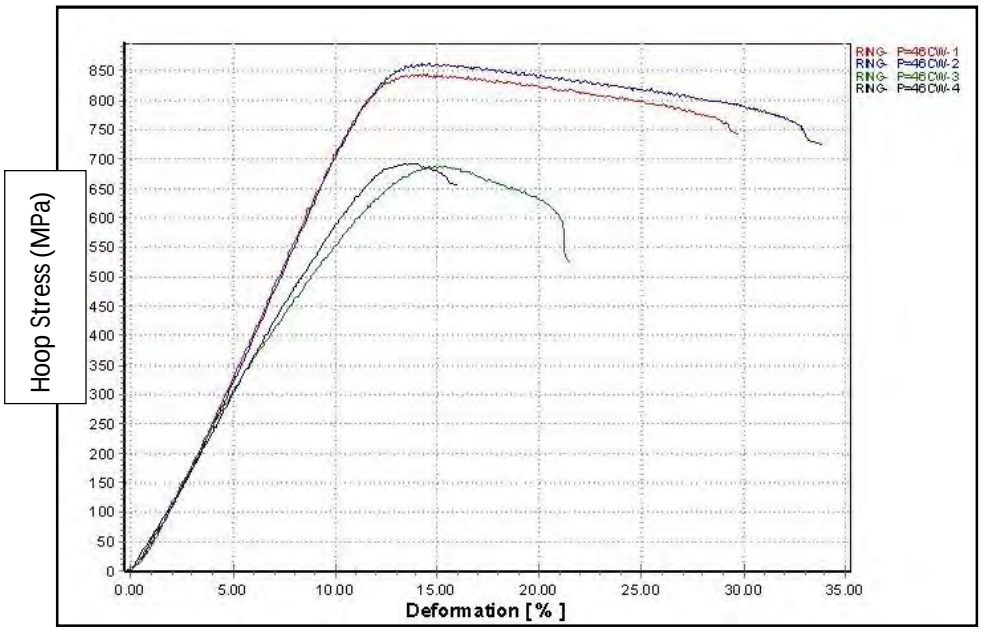

Figure 9. Hoop stress vs. deformation curves in the ring tension tests on 15-15 Ti 46%CW specimens

Most often the specimens are broken in one part from two gauged zone, inside of the calibrated narrowing section, as can be seen in Figure 9 for 15-15Ti, 24% CW. This happened at temperature Tcam but also at temperature of 500°C.

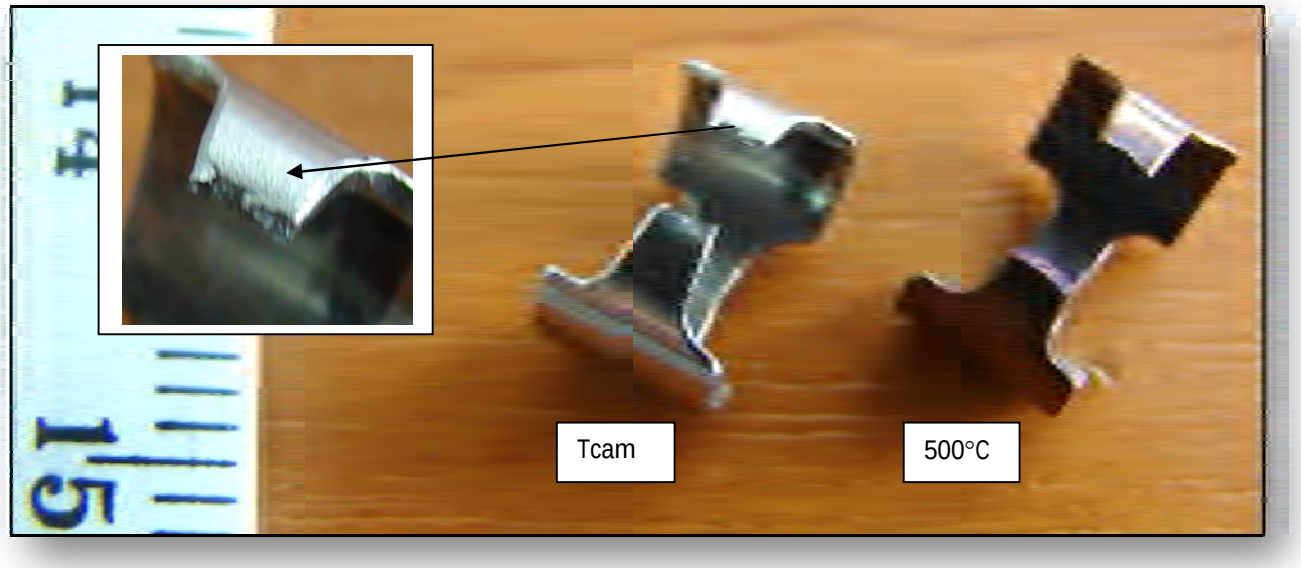

Figure 9. Macroscopic aspects of 15-15Ti, 24% , after ring tension test

For the 15-15Ti specimen with 46% CW the macroscopic aspect after ring tension test is displayed in Figure 10.

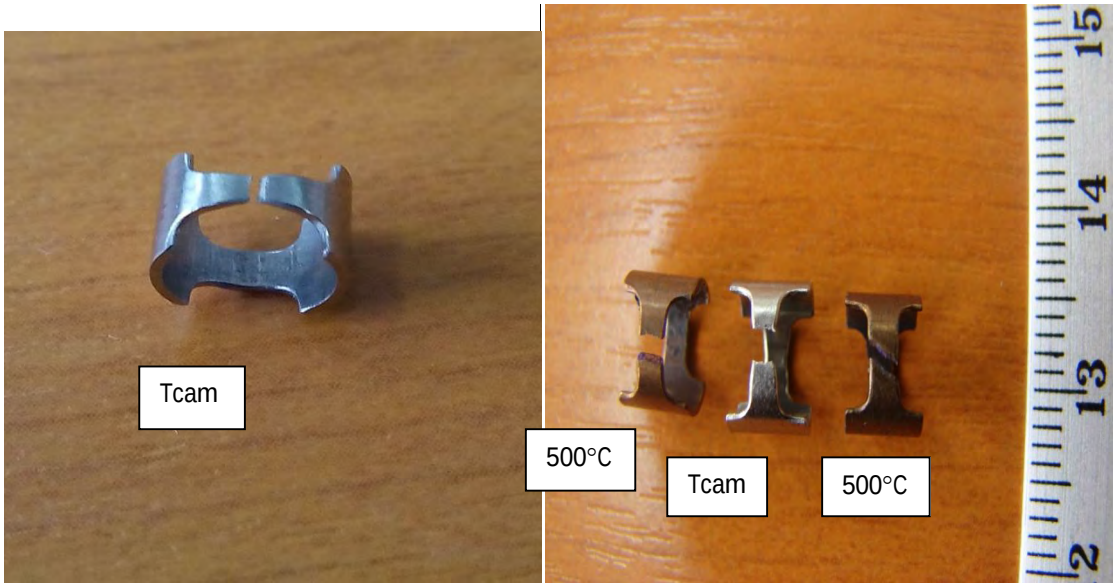

Figure 10. Macroscopic aspects of 15-15 Ti, 46%, after ring tension test

The ultimate hoop tensile strength (UHTS) decreases with temperature for 15-15Ti 24%CW; in this case the values of UHTS at 500°C is around 20% lower than UHTS at Tcam (see Figure 11). For 15-15Ti, 46% CW, the same strength is 18% lower at 500°C as against Tcam (Figure 12).

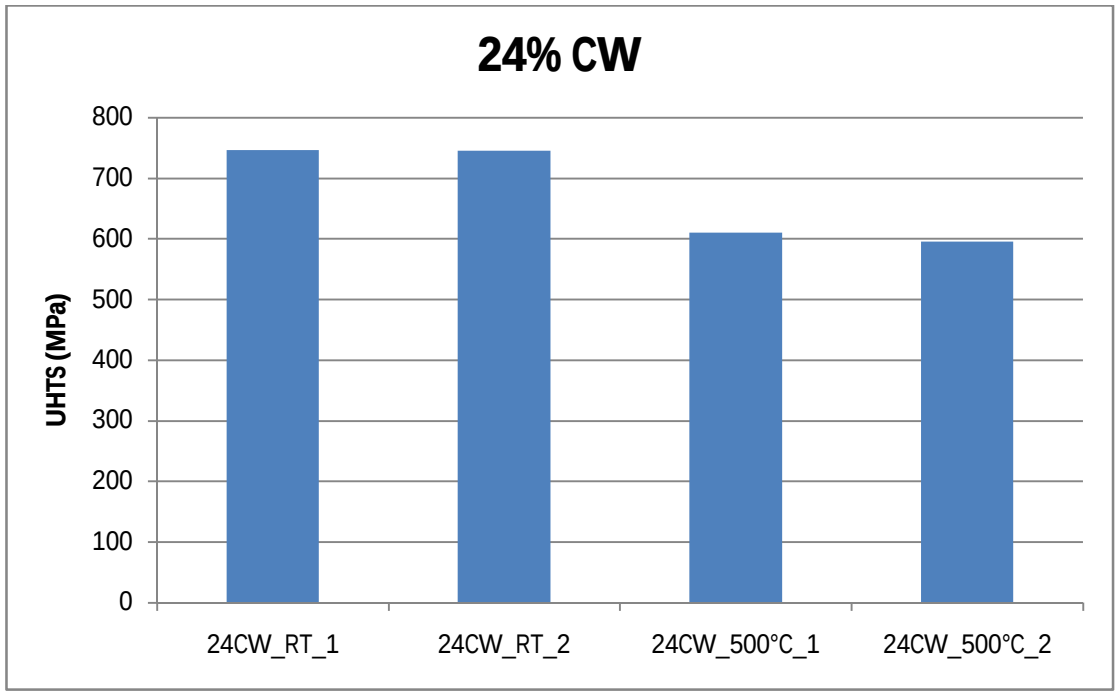

Figure 11. Ultimate hoop tensile strength (UHTS) from ring tension tests vs. temperature for 15-15Ti (24%CW)

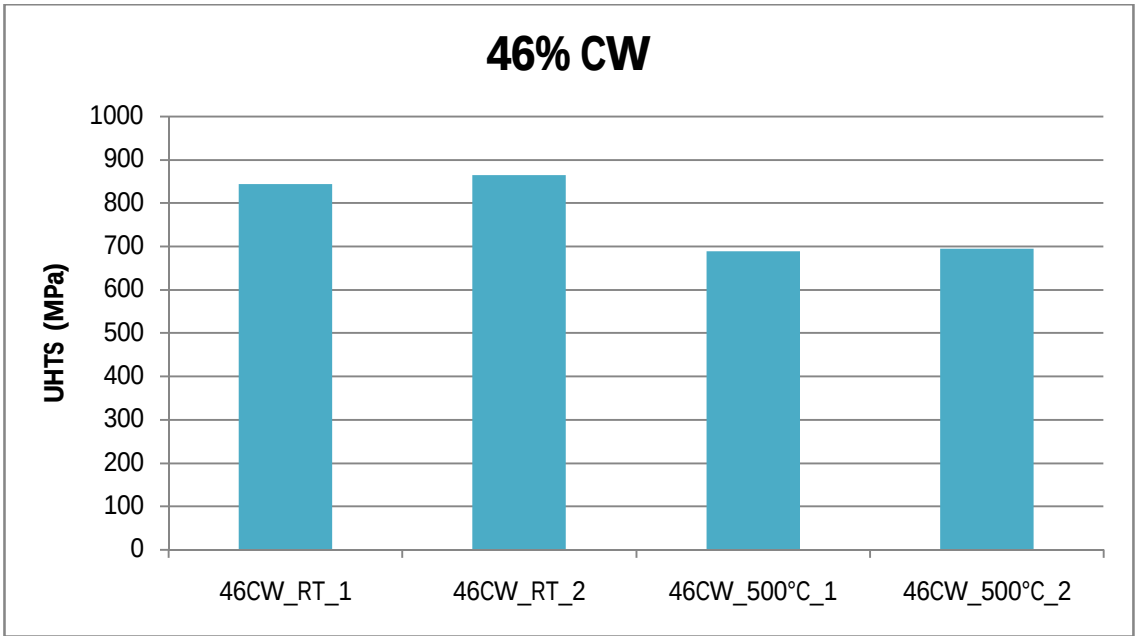

Figure 12. Ultimate hoop tensile strength (UHTS) from ring tension tests vs. temperature for 15-15Ti (46%CW)

The mechanical properties are much better for the 15-15Ti specimen with 46%CW, than those with 24%CW at each temperature of tests (Figure 13 and 14).

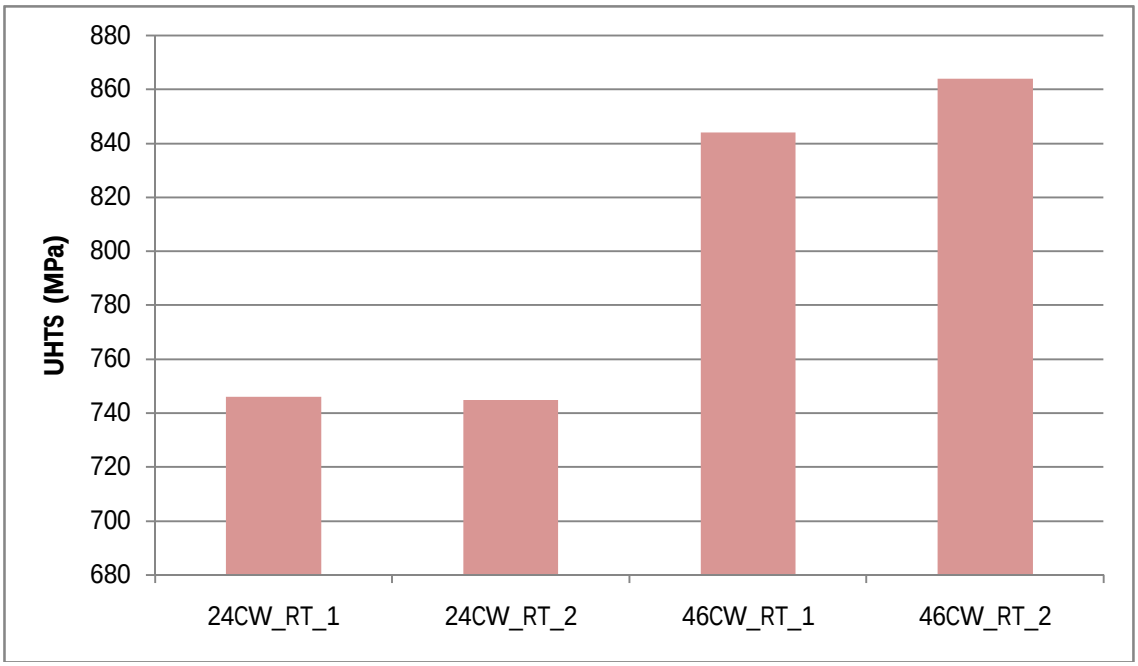

Figure 13. Ultimate hoop tensile strength (UHTS) vs. CW for 15-15 Ti at room temperature

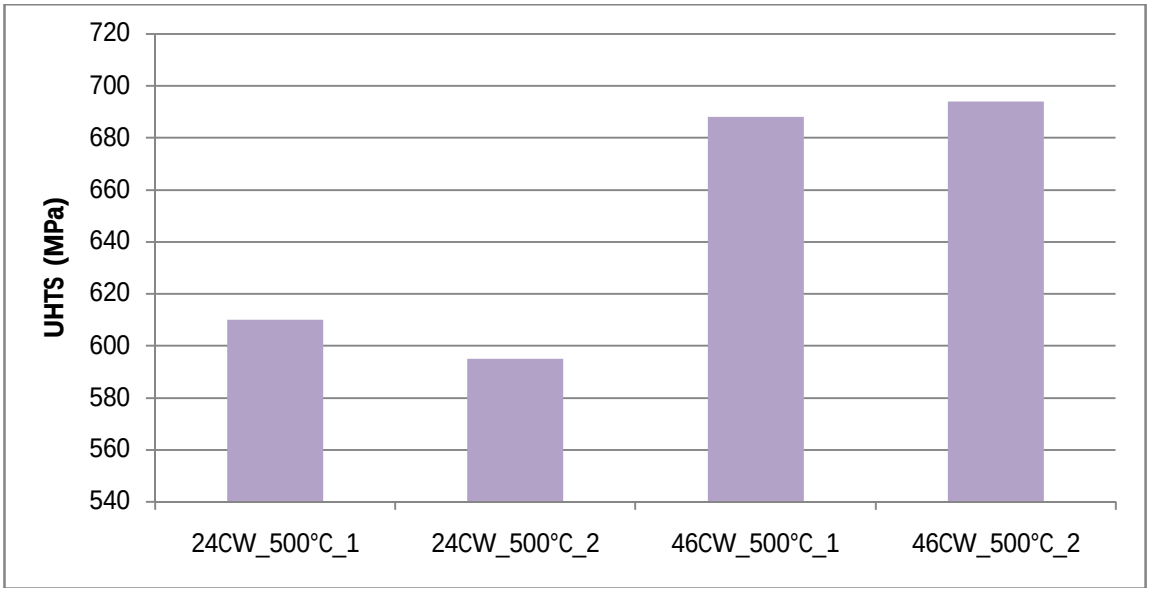

Figure 14. Ultimate hoop tensile strength (UHTS) vs. CW for 15-15 Ti at 500°C

Experimental results for temperature 600°C

To carry out the ring tests at high temperatures is a challenge for test systems and grips. Therefore, to reduce the coefficient of friction between clamping system and specimens, the literature recommends using Teflon tape. Using Teflon is, however, limited by temperature. From our experience we can say that Teflon can be properly used to a maximum of 500°C. Above this temperature Teflon burns.

For this work the intention was to conduct the tests at higher temperatures like as 600°C to 800°C, in which Teflon tape cannot be used.

In this case the option was to reduce the friction coefficient by using the colloidal graphite. The coating was performed by spraying graphite samples diluted with isopropyl alcohol. The dilution ratio was 1: 3. Figure 15 shows the ring tension specimens covered with the colloidal graphite.

Figure 15. The ring tension specimens covered with the colloidal graphite.

The sample heating has been done about 200 C°/min and keeping the constant temperature was 2400 seconds to allow the temperature uniformity throughout the system (grips, sample). The tests were conducted at 600°C under normal conditions, and the fracture locating is inside of the calibrated narrowing section (Figure 16).

Figure 16. Tested ring specimen at 600°C

Figure 17 displays the ring tensile curves for specimens of 15-15Ti for both cold works. At 600°C the UHTS values are of 590 MPa (24 %CW) and around 670 MPa for 46% CW.

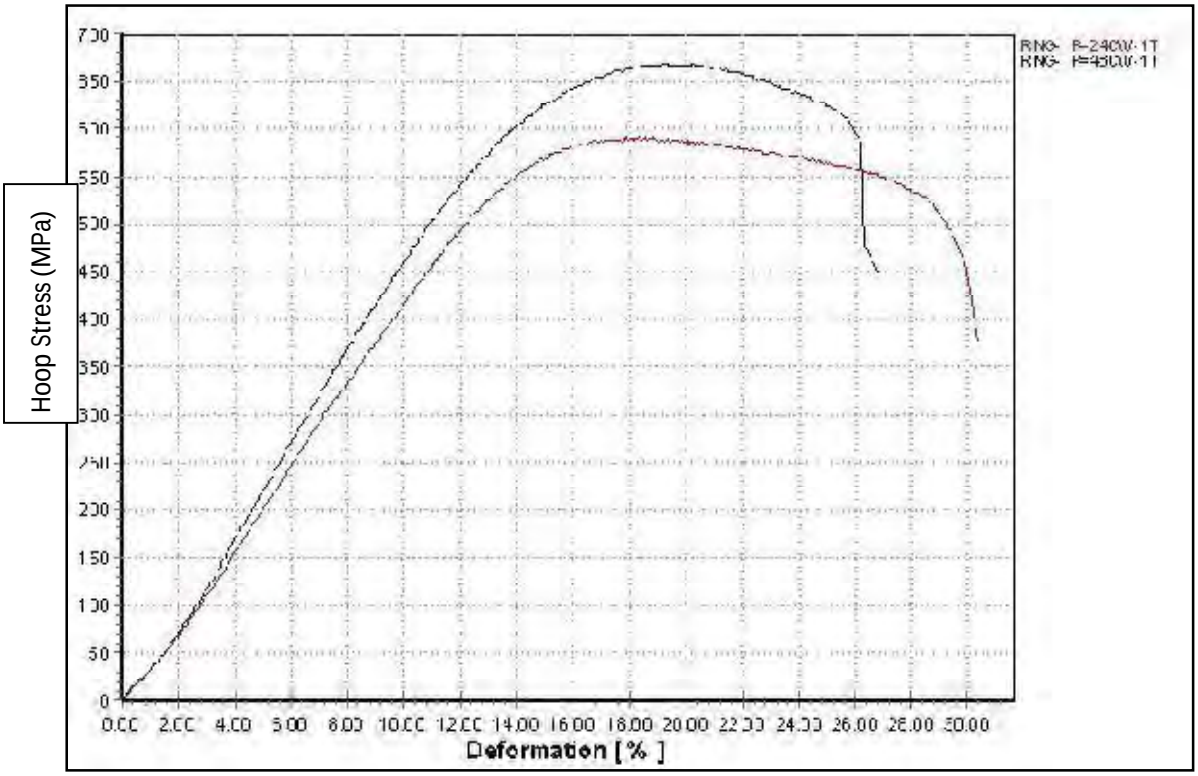

Figure 17. The hoop stress vs. deformation curves at 600°C (24 %CW and 46% CW)

The ring tension tests at 800°C were unsuccessful and the results were not valid.

Methalografical analyses

In the metallographic analyses were examined the grain microstructure in the radial-transversal section (Figure 18 and Figure 19) and in the radial-longitudinal section (Figure 20 and Figure 21).

Figure 18. Microstructural morphology in transversal section for 15-15 Ti, 24% CW

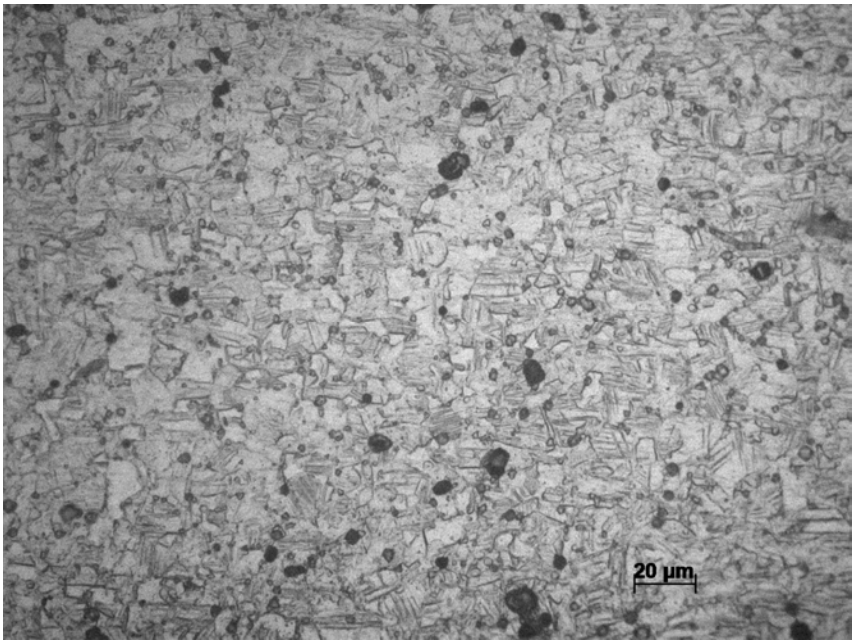

Figure 19. Microstructural morphology in transversal section for 15-15 Ti, 46% CW

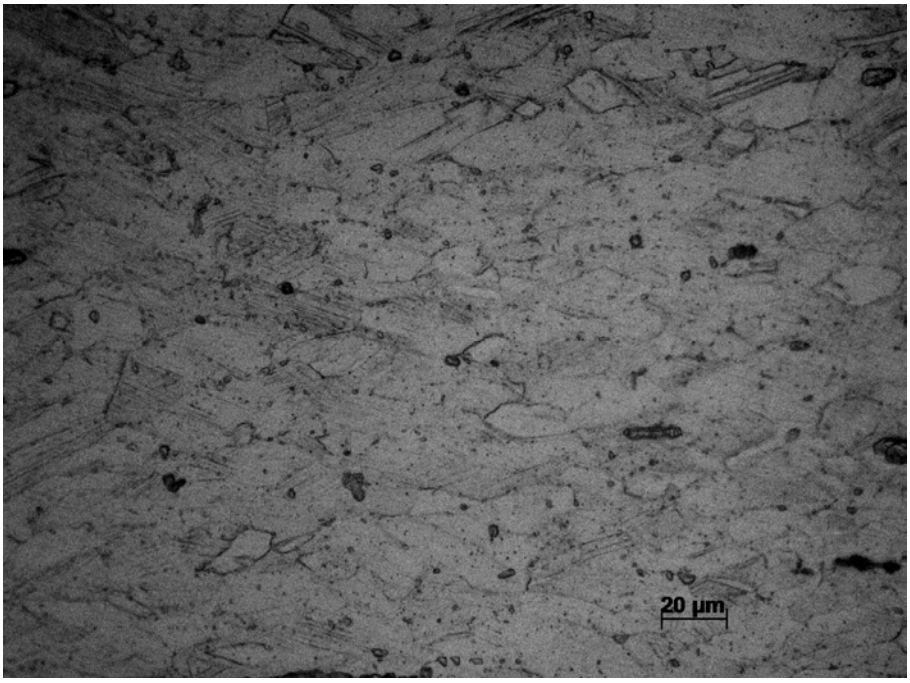

Figure 20. Microstructural morphology in longitudinal section for 15-15 Ti, 24% CW

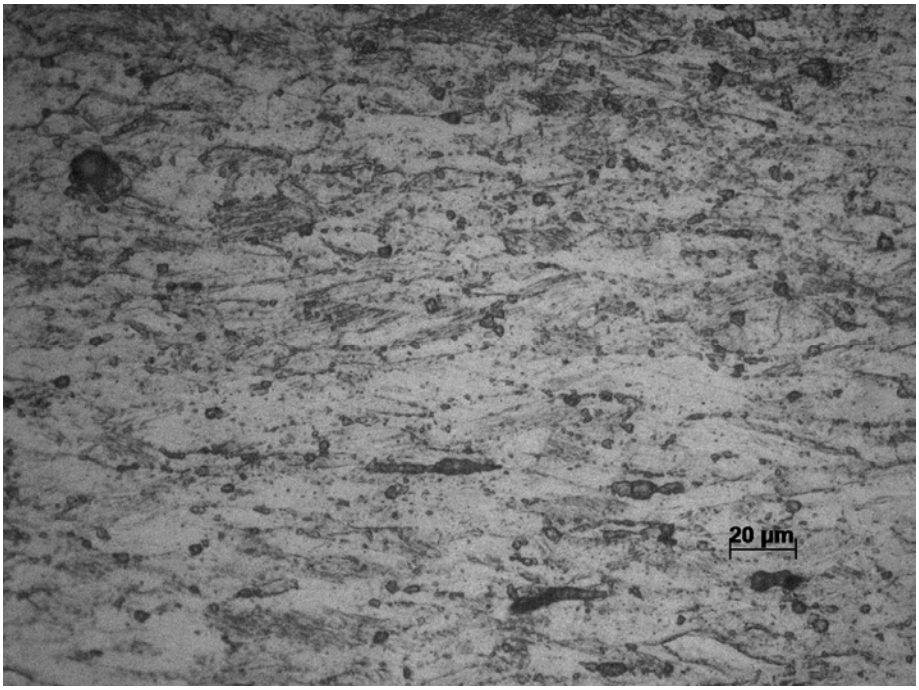

Figure 21. Microstructural morphology in longitudinal section for 15-15 Ti, 46% CW

For 15-15Ti, 46%CW, the grain morphology is similar to 15-15Ti, 24%CW, but they are smaller. In the radial-transversal section the grains are equiaxed but dimensions for first alloy are smaller. For the radial-longitudinal section one can see elongated grains in axial direction, and also for 15-15Ti 46% CW

with smaller dimensions. It seems that this microstructural feature explains the difference in UHTS of tested specimens versus cold work types.

Results analysis

In the Table 1 are resumed the mechanical properties from the ring tension tests, for 15-15Ti with two cold work processing in the circumferential direction. For comparison purpose, the UTS corresponding values from specifications [5, 6] are given, but for them the direction of obtaining (longitudinal or circumferential) are not known.

Table 1. Ultimate Tensile Strength for 15-15Ti (TASTE PP) in MPa

Specimen type	Tcam	500°C	600°C
UHTS (MPa); 24% CW	746; 745	595; 610	590
UHTS (MPa); 46% CW	844; 864	688; 694	670
UTS (MPa); 24% CW [5]	809		
UTS (MPa); 46% CW [6]	950		

At room temperature the values of UHTS obtained in the ring tension tests are lower with 6-10% than those from mentioned specifications. The experimental conditions which were used to obtain UTS in reference [5, 6] are not known, and the explanation of these small differences cannot be done.

In the preparing of the ring tension test for 15-15Ti, some preliminary test were performed on the zircaloy-4 specimens, together with the some modeling of the test by means of Finite Element Method, and the agreement was acceptable. In the case of applying the Finite Element Modelling for the uniaxial ring tensile test for 15-15Ti we have to mention that the works are in-progress and much effort should be done for the stress-strain predictions at various temperatures.

Conclusions

RATEN ICN performed the ring tension tests on the 15-15Ti specimens in the framework of EERA JPNM Pilot project TASTE. The ring tension test is a test for determining material properties only in the hoop direction of a tube.

The paper presents the experimental procedure, the ring tension test methodology, the experimental results at various temperatures and the analyses of results. The following results could be mentioned:

- The methodology of the ring tension tests was set up;
- The ring tension tests on 15-15Ti with 24%CW and 46% were carried out at temperatures: Tcam, 500°C, 600°C;
- The ultimate hoop tensile strength for 15-15Ti, 46 %CW is better than those of 15-15Ti, 24 %CW at all tested temperatures;
- The microstructural analysis reveals a finer grain sizes of 15-15Ti, 46CW to 15-15Ti 24%CW, that explains a higher UHTS values for first one.

References

[1] Arsene, S. and Bai, J., "A New Approach to Measuring Transverse Properties of Structural Tubing by a Ring Test-Experimental Investigation," Journal o/Testing and Evaluation, Vol. 26, No. I, January 1998, pp. 26-30.J. Test. Eval. 26 (1998) 26–30.

[2] Arsene, S., Bai, J., "A new approach of measuring transverse properties of structural tubing by a ring test", Journal of Testing and Evaluation 24 (1996), 386.

[3] Chris P. Dick, Yannis P. Korkolis, "Mechanics and full-field deformation study of the Ring Hoop Tension Test", International Journal of Solids and Structures 51 (2014) 3042–3057.

[4] Christopher P. Dick, Yannis P. Korkolis, "Assessment of anisotropy of extruded tubes by ring hoop tension test", Procedia Engineering 81 (2014) 2261 – 2266.

[5] Rémi Delville, Specifications DIN 1.4970 24% CW cladding tubes TASTE project –SCK·CEN, May 2014

[6] Rémi Delville, Specifications DIN 1.4970 46% CW cladding tubes TASTE project –SCK·CEN, May 2015

Appendix E

Ring Compression Tests at room temperature accompanied by Finite Element Analysis in order to predict YS and UTS

ENEA report by Carlo Cristalli and Rosario Giammusso

Intermediate Report on the activities carried out in the frame of EERA Pilot Project

TASTE

Testing and ASsessment methodologies for material characterization of thin-walled cladding TubEs

Ring Compression Tests at room temperature accompanied by Finite Element Analysis in order to predict YS and UTS

Authors:

Carlo Cristalli

Rosario Giammusso

Ring Compression Tests at room temperature to predict YS and UTS

Index:

1. **Introduction**……..p.1
2. **Material**……p.3
3. **Finite Element Analysis**……p.4
4. **Experimental results**……p.8
5. **Analysis of the results; Correlation between Ring Compression Tests (Collapse Load) and tensile tests (Rp02 and UTS**)……..p.12
6. **Conclusions**…….p.19
7. **References**……..p.20

1. Introduction

This Ring Compression test consists in the compression of a pipe between two parallel planes in order to achieve a characteristic curve reporting load as function of the displacement. In ring compression tests the specimen is simply compressed perpendicular to the tube axis under displacement or load control. Among the equivalent stresses distributed in the entire ring, the maximum value of these stresses is usually located close to the inner surface at the 12o'clock position. The ring-compression test is a good ductility screening test. For determining tensile and creep properties the test method has no sensitivity to friction between the ring and the loading device. The main shortcomings are that the deformation is highly non-homogenous and undergoes simultaneously tensile and compressive deformation. The assessment is therefore very complex. In particular for extracting true stress/true strain from the force/deflection data which must be done indirectly via iterative process which may lead to non-unique solutions. Several methods have been taken into account, in literature [1-14], in order to correlate the load-displacement curve resulting from this test to the mechanical properties of the material (Yield Stress, UTS, K_{IC}).

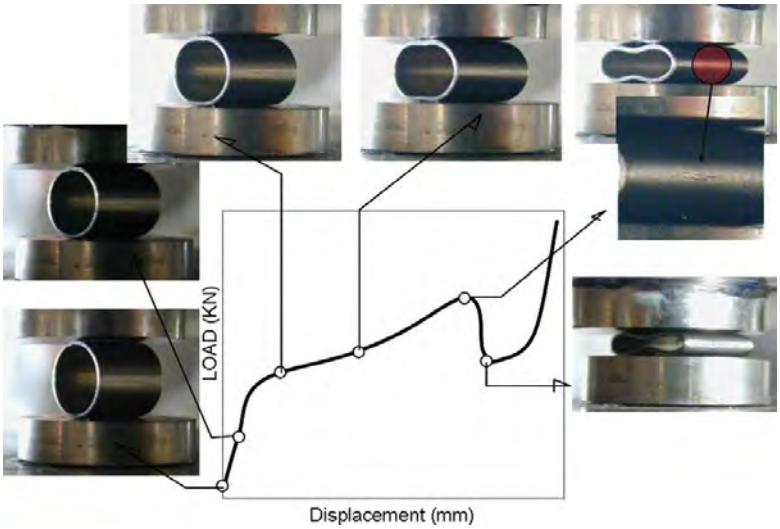

Fig. 1: Stages of Ring Compression Test [1]

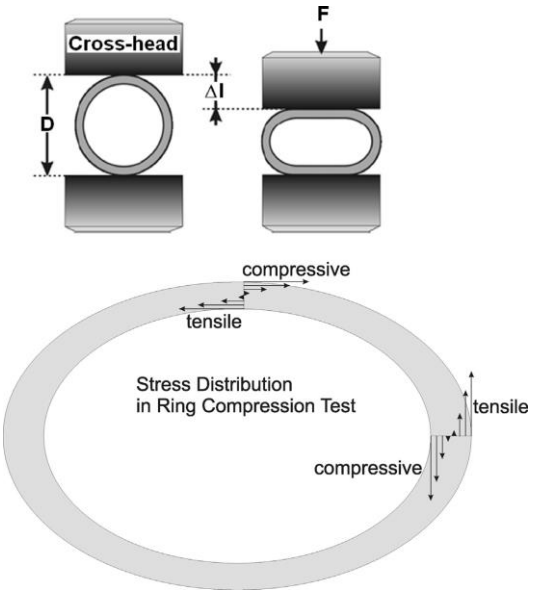

Fig. 2: Principal experimental setup and mechanics of RCT [2]

2. Material

The investigated material is 15-15 Ti austenitic steel. It has been produced by Sandvik and manufactured in the shape of tubes (outside diameter 6,5 mm, thickness 0,45 mm). The tubes have been supplied to ENEA by SCK-CEN in two manufacturing conditions; namely 24 % and 46 % cold working ratio. The following tables (tab. 1-2) report the results of the tensile tests performed by the manufacturer (Sandvik) on the two batches of 24% and 46% cold worked material.

		Resistance	***Elasticity***	***Elongation***
		Rm (N/mm2)	Rp0.2 (N/mm2)	A (%) sur 5.65√So
Requis **/** *Required***:**	≤300 MPa	≥ 760 MPa	620 / 840 MPa	≥ 18%
Résultats **/** *Results* ***Batch* 90770**	235 MPa / 236 MPa *	810 / 817 / 801 MPa	695 / 691 / 686 MPa	26.4% / 26.4% / 23.5%
Résultats **/** *Results* ***Batch* 90771**	235 MPa / 236 MPa *	823 / 817 / 841 MPa	708 / 691 / 722 MPa	25.0% / 23.5% / 25.0%

*Results coming from tensile tests performed on a « post series » heat-treated in the same conditions as batches 90770 and 90771 and coming from the same batch of hollows.

Table 1 – Summary of tensile properties measured on 24% cold-worked tubes

	Resistance	***Elasticity***	***Elongation***
	Rm (N/mm2)	Rp0.2 (N/mm2)	A (%) sur 5.65√So
Requis **/** *Required***:**	For information	> 900 MPa	For information
Résultats **/** *Results*	947-947-957 MPa	924-926-928MPa	9-10-12.%

Table 2 - Summary of tensile properties measured on 46% cold-worked tubes.

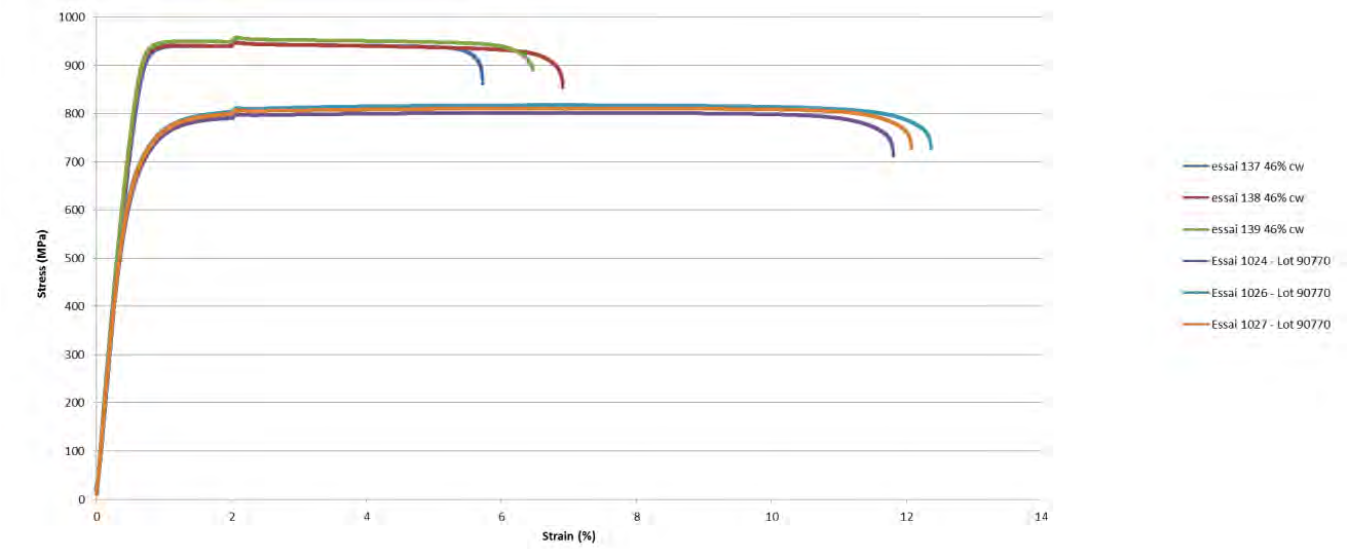

Fig. 3 – Stress strain curves of the 24% and 46% cold worked material

The tubes have been cut to three different lengths: 6 mm, 20 mm and 65 mm, corresponding respectively to 1, 3 and 10 diameters.

3. Finite Element Analysis

3.1 Finite Element Model implementation

The principle experimental setup of the Ring Compression Test has been analyzed from mechanical point of view by means of the commercial code ABAQUS version 6.14.

The finite element model utilizes two-dimensional continuum elements. Symmetry of the ring specimen is used to reduce the number of modeled elements. Based on the available plane of symmetry the model reduces to a half of the entire ring (see Fig. 4). Furthermore, a plane strain condition was postulated for the elements. That is, the finite element representing the ring specimen allows radial and circumferential strain of the ring, but does not allow axial strain. Comparable to the load imposed in the real RCT, in the FE model some fictitious contact surfaces are implemented The resulting force on the cross-head is modeled by contact surfaces with a friction coefficient of 0.0 (see contact surfaces in Fig. 4). The force predicted by FEM has to be multiplied by a factor of 2 because the FE model has been reduced for symmetrical reason. The other boundary conditions of Finite Element Model have been reported in Fig. 4.

A mesh independency analysis has been performed to select an optimized spatial discretization which allows accurate results to be obtained saving calculation time. A mesh composed of ~9200 nodes connected in ~2900 elements has been selected (Fig. 3, right), that allows numerical simulations to be carried out in about 15 minutes, running in parallel on a 4 CPU workstation equipped with 64 GByte of RAM. In particular, the parts of the model were meshed by means of 8-node CPE8 plane strain elements.

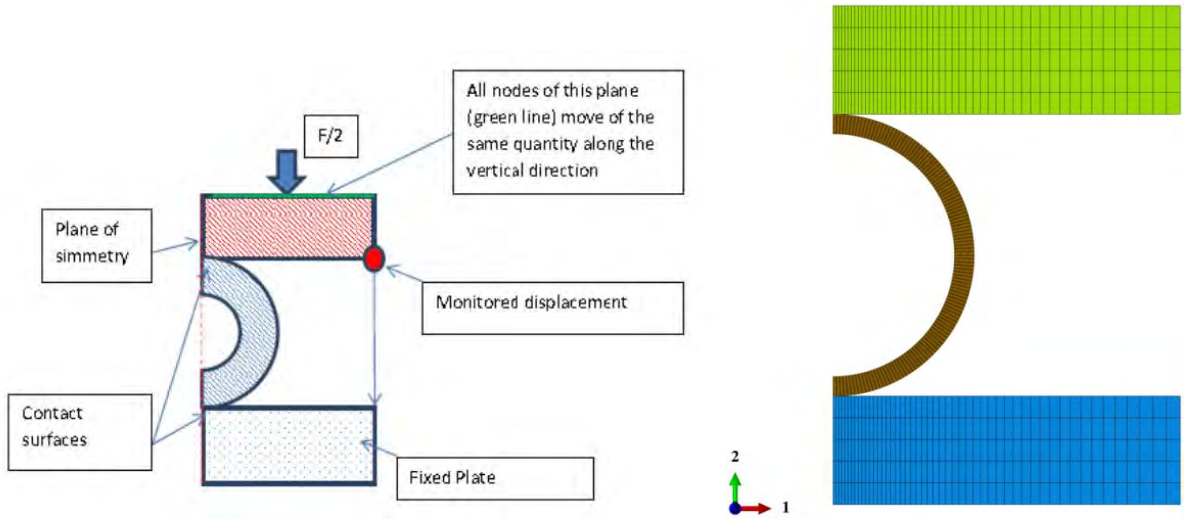

Fig. 4 –Boundary conditions (left) and mesh (right) of the Finite Element Model

3.2 Results of the mechanical analyses

FEM prediction of RCT requires the mechanical properties of the ring. These properties are taken from the results of the tensile tests performed by Sanvik and SCK-CEN on the material of the batches used for the fabrication of the claddings. In the frame of this study, the thermo-mechanical properties of the material have been assumed to depend uniquely on cold working rate and the ring mechanical behavior is assumed to be isotropic elastic–plastic. The isotropic strain-hardening tensile law is modelled using a power-law: $\sigma = K (\varepsilon_p^n)$, where σ and ε_p are the equivalent Von–Mises stress and the corresponding equivalent plastic strain respectively and, K and n are two material parameters to be identified.

The loading device stiffness is known to be significantly higher than the sample stiffness. It is anyway assumed to be an elastic body with a large Young modulus, but material properties for loading device are expected to have a negligible influence on stress and strain distribution in the ring.

The contact between the ring and the loading device is assumed to be perfect, without friction. To this purpose a small-sliding contact definitions have been prescribed between all surfaces that come in contact.

Inside an Instron machine a movable cross-head squeezes the ring specimen with a controlled displacement. The displacement Δl of the cross-head of the Instron machine provokes a reaction force F. That force is computed and plotted versus the displacement of the movable cross-head squeezes, see Fig. 5 and 6. In the FEA two essays have been considered: essay 1027 and essay 137.

The first graph (Essai 1027 lot 90770) refers to the claddings fabricated with 24% cold working rate while the second (Essai 137 lot 91261) refers to the claddings fabricated with 46% cold working rate.

It has to be underlined that the experimental curves is not reproduced totally by the numerical results because the elastic-plastic properties have been extracted for low values of the total deformations (< 12%). The correlation between FEM simulation and experimental data is good up to the elbow of the collapse stress. After the elbow has been exceeded the plastic behavior of the material prevails and the FEM seems no longer able to reproduce the experimental data correctly. This is due to the lack of expertize in modeling correctly the plastic behaviour of the material from tensile tests data. Nevertheless, a complete modeling of the total Load –Displacement behaviour isn't considered essential, at this stage.

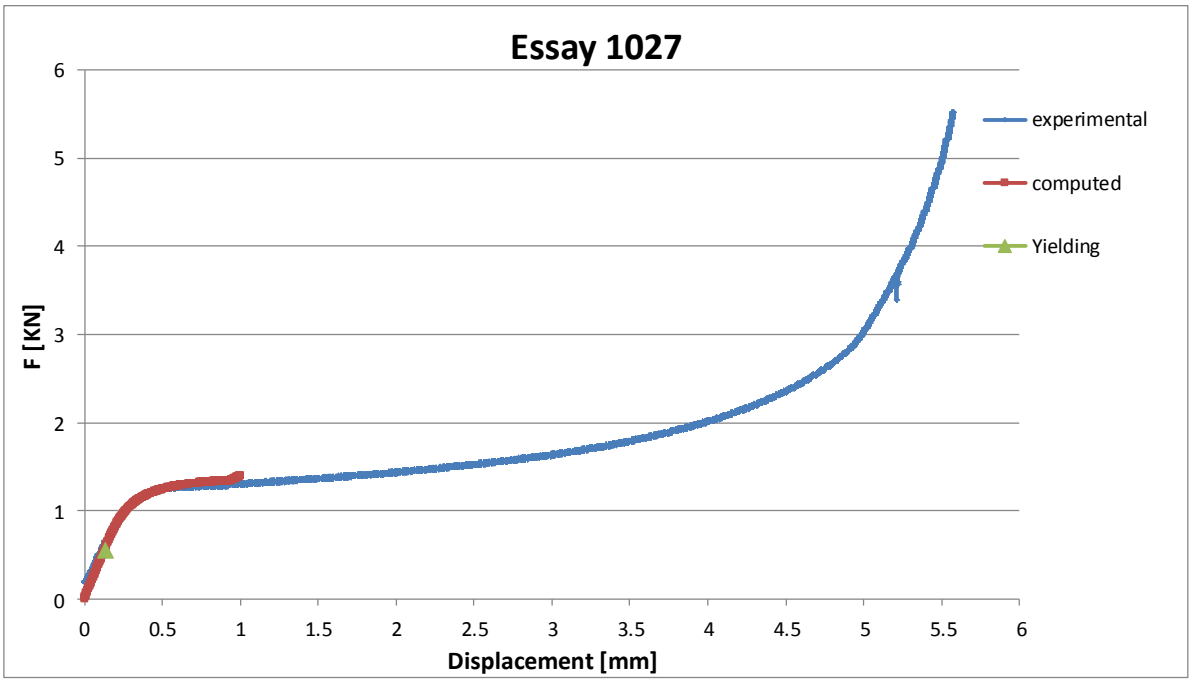

Fig. 5 – Force-Displacement: Essay 1027 lot 90770

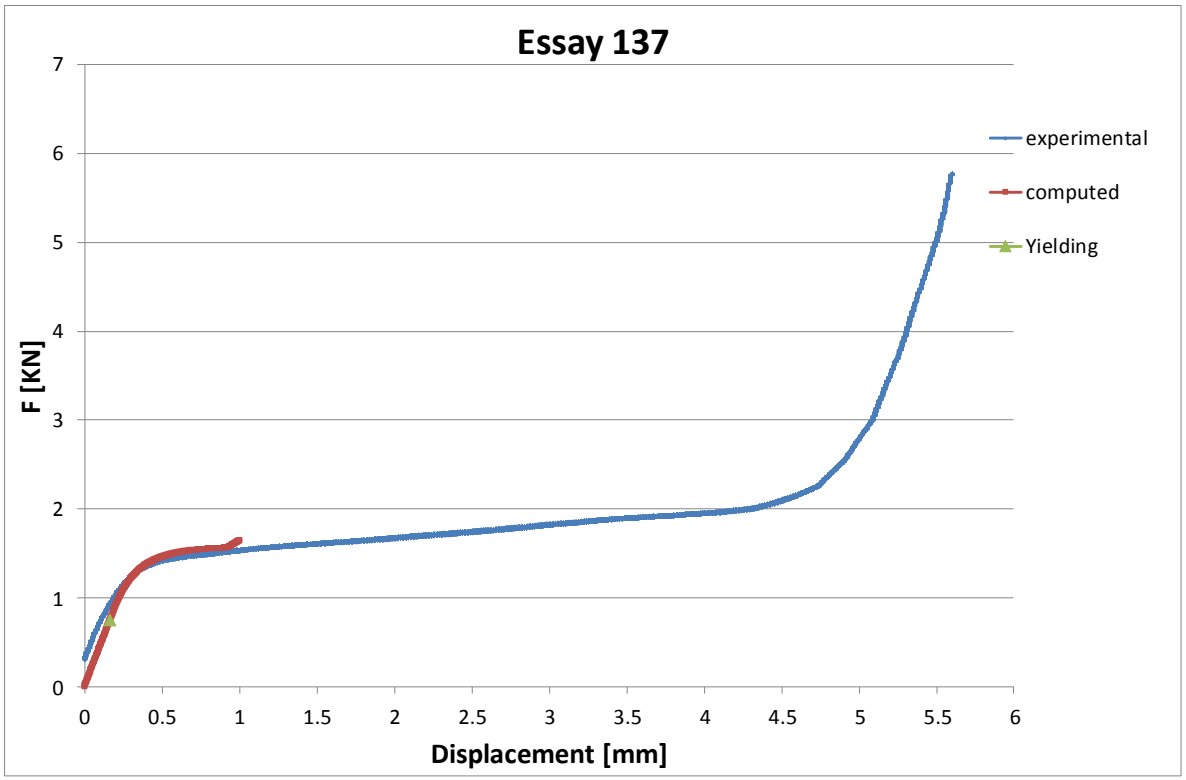

Fig. 6 – Force-Displacement: Essay 137 lot 91261

As we can observe in the previous plots, the Yield Stress is locally exceeded well before the achievement of the collapse load (elbow in the load displacement curve).
Yielding condition at the 12 o'clock position at inner rim is reached for a value of displacement of 0.132 mm and a Force of 0.56 KN for the essay 1027.

Yielding condition at the 12 o'clock position at inner rim is reached for a value of displacement of 0.164 mm and a Force of 0.745 KN for the essay 137.
Von Mises equivalent stresses at various positions of the rings have been reported on Fig. 7 and 8. Compressing the ring between two parallel plates induces in the 3 o'clock position at outer rim of ring and in the 12 o'clock position at inner rim of ring tensile stresses while in the 3 o'clock position at inner rim of ring and in the12 o'clock position at outer rim of ring compressive stresses prevail. The more the ring is compressed the larger the tensile stresses will be and may finally lead to failure of the ring material. Such failures occur preferentially at the 12'o clock position at inner rim.

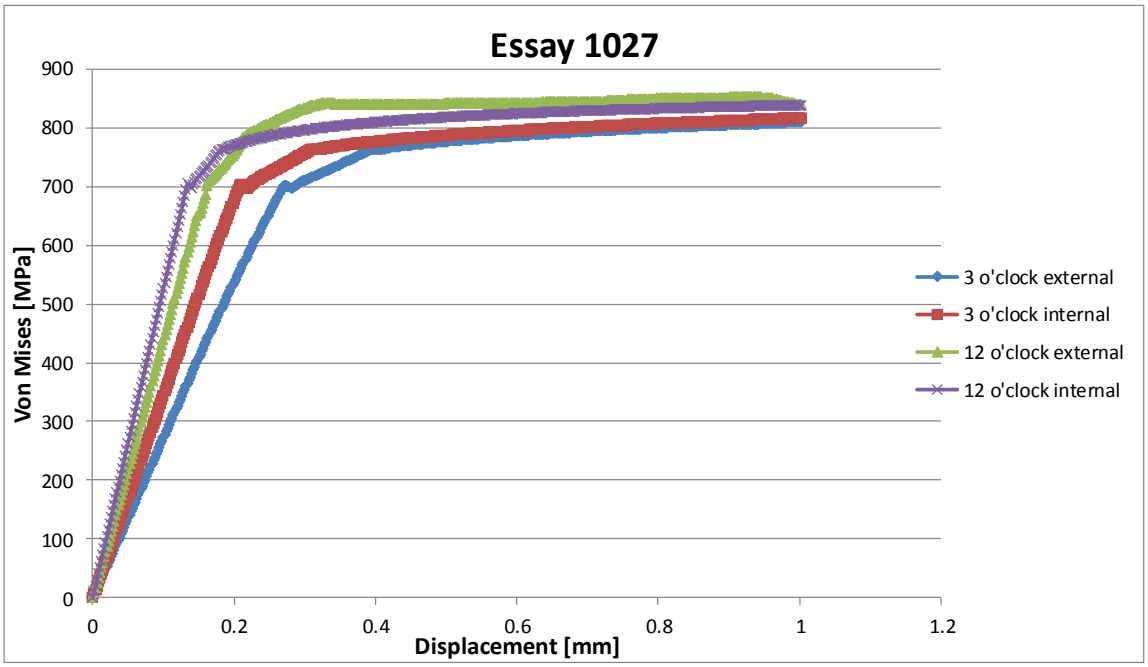

Fig. 7 –Von Mises: Essay 1027 lot 90770

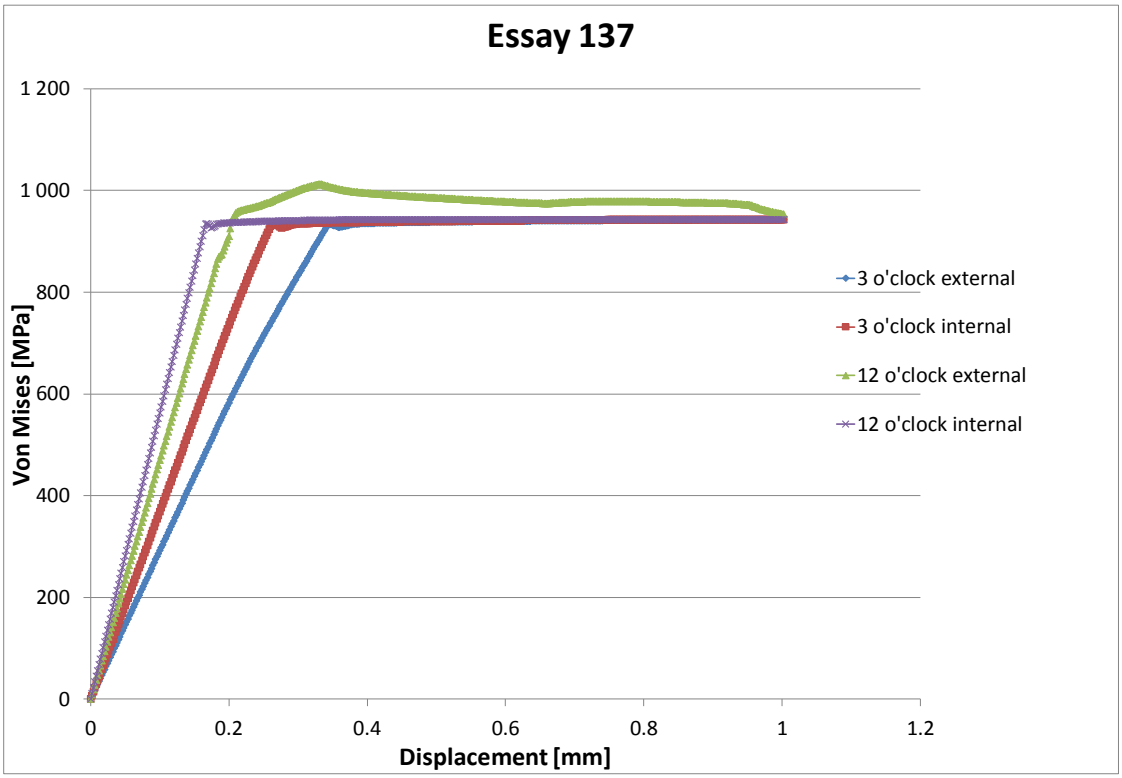

Fig. 8 – Von Mises: Essay 137 lot 91261

2. Experimental results

The Ring Compression tests were carried out at room temperature inside the laboratory of ENEA Brasimone with Tensile machine MetroCom. E50 (Fig. 9, left). equipped with a 50 kN Load cell - MTS 3187-104.
Each test has been performed at room temperature keeping the speed of the crosshead constant to 0,2 mm/min. The test has been stopped when the tube resulted completely flattened. For each tube length three tests have been performed (fig. 9, right).

Fig. 9: Metrocom E50 Machine (left); flattened tubes after testing (right)

The typical curve resulting from the ring compression test is reported in the following graph (fig. 10).

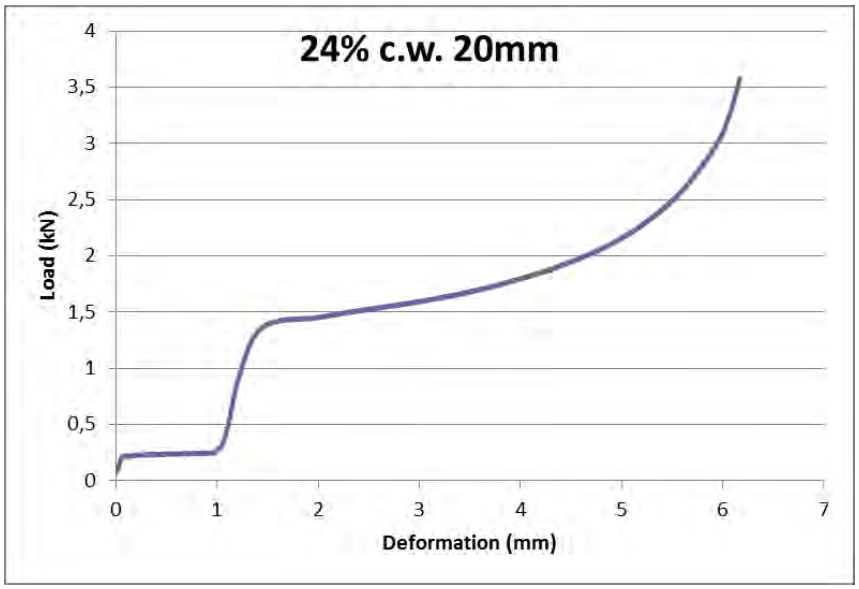

Fig. 10: Load – Deformation curve of the 20 mm length tube (24% c.w.)

The obtained curve can be approximately divided into three stages. In the first stage the load remains almost constant at the increasing deformation; this means that, during this phase, the plays in the crosshead grip assembly are being exhausted. This portion of the curve will be neglected in the analysis aimed at the determination of the tensile properties of the material. In the following portion of the curve the load increases rapidly with the deformation up to an elbow corresponding to the collapse load (see later). Once exceeded this elbow, the load increases again with a parabolic law up to the complete crushing of the tube.

Hereafter the Load-Displacement curves obtained in the tests performed on the 6 mm length samples are reported (fig. 11).

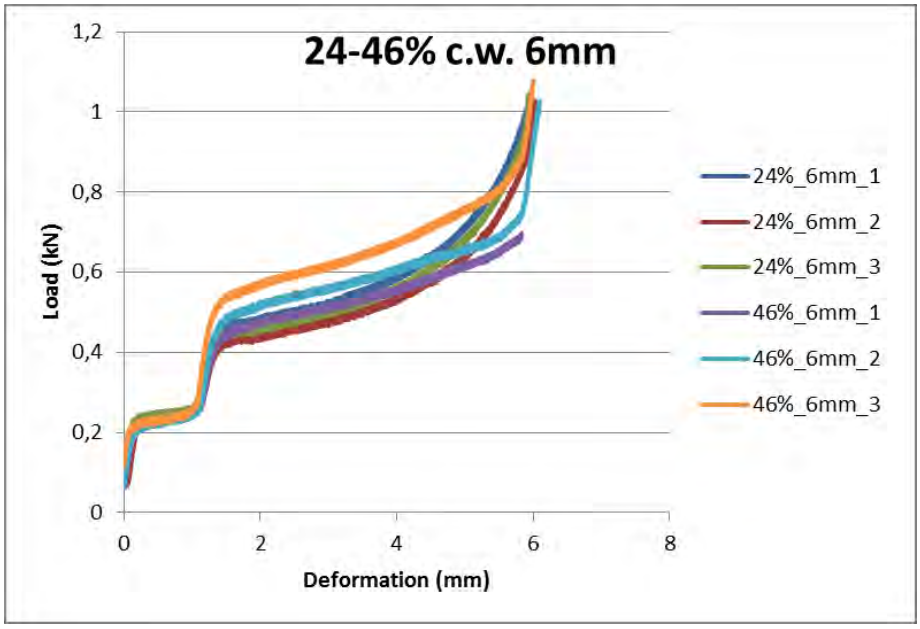

Fig. 11: Load – Deformation curves of the 6 mm length tubes (24% and 46% c.w.)

The elbow of the curves, corresponding to the Collapse Load, can be put in relation to the tensile properties in agreement to literature [1,11]. Detailed calculations aimed at the correlation between the Collapse Load and the tensile properties of the material are reported in the next paragraph. Comparing the results of the two c.w. conditions we can notice a larger spread in the curves obtained on the tubes with the higher c.w. ratio. The Collapse Load resulting from the more severe c.w. ratio appears averagely higher, as expected.
In the following graph (fig. 12) the Load-Displacement curves obtained after the tests performed on the 20 mm length samples are reported.

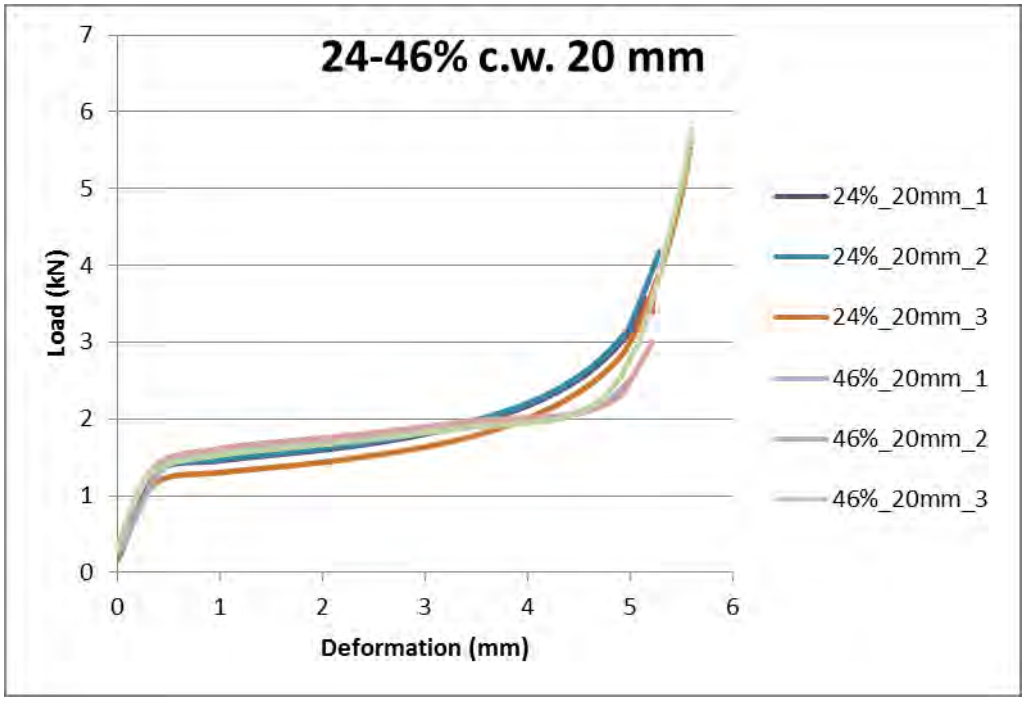

Fig. 12: Load – Deformation curves of the 20 mm length tubes (24% and 46% c.w.)

Despite the previous tests the larger scatter appears now with the 24% c.w. ratio. The Collapse Load resulting from the more severe c.w. ratio appears averagely higher, as expected.
Below the Load-Displacement curves obtained after the tests performed on the 20 mm length samples are reported (fig. 13).

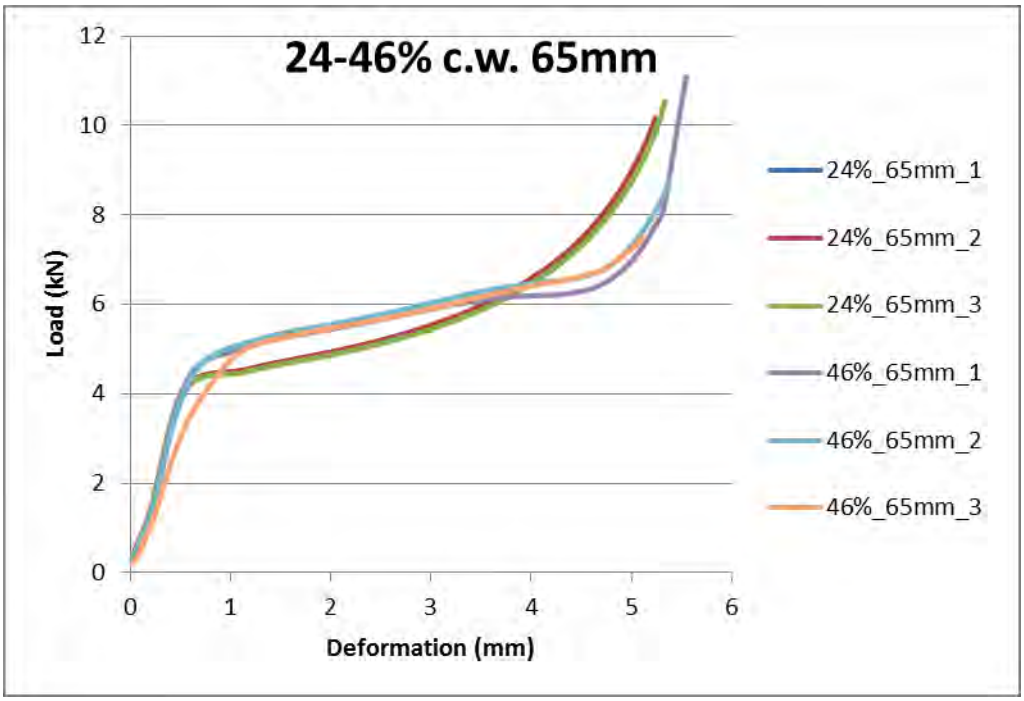

Fig. 13: Load – Deformation curves of the 65 mm length tubes (24% and 46% c.w.)

We can notice that the scatter in the results appears markedly lower. On the other hand, the Collapse Load resulting from the more severe c.w. ratio appears averagely higher, as expected. We can deduce that both the scatter in the results and the enhancement of the Collapse Load with the c.w. ratio decrease at the increasing tube length.

Hereafter all the tests performed at room temperature are reported (fig. 14).

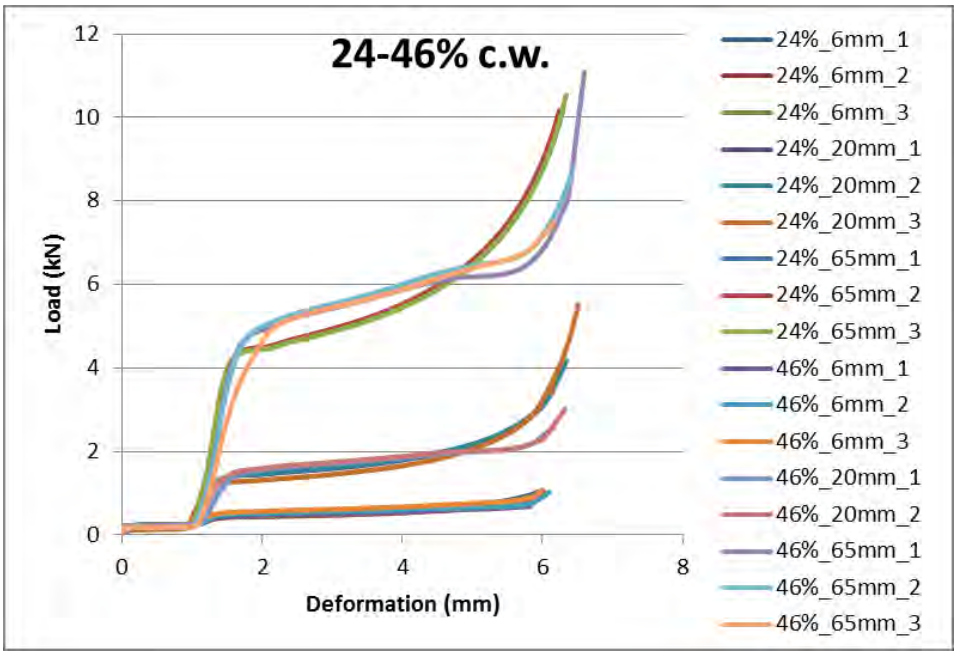

Fig. 14: Load – Deformation curves of the 24% and 46% c.w. tubes

2. Analysis of the results; Correlation between Ring Compression Tests (Collapse Load) and tensile tests (R_{p02} and UTS)

The Collapse Stress has been calculated in agreement with [1, 11] according to the following formulation:

1) $Collapse\ Stress = \frac{\alpha P_0 R_0}{t_0^2 l}$

With:

α = 0,866 for tubes (longer than one diameter) or 1 for rings (length shorter than one diameter);

R_0 = initial outer radius;

t_0 = tube thickness;

l = length of the ring;

P_0 = initial collapse load, obtained by the graphical intersection between the linear interpolation of the first and second stages of the load-displacement curve.

The Collapse Stress has been correlated to the Yield Stress ($R_{p0,2}$) and Ultimate Tensile Stress (UTS) through the following coefficients;

2) $K_{R_{p02}} = \frac{Collapse\ Stress}{R_{p02}}$

3) $K_{UTS} = \frac{Collapse\ Stress}{UTS}$

The Collapse Stress and the ratios to the R_{p02} and to the UTS have then been identified for each tube length and c.w. ratio.

For 6 mm length, 24% c.w.;

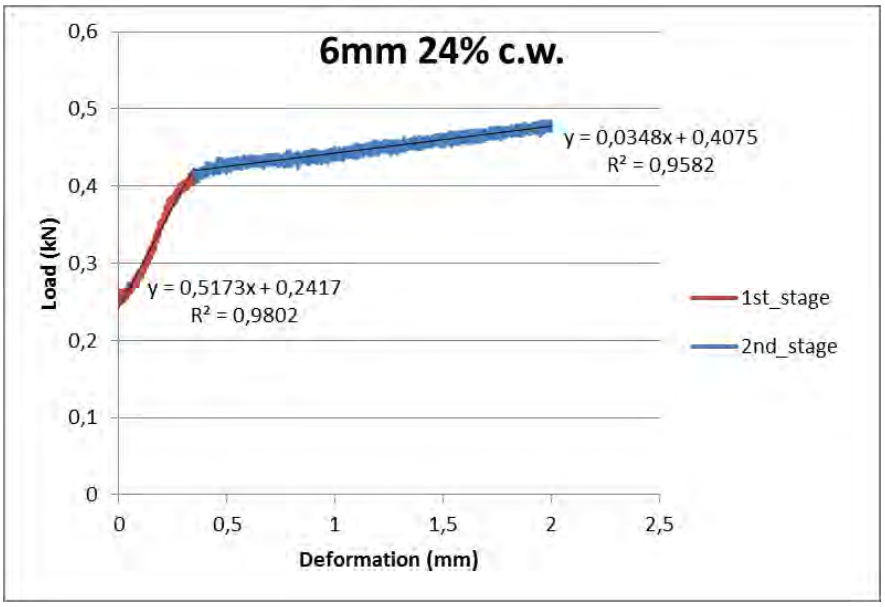

Fig. 15: Linear Interpolation to determine Collapse Load (6mm 24% c.w. tube)

Coefficient	Value	Unit
α	1	-
R_0	3,25	mm
t	0,45	mm
L	6	mm
Collapse Load	0,45	kN
Collapse Stress	1215,27	Mpa
Rp02 (avg., SCK-CEN)	699	Mpa
UTS (avg., SCK-CEN)	818	Mpa
KRp02	1,74	-
KUTS	1,49	-

Tab. 3: Coefficients used in the calculation of the Collapse Stress (6mm 24% c.w. tube)

	Collapse Stress (Mpa)	KRp02	KUTS
Tube_1	1221,7	1,75	1,49
Tube_2	1215,27	1,74	1,49
Tube_3	1168	1,67	1,42
Δ %	4,6 %	5 %	4,6 %

Tab. 4: Coefficients obtained after three repetitions of the test (6mm 24% c.w. tube)

For 20 mm length, 24% c.w.;

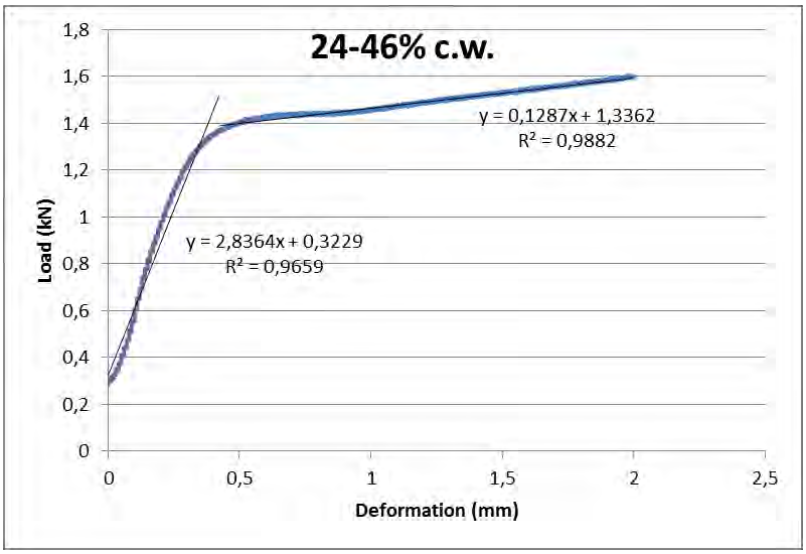

Fig. 16: Linear Interpolation to determine Collapse Load (20 mm 24% c.w. tube)

Coefficient	Value	Unit
α	0,866	-
R_0	3,25	mm
t	0,45	mm
L	20	mm
Collapse Load	1,38	kN
Collapse Stress	962,05	Mpa
Rp02 (avg., SCK-CEN)	699	Mpa
UTS (avg., SCK-CEN)	818	Mpa
KRp02	1,38	-
KUTS	1,18	-

Tab. 5: Coefficients used in the calculation of the Collapse Stress (20 mm 24% c.w. tube)

	Collapse Stress (Mpa)	KRp02	KUTS
Tube_1	962,05	1,38	1,18
Tube_2	974,29	1,39	1,19
Tube_3	846,9	1,21	1,04
Δ %	15 %	15 %	15 %

Tab. 6: Coefficients obtained after three repetitions of the test (20 mm 24% c.w. tube)

For 65 mm length, 24% c.w.;

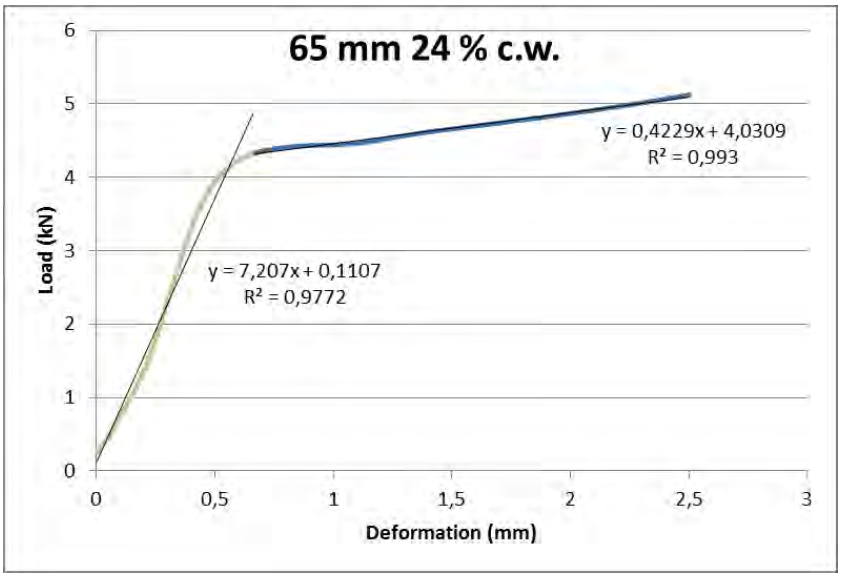

Fig. 17: Linear Interpolation to determine Collapse Load (65 mm 24% c.w. tube)

Coefficient	Value	Unit
α	0,866	-
R_0	3,25	mm
t	0,45	mm
L	65	mm
Collapse Load	4,28	kN
Collapse Stress	914,17	Mpa
Rp02 (avg., SCK-CEN)	699	Mpa
UTS (avg., SCK-CEN)	818	Mpa
KRp02	1,31	-
KUTS	1,12	-

Tab. 7: Coefficients used in the calculation of the Collapse Stress (65 mm 24% c.w. tube)

	Collapse Stress (Mpa)	KRp02	KUTS
Tube_1	926,32	1,33	1,13
Tube_2	922,5	1,32	1,13
Tube_3	914,17	1,31	1,12
Δ %	1,3 %	1 %	1,3 %

Tab. 8: Coefficients obtained after three repetitions of the test (65 mm 24% c.w. tube)

For 6 mm length, 46% c.w.;

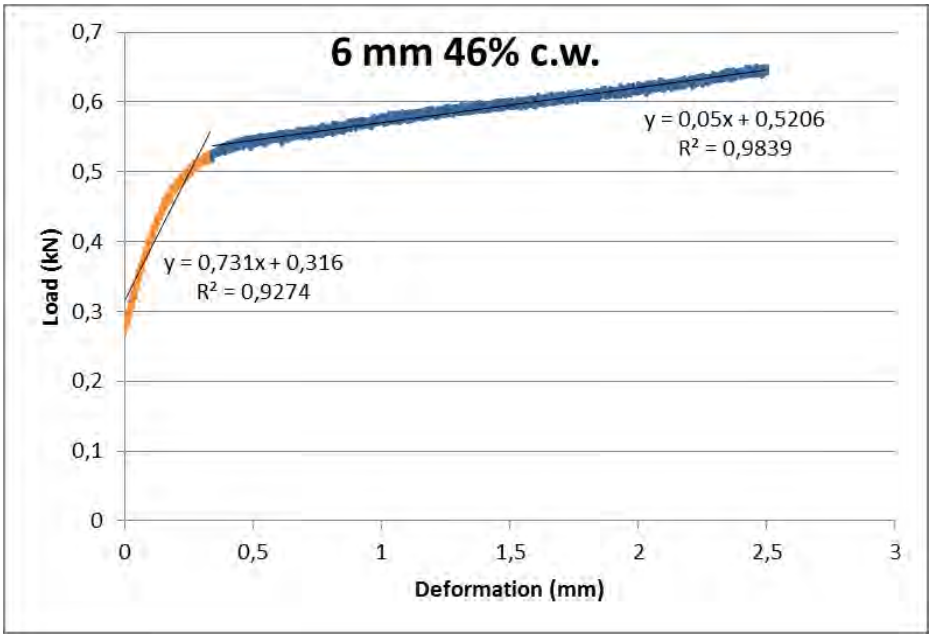

Fig. 18: Linear Interpolation to determine Collapse Load (6 mm 46% c.w. tube)

Coefficient	Value	Unit
α	1	-
R_0	3,25	mm
t	0,45	mm
L	6	mm
Collapse Load	0,54	kN
Collapse Stress	1432,73	Mpa
Rp02 (avg., SCK-CEN)	926	Mpa
UTS (avg., SCK-CEN)	950,3	Mpa
KRp02	1,55	-
KUTS	1,51	-

Tab. 9: Coefficients used in the calculation of the Collapse Stress (6 mm 46% c.w. tube)

	Collapse Stress (Mpa)	KRp02	KUTS
Tube_1	1197,62	1,29	1,26
Tube_2	1312,65	1,42	1,38
Tube_3	1432,73	1,55	1,51
Δ %	19 %	16 %	16,4 %

Tab. 10: Coefficients obtained after three repetitions of the test (6 mm 46% c.w. tube)

For 20 mm length, 46% c.w.;

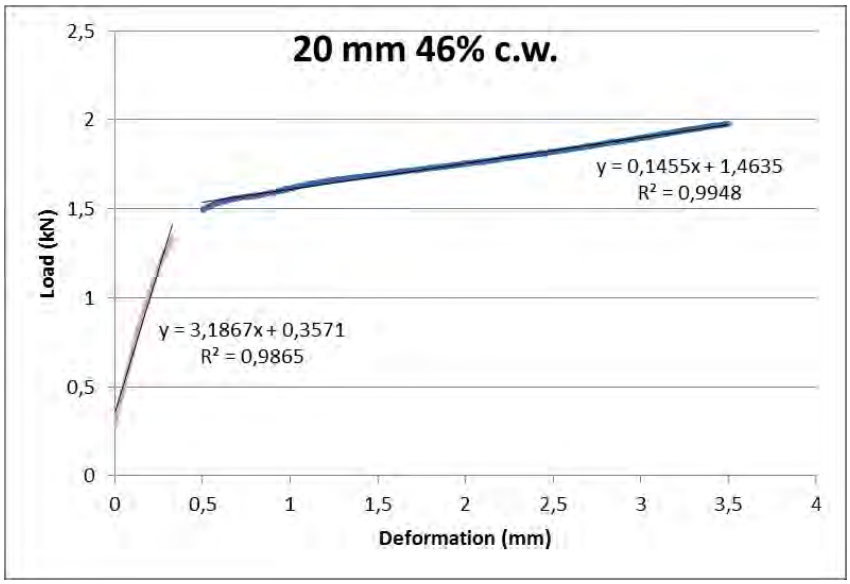

Fig. 19: Linear Interpolation to determine Collapse Load (20 mm 46% c.w. tube)

Coefficient	Value	Unit
α	0,866	-
R_0	3,25	mm
t	0,45	mm
L	20	mm
Collapse Load	1,52	kN
Collapse Stress	1053,83	Mpa
Rp02 (avg., SCK-CEN)	926	Mpa
UTS (avg., SCK-CEN)	950,3	Mpa
KRp02	1,14	-
KUTS	1,12	-

Tab. 11: Coefficients used in the calculation of the Collapse Stress (20 mm 46% c.w. tube)

	Collapse Stress (Mpa)	KRp02	KUTS
Tube_1	1044,53	1,13	1,1
Tube_2	1053,83	1,14	1,1
Tube_3	1001,37	1,08	1,05
Δ %	4,3 %	4 %	4,3 %

Tab. 12: Coefficients obtained after three repetitions of the test (20 mm 46% c.w. tube)

For 65 mm length, 46% c.w.;

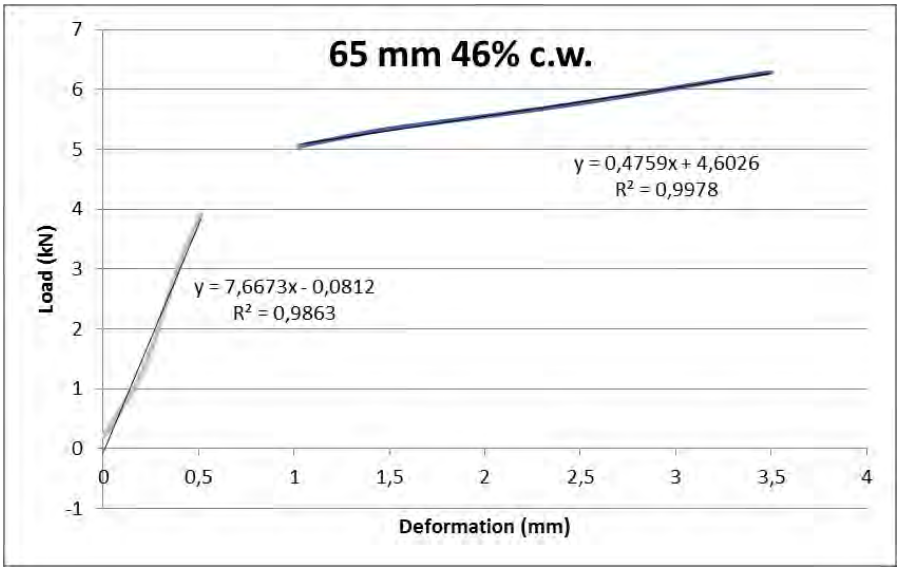

Fig. 20: Linear Interpolation to determine Collapse Load (65 mm 46% c.w. tube)

Coefficient	Value	Unit
α	0,866	-
R_0	3,25	mm
t	0,45	mm
L	65	mm
Collapse Load	4,91	kN
Collapse Stress	1050,44	Mpa
Rp02 (avg., SCK-CEN)	926	Mpa
UTS (avg., SCK-CEN)	950,3	Mpa
KRp02	1,13	-
KUTS	1,1	-

Tab. 13: Coefficients used in the calculation of the Collapse Stress (65 mm 46% c.w. tube)

	Collapse Stress (Mpa)	KRp02	KUTS
Tube_1	1026,04	1,11	1,08
Tube_2	1050,44	1,13	1,1
Tube_3	1063,55	1,15	1,12
Δ %	3,6 %	4 %	3,5 %

Tab. 14: Coefficients obtained after three repetitions of the test (65 mm 46% c.w. tube)

The following diagrams (fig. 21 -22) compare the calculated ratios to the Rp02 and to the UTS for each tube length and c.w. ratio;

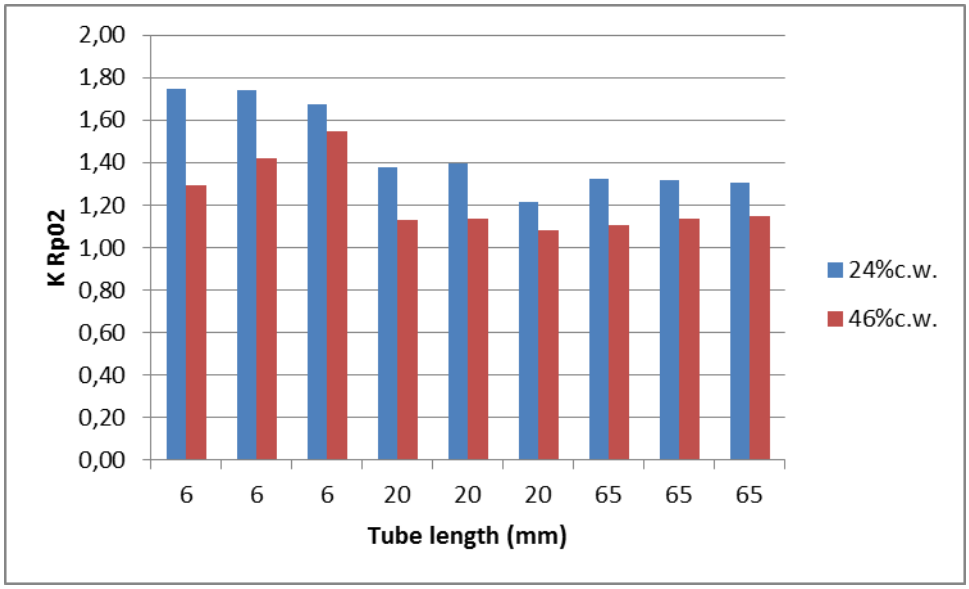

Fig. 21: Ratios to the Rp02 obtained after three repetitions of the test (24% c.w. tube)

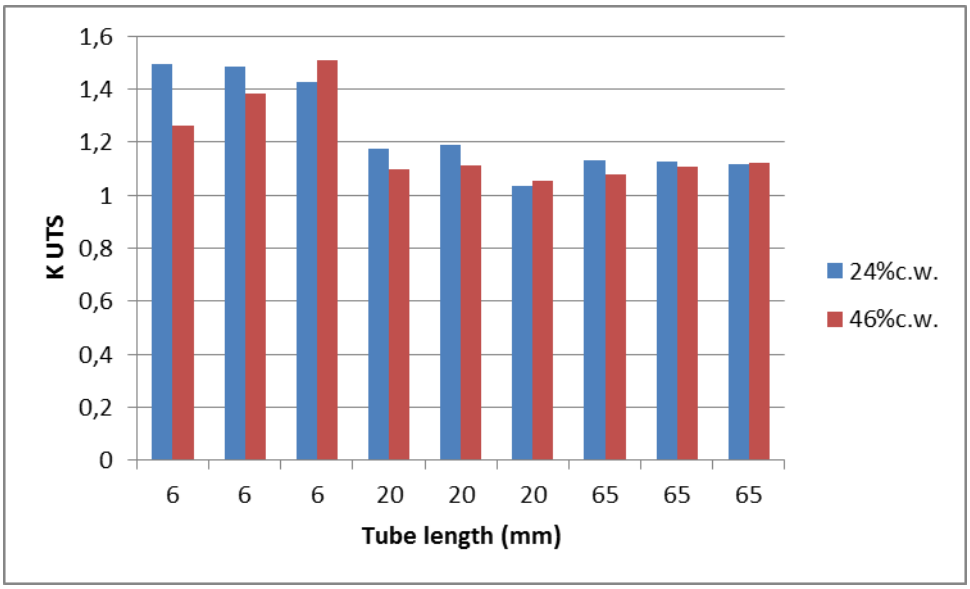

Fig. 22: Ratios to the UTS obtained after three repetitions of the test (46% c.w. tube)

In each of the tested cases neither the Rp02 nor the UTS are approximated exactly by the Collapse Stress, as literature suggests [1,11]. The ratio of the tensile properties (Rp02 and UTS) to the Collapse Stress, in fact, always results higher than 1, meaning that the Collapse Stress always occurs once both the Rp02 and the UTS have been exceeded.

The statistical scatter of the results with the same testing conditions remains within 5 % and therefore acceptable just in four of the six investigated experimental conditions. The 6 mm 46% c.w. and the 20 mm 24% c.w. tubes don't fit this requirement being the scatter of the results, in these cases, in the range of 15%.

Some sources in literature put the Collapse Stress in relation to the Yield Stress [1], other sources to the UTS [11]. It's expected that, in a correctly working method, the ratios to the tensile properties remain the same with the changing c.w. condition; in other words, once determined the ratio to the Yield Stress or to the Ultimate Tensile Stress, this should be kept constant with the variation of the chosen property (namely YS or UTS). This experimental campaign at room temperature shows that the ratio to the Yield Stress doesn't remain constant with the changing cold working condition. Therefore it's preferable to run the method as a screening procedure for the evaluation of the UTS more than the Yield Stress (Rp02).

Even limiting the validity of the screening procedure to the assessment of the UTS, the equivalence of the ratios (Collapse Stress to UTS) in the two cold working conditions seems to be verified, with good approximation, only with the largest values of the cladding length. Therefore, the main outcome of this room temperature experimental campaign is that the tensile property that can be better assessed by means of the Ring Compression testing procedure is the UTS, but just for large values of cladding length, possibly in the range of ten diameters.

5. Conclusions

Inside a 50 kN press a movable cross-head squeezes a ring specimen with a controlled displacement. This Ring Compression Test screening procedure has been analyzed through two parallel approaches; by Finite Element Analysis and through an experimental campaign at room temperature.

The displacement Δl of the cross-head of the machine provokes a reaction force F in the machine depending on the ring specimen stiffness. That force has been measured, computed and plotted versus the

imposed displacement. The predicted reaction force from displacing the FEs is comparable to the measured reaction force of RCT. The main outcome of the FEA is that the Yield Stress is locally exceeded well before the achievement of the collapse load. The correlation between FEM simulation and experimental data is good up to the elbow of the collapse stress in both cold working conditions. Therefore the FEM proves a suitable instrument to simulate the process up to the achievement of the Collapse Load. After the elbow has been exceeded the plastic behaviour of the material prevails and the FEM seems no longer able to reproduce the experimental data correctly. This is due to the lack of expertize in modeling correctly the plastic behaviour of the material from tensile tests data. Nevertheless, a complete modeling of the total Load –Displacement behaviour isn't considered essential, at this stage.
The main outcome of the room temperature experimental campaign is that the tensile property that can be better assessed by means of the Ring Compression testing procedure is the UTS, but just for large values of cladding length, possibly in the range of ten diameters.

6. References

1. T. Yella Reddy and S.R. Reid "On obtaining Material Properties from the Ring Compression Test" Nuclear Engineering and Design 52 (1979) 257-263
2. R. Yamada, M. Suzuki and Y. Harayama, Nucl. Eng. Des. 44 (1977) 75.
3. T.Y. Reddy, Ph.D. Thesis, University of Cambridge (1978)
4. R.H. Burton and J.M. Craig, B.Sc. (eng) Rept., University of Bristol (1963).
5. J.A. DeRuntz and P.G. Hodge, Jr., J. Appl. Mech. 31 (1963) 391.
6. R.G. Redwood, J. Appl. Mech. 32 (1964) 357.
7. S.R. Reid and T.Y. Reddy, Int. J. Solid Structures 14 (1978) 213.
8. J. Herb, J. Sievers, H.G. Sonnenburg, "A new cladding embrittlement criterion derived from ring compression tests" Nuclear Engineering and Design 273(2014)615–630
9. M.A. Martin-Rengel, F.J. Gómez Sánchez, J. Ruiz-Hervías, L. Caballero "Determination of the hoop fracture properties of unirradiated hydrogen-charged nuclear fuel cladding from ring compression tests" Journal of Nuclear Materials 436 (2013) 123–129
10. M.A. Martín-Rengel, F.J. Gómez, J. Ruiz-Hervías, A.Valiente, "Obtention of fracture properties of unirradiated hydrogen-charged fuel cladding from ring compression test", 2009 Water Reactor Fuel Performance Meeting, September 6–10, 2009, Paris, France, paper no. 2212, 2009.
11. V. Busser, M.C. Baietto-Dubourg, J. Desquines, C. Duriez, J.P. Mardon "Mechanical response of oxidized Zircaloy-4 cladding material submitted to a ring compression test" Journal of Nuclear Materials 384 (2009) 87–95
12. Lacki, P.a, Adamus, J.a, Motyka, M.b, Sieniawski, J.b "Theoretical and experimental analysis of a ring compression test for Ti-6Al-4V titanium alloy"
13. Cristino, V.A.M., Rosa, P.A.R., Martins, P.A.F. "The Role of Interfaces in the Evaluation of Friction by Ring Compression Testing "
14. M. Nemat-Alla, Int. J. Mech. Sci. 45 (2003) 605.

Europe Direct is a service to help you find answers to your questions about the European Union.

Freephone number (*)**:**

00 800 6 7 8 9 10 11

(*) The information given is free, as are most calls (though some operators, phone boxes or hotels may charge you).

More information on the European Union is available on the internet (http://europa.eu).

HOW TO OBTAIN EU PUBLICATIONS

Free publications:

- one copy:
  via EU Bookshop (http://bookshop.europa.eu);
- more than one copy or posters/maps:
  from the European Union's representations (http://ec.europa.eu/represent_en.htm);
  from the delegations in non-EU countries (http://eeas.europa.eu/delegations/index_en.htm);
  by contacting the Europe Direct service (http://europa.eu/europedirect/index_en.htm) or
  calling 00 800 6 7 8 9 10 11 (freephone number from anywhere in the EU) (*).

  (*) The information given is free, as are most calls (though some operators, phone boxes or hotels may charge you).

Priced publications:

- via EU Bookshop (http://bookshop.europa.eu).

KJ-1A-28746-EN-N

JRC Mission

As the science and knowledge service of the European Commission, the Joint Research Centre's mission is to support EU policies with independent evidence throughout the whole policy cycle.

EU Science Hub
ec.europa.eu/jrc

@EU_ScienceHub

EU Science Hub - Joint Research Centre

Joint Research Centre

EU Science Hub

Publications Office

doi:10.2760/49859

ISBN 978-92-79-75429-6